CORE-WIDE PROBABILISTIC EVALUATION OF HOT SPOT TEMPERATURE IN REACTOR CORE THERMAL AND HYDRAULIC DESIGN

〔原子炉炉心熱流力設計に於けるホットスポット温度の確率論的多点評価〕

1979

Katsuhiro Sakai

CONTENTS

Chapter 1 Introduction ---------- 1

1.1 General introduction ---------- 1

1.2 Conventional design method and its technical problems -- 3

1.2.1 Roles of core thermal and hydraulic design in nuclear reactor design ---------- 4

1.2.2 Method and technical problems in conventional core thermal and hydraulic design ---------- 5

1.3 Objectives of the present studies and the related technical significance ---------- 11

1.3.1 Parameters affecting the core temperature ---------- 12

1.3.2 Necessity of a probabilistic method for evaluating the core temperature ---------- 12

1.3.3 A new method of evaluating a hot spot factor ------- 12

References ---------- 22

Chapter 2 Evaluation of fuel pin bundle deflection and its effect on the core temperature ---------- 27

2.1 Introduction ---------- 27

2.2 Analytical formulation ---------- 28

2.2.1 Assumption underlying the pin bundle deflection analysis ---------- 28

2.2.2 Equations governing fuel pin deflection ---------- 29

2.2.3 Boundary conditions ---------- 34

2.2.4 General solution of the deflection equation -------- 38

2.2.5 Equilibrium matrix equation for fuel pin bundle deflection ---------- 40

2.2.6 Subchannel analysis method in a fuel subassembly --- 50
2.2.7 Computational scheme ---------- 50
2.3 Experimental investigation on lateral drag coefficients of a fuel pin ---------- 51
2.3.1 Introduction ---------- 51
2.3.2 Experimental facilities and methods ---------- 51
2.3.3 Data analyses and results ---------- 53
2.4 Numerical results and discussion ---------- 56
2.5 Conclusions ---------- 68
Appendix 2A ---------- 77
References ---------- 81
Chapter 3 Probabilistic evaluation of fuel pin gaps due to the variation of core design parameters ---------- 83
3.1 Introduction ---------- 83
3.2 Analytical formulation ---------- 84
3.2.1 Assumptions underlying the probabilistic evaluation of fuel pin gaps ---------- 84
3.2.2 Probabilistic variation in fuel pin gaps ---------- 84
3.3 Computational scheme ---------- 90
3.4 Numerical results and discussion ---------- 91
3.4.1 Sensitivity of uncertainties ---------- 91
3.4.2 Evaluation of higher order terms ---------- 96
3.4.3 Probabilistic distribution of the pin gap ---------- 97
3.5 Conclusions ---------- 97
References ---------- 109
Chapter 4 Probabilistic evaluation of subassembly coolant flow rates due to the variation of core design parameters --- 111

4.1 Introduction ---------- 111

4.2 Analytical formulation ---------- 112

4.2.1 Nominal calculation ---------- 113

4.2.2 Evaluation of pressure loss performance ---------- 113

4.2.3 Probabilistic variation in coolant flow rate ------- 117

4.3 Numerical results and conclusions ---------- 123

4.3.1 Sample calculation 1 ---------- 125

4.3.2 Sample calculation 2 ---------- 126

4.3.3 Conclusions ---------- 126

References ---------- 135

Chapter 5 General discussion and conclusions ---------- 137

Nomenclature ---------- 144

Acknowledgement ---------- 152

Author's personal record ---------- 153

Chapter 1

Introduction

1.1 General introduction

Thermal and hydraulic design of an LMFBR core plays an important role in connection to the optimization of fuel subassemblies and reactor core structures as well as reactor inlet and outlet coolant temperature in the nominal operating condition with respect to reactor core performance, economy and safety, which are the prime objectives of LMFBR design.

In core thermal and hydraulic design, the maximum operating temperature is limited by the criterion that the core temperature should not exceed critical values. It is therefore necessary to accomplish a method of core-wide temperature analyses with related quantitative reliability evaluation in order to assure safety performance of a reactor core under consideration.

Some uncertainties due to manufacturing and assembling tolerances associated with the dimensions and geometries of fuel subassemblies and core internals and the experimental ambiguities included in material properties are inherently related to the core temperature and it is necessary to take into consideration the deviation of the core temperature due to these uncertainties in evaluating the safety performance of a reactor under design criteria.

In conventional hot spot analyses[1] ~ [13], neglecting completely the effect due to the mutual dependency of various parameters previously mentioned on the core temperature, it is assumed that the temperature dependency on the statistical deviations of these parameters is linear and the resulting probabilistic core temperature variation due to the statistical deviations of these parameters is of the normal distribution. The reliability level associated with the core temperature variation thus evaluated is less

accurate neglecting the effect of the mutual correlation among these factors, and therefore conservative engineering judgements for a safety margin have been employed in the conventional hot spot analyses. In this paper, the probabilistic temperature variation due to the statistical deviation of the previously mentioned uncertain parameters is discussed taking into consideration the thermomechanical correlation among fuel pins, fuel subassemblies and core internal structures, coolant flow correlation among coolant channels and the temperature dependency of core material properties based on the factory data and experiments.

An engineering hot spot factor is evaluated in terms of confidence level related to the safety performance of a reactor core based on the probabilistic temperature variation thus obtained. The importance of the following three subjects on the probabilistic evaluation of the core temperature related to engineering hot spot factors is discussed in chapters 2, 3 and 4, which have not been considered in conventional core design analyses, respectively.

(i) Experimental investigation of the lateral drag coefficient of fuel pins under coolant flow, which is necessary to determine fuel pin deflection modes in reactor operating condition, and evaluation of fuel pin deflection modes and the core temperature under the fuel pin deflection within a fuel subassembly[14] ~ [18].

(ii) Evaluation of fuel pin gap probabilistic distribution taking into consideration the manufacturing and assembling tolerances associated with fuel subassemblies, and the ambiguity in thermal and hydraulic parameters of material properties and hydraulic experimental data with the sensitivity of these uncertainties to fuel pin gaps[19] ~ [21].

(iii) Evaluation of the probabilistic distribution of coolant flow rate in a fuel subassembly taking into consideration the coolant flow correlation among core internal coolant flow channels under manufacturing and assembling

tolerances associated with core internals and the umbiguity in thermal and hydraulic parameters[22] ~ [25].

In chapter 5, general discussion on the results obtained through the present studies is presented.

1.2 Conventional design method and its technical problems

In thermal and hydraulic design of a nuclear reactor core, the operating temperature is limited by the criterion that the temperature of core components should not exceed the critical values. In an LMFBR, coolant temperature should be sufficiently below its boiling point, cladding temperature should not exceed the critical values, which provokes an unacceptable creep rate of cladding material, and fuel temperature should be lower than its melting point.

Some uncertainties due to manufacturing and assembling tolerances and experimental ambiguities are inherently included in the parameters, from which the core temperature is influenced. It is therefore necessary to take an adequate design safety margin, which takes into account the effect of all statistical deviations of uncertainties on the core temperature. In the conventional evaluation of such a safety margin [1] ~ [13], the thermomechanical correlation among fuel pins, fuel subassemblies and core internal structures, the coolant flow correlation among coolant channels and the temperature dependency of material properties are not taken into consideration in relation with the core hot spot temperature. It is assumed that the variation of the core temperature due to uncertainties can be dealt with by individual hot spot subfactors, which correspond to safety coefficients for the maximum deviation in the core temperature from the design nominal value.

Errors thus introduced in the evaluation of the core temperature neglecting the effect of the above mentioned correlations among uncertainties cause to lower the reliability level in safety performance of the core, and a conservative safety margin based on engineering judgements was to be employed in the

conventional thermal and hydraulic design. However, in order to improve the core performance and the related safety evaluation, these correlations should be taken into consideration in thermal and hydraulic design. In this section, the associated technical problems will be reviewed.

1.2.1 Roles of core thermal and hydraulic design in nuclear reactor design

In order to assure the core performance under designed thermal efficiency and neutron doubling time and to improve the core economy with respect to fuel inventory and power generating cost, design parameters should be optimized so that high power density, high coolant outlet temperature and large coolant temperature difference are obtained. Here, we define (i) structual design parameters, (ii) thermal and hydraulic parameters, and (iii) core design parameters as follows:

(i) Structual design parameters include dimensions and geometries of fuel subassemblies and core internals such as fuel pin diameter, fuel pin pitch, spacer wire diameter, wrapping pitch of spacer wires, flat to flat distance of wrapper tubes, core height, number of fuel pins in a fuel subassembly, number of fuel subassemblies in a reactor core and diameter of orificing holes in orificing devices, etc..

(ii) Thermal and hydraulic parameters include material properties such as coolant density, specific heat and thermal conductivity of coolant and core structual materials and hydraulic data such as coolant pressure loss coefficient, lateral drag coefficient of a fuel pin and coolant mixing coefficient, etc..

(iii) Core design parameters consist of structual design parameters, and thermal and hydraulic design parameters described above.

In the preliminary stage of core thermal and hydraulic design, the effect of structual design parameters on the core temperature is analyzed and the

structures of fuel subassemblies and core internals are optimized so as to attain the compact core with improved cooling efficiency, namely

(i) a fuel subassembly has features of a small fuel pin diameter, 5 ~ 7mm which corresponds to about one half of a light water reactor fuel pin and a closely spaced fuel pin bundle with pitch to diameter ratio of about 1.2 which is smaller by 20 ~ 30% than that of a light water reactor[9] ~ [13], and

(ii) the core internals include orificing devices within coolant flow channels, and high and low pressure plenums to regulate a subassembly coolant flow rate based on a heat generation rate[9] ~ [11], [13].

Once fuel subassemblies and core internals are optimized, hot spot temperatures are calculated based on a detailed heat generation distribution utilizing the related hot spot subfactors which are the safety margins for the uncertainties in core design parameters and finally various possible combinations of reactor inlet and outlet coolant temperature fulfiling the thermal and hydraulic design criteria are evaluated and usually summarized in a diagram called core permissible operation temperature bounds[10], [11].

Based on this diagram, reactor inlet and outlet coolant temperature is optimized taking into consideration the feasibility studies regarding nuclear steam supply system design with turbine steam quality, heat transfer area of intermediate heat exchangers and steam evapolators and coolant circulation pump pressure head.

A flow sheet of core thermal and hydraulic design procedures in a detailed design stage is shown in Table 1.1.

1.2.2 Method and technical problems in conventional core thermal and hydraulic design

In core thermal and hydraulic design, operating temperature is limited by the design criterion that the core temperature should not exceed the critical

Table 1.1 Thermal and hydraulic design procedures in detailed design stage

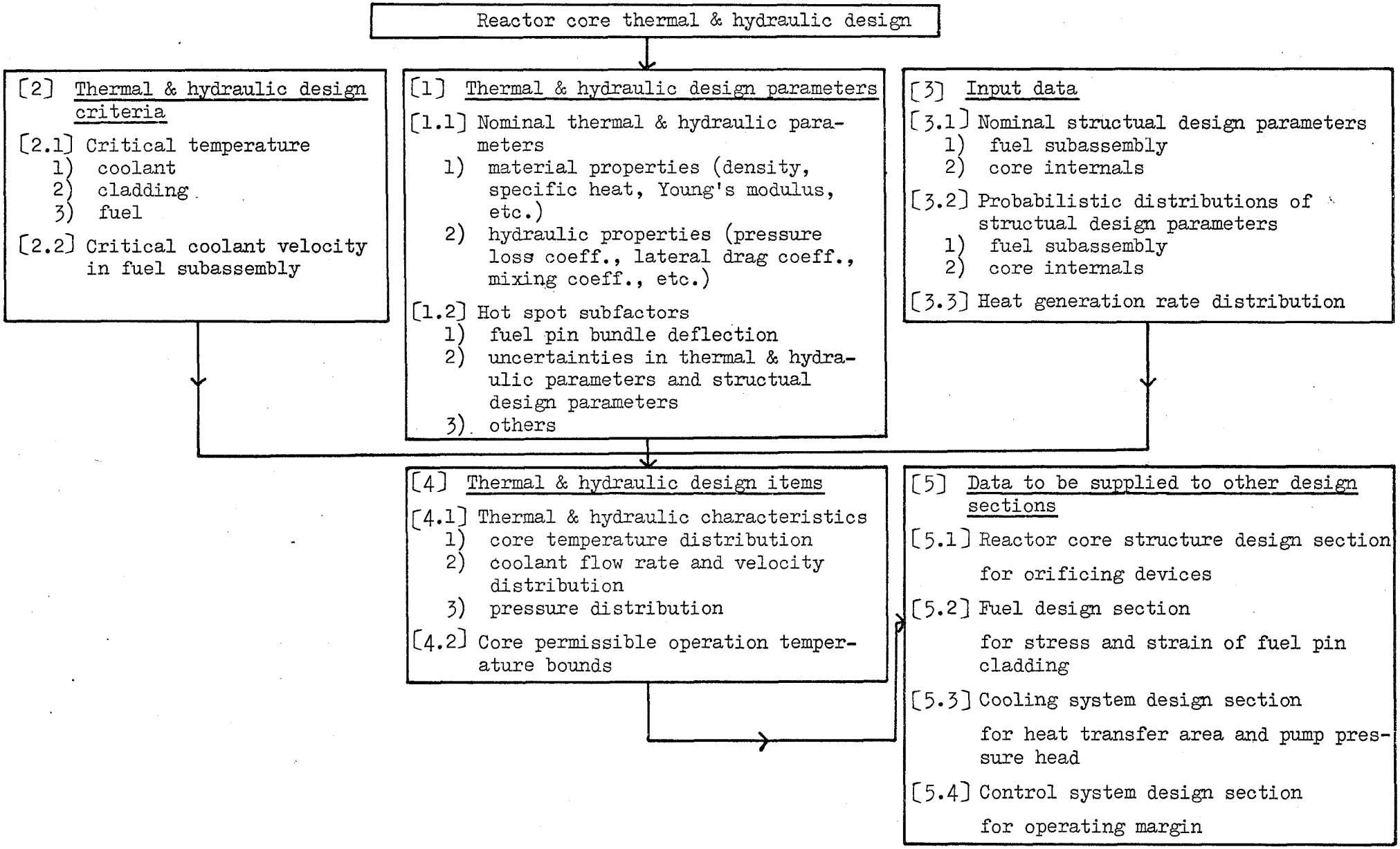

values in relation to core safety. Therefore, it is necessary to accomplish methods of detailed core temperature analyses and core temperature reliability analyses in order to assure most reasonably reactor core performance and core safety. In the following sections, we will review and discuss various design parameters related to core thermal and hydraulic design, methods of hot spot analyses and the related technical problems in the conventional core thermal and hydraulic design.

1) Technical problems in thermal and hydraulic parameters

i) Material properties

There are two kinds of material properties employed in core thermal and hydraulic design, namely,

a) the material properties, which directly affect the core temperature such as coolant density, specific heat and thermal conductivity, etc. and

b) the mechanical properties of materials which indirectly affect the core temperature such as Young's modulus and linear thermal expansion coefficient, etc..

These material properties have been experimentally investigated in sufficient cases[26)~(32)] and there may not be any further problems concerning with these material properties.

ii) Hydraulic parameters

Lateral drag coefficient of a wire-spaced fuel pin in coolant flow[16)~(18)], which corresponds to the hydrodynamical drag force normal to a fuel pin center axis, is necessary in evaluating the equilibrium configuration of a wire-spaced fuel pin bundle in a reactor operating condition, in connection to the core temperature. However, this coefficient has not been investigated yet. Its experimental investigation and the contribution of lateral drag force to the equilibrium configuration of a fuel pin bundle in a reactor operating condition will be discussed in chapter 2. The other coefficients such as

pressure loss coefficient and coolant mixing coefficient, etc. have sufficiently been investigated[33] ~ [44] and there may not be any further problems involved in these values.

2) Conventional hot spot analyses and the related technical problems

i) Conventional hot spot analyses

In order to take into consideration the ambiguity in the core temperature due to uncertainties inherent with core design parameters (structual design parameters and thermal and hydraulic parameters), the following procedures are conventionally employed. A function representing the core temperature at certain point within a core is expanped into Taylor's series with respect to all design parameters at their nominal values and the series are truncated at the first order terms, where each design parameter is considered to be an independent variable. The zeroth order term corresponds to the nominal core temperature at the specified point and the first order terms represent the contribution to the core temperature due to the deviation of each independent parameter.

We define a hot spot subfactor for the core temperature due to a design parameter F_λ to be $1 + \Delta T_1(F_\lambda)/\Delta T_0$, where ΔT_0 is the nominal temperature rise at the specified point and $\Delta T_1(F_\lambda)$ is the maximum value of the first order derivative term with respect to F_λ. In a former core design concept, hot spot subfactors due to all design parameters were cumulatively multiplied to obtain a hot spot factor for the core temperature which gave an extremely conservative design value[1]. A large safety margin under such a cumulative method of core hot spot analyses corresponds to the lowering in reactor operating temperature and consequently to the reduction in core economy.

Thus a statistical treatment of uncertainties associated with design parameters was proposed on such premises that uncertain parameters may vary independently one another and that the probabilistic variation of the core

temperature due to these parameters is of the normal distribution[2]. With such a probability concept, a hot spot factor corresponding to the confidence level of $3\sigma_v$ was investigated by H. Chelemer and L. S. Tong[3], where these hot spot analyses were conducted with respect to the nominal hottest spot within a core and hot spot subfactors were combined statistically or cumulatively, according to their natures.

However, under probabilistic aspects of core hot spot analyses, any point within a core may have the probability of being the hottest spot in a core besides the nominal hottest spot. Therefore in evaluating the safety confidence level related to core design values, the probability of core temperature exceeding the design criteria should account for probabilistic temperature variations at all points within a core[4]. In such core-wide hot spot analyses, uncertainties affecting the core temperature should be classified into two categories according to their natures, namely (i) local uncertainties, which affect the temperature at an individual spot independently within a reactor, and (ii) global or core-wide uncertainties, which affect the temperature at all spots within a zone to the same extent. Amendola[5], [6] and others[7] developed a method of evaluating the probability that there exists no hot spot in the core exceeding the core temperature design criteria taking into consideration a core-wide probabilistic temperature variation. Then, P. L. Arnsberger[8] and K. Sakai[45] proposed a method of evaluating the probability for several hot spots in a core exceeding the core temperature design criteria.

In these core-wide hot spot analyses, mathematical treatment for calculating a safety reliability level is considerably rigorous, while physical treatments on thermomechanical correlation within a core, coolant flow correlation among coolant channels and subchannels and the temperature dependency of material properties are followed after the conventional concepts.

ii) Technical problems in the conventional hot spot analyses

a) Technical problems associated with the methods of hot spot temperature evaluation

Accuracy in the evaluation of hot spot temperature should be improved by taking into consideration the following subject matters which have been neglected in the conventional hot spot temperature analyses.

(i) The thermomechanical correlation among fuel pins[14]~[21], fuel subassemblies and core internal structures[46], [47] in relation with the core hot spot temperature should be taken into consideration.

(ii) The coolant flow correlation among coolant subchannels[14]~[21] in a fuel subassembly and coolant channels[22]~[25] among in a reactor core due to uncertainties included in core design parameters in connection to the hot spot temperature should be taken into consideration.

(iii) The effect of the temperature dependency of material properties, especially thermal conductivity of fuel pellets on the core hot spot temperature, should not be neglected [48]~[50].

(iv) Because of the mutual dependency among core design parameters due to the above-mentioned correlations and temperature dependency of material properties on the core temperature, the contribution of each parameter to the core hot spot temperature is not linear.

(v) Some of the uncertainties associated with core design parameters have off-normal distributions and the resulting core hot spot temperature can not be treated as normally distributed [19]~[25], [49], [50].

b) Technical problems in the evaluation of hot spot subfactors

(i) Hot spot subfactors for the coolant temperature rise due to thermal, hydrodynamical and irradiation-induced fuel pin deflection and the resulting fuel pin gap variation play an important role in connection to thermal and hydraulic characteristics of fuel subassemblies[51], [52], especially for loosely packed wire-spaced fuel pin bundles[14]~[18], and a method of

evaluating probabilistic fuel pin gap distribution in a reactor operating condition should be developed instead of presuming a normal pin gap distribution. The related discussion will be given in chapter 2.

(ii) The effect of variation in core design parameters on the core temperature through subchannel coolant flow rate correlation related to subchannel areas and fuel pin gaps should probabilistically be evaluated where fuel pin gaps substantially show off-normal distributions due to the confinement of a fuel pin bundle within a wrapper tube [19]~[21]. Conventionally, these pin gaps have been considered normally distributed and the error due to such assumption will be discussed in chapter 3 together with the sensitivity of uncertainties to fuel pin gaps.

(iii) A method of probabilistically evaluating the effect of variation in core design parameters on the core temperature through fuel subassembly coolant flow rate correlation under constant coolant flow rate at a core inlet should be developed where uncertainties are to be classified into several categories according to their scopes of influence [22]~[25]. The related discussion will be given in chapter 4.

1.3 Objectives of the present studies and the related technical significance

In order to optimize core safety performance under the core temperature design criteria, designed thermal efficiency and neutron economy, it is necessary to accomplish a reliable method of hot spot temperature analyses. Objectives of the present studies are therefore to accomplish a method of core temperature reliability analyses taking into consideration the mutual dependency among core design parameters on the core temperature, which were not conventionally accounted for, and a method of evaluating a hot spot factor with the corresponding core confidence level within statistical variations of all uncertainties.

1.3.1 Parameters affecting the core temperature

Before coming to detailed discussions on core temperature analyses, we will select some of the sensitive parameters to the core temperature, which are shown in Table 1.2. These sensitive parameters are as follows:

Block [1] in Table 1.2; thermal and hydraulic parameters, and structual design parameters.

Block [2] in Table 1.2; fuel pin gaps and geometries of coolant subchannels within a fuel subassembly taking into consideration fuel pin deflection due to mechanical interactions among fuel pins as well as among fuel subassemblies.

Block [3] in Table 1.2; subchannel coolant flow rates within a fuel subassembly under the condition of a constant subassembly coolant flow rate as well as subassembly coolant flow rates within a reactor core under the condition of a constant coolant flow rate at a core inlet.

1.3.2 Necessity of a probabilistic method for evaluating the core temperature

Some statistical ambiguities are inherently included in core design parameters affecting the core temperature as listed in Block [1] in Table 1.2. Therefore, an evaluation of core temperature reliability level needs to be discussed in terms of probabilistic procedures. Namely, whether the core temperature satisfies the design criteria should be discussed in terms of a corresponding confidence level A and a hot spot factor H.S.F. (A), which are defined in the following section.

1.3.3 A new method of evaluating a hot spot factor

Because of the mutual dependency among core design parameters due to thermomechanical and coolant flow correlations and the dependency of material properties on the core temperature, the core hot spot temperature can not substantially be computed in terms of individual hot spot subfactors. A hot spot factor corresponding to a confidence level A should be determined taking

Table 1.2 Sensitive parameters to the core temperature

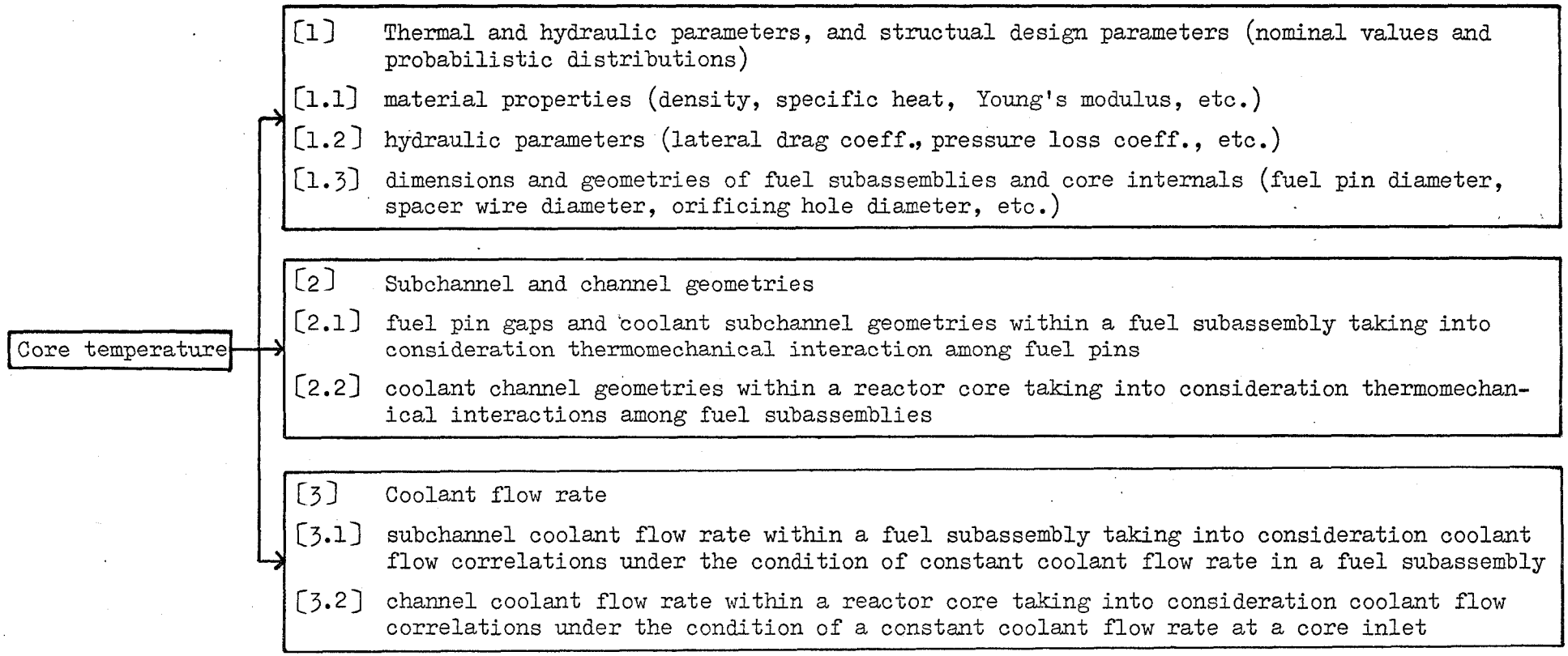

into consideration the above-mentioned mutual dependency among all parameters and their probabilistic variations.

In the present studies, a hot spot factor is expressed in terms of two subfactors being responsible for the inner-subassembly correlation and the inter-subassembly correlation for computational convenience as to be explained later on. Procedures employed in the present analyses are shown in Table 1.3 and are explained in detail as follows:

FBR thermal and hydraulics may be divided into following two parts, namely

Block [1], inner-subassembly thermal and hydraulics, and

Block [2], inter-subassembly thermal and hydraulics.

A schematic representation of reactor core internal structures in a case of a typical prototype LMFBR which correspond to Block [2] is given in Fig. 1.1, and subassembly internal structures with a fuel pin bundle of a corresponding LMFBR fuel subassembly are shown in Fig. 1.2.

Block [1] includes the following analytical procedures.

Block [1.1]: For the nominal values of thermal and hydraulic parameters and fuel subassembly structual parameters, fuel pin deflection and subchannel temperature analyses within a fuel subassembly are to be performed taking into consideration fuel pin deflection as well as subchannel coolant flow correlations under the condition of constant subassembly coolant flow rate. These subjects will be discussed in chapter 2.

Block [1.2]: Conditional probabilistic distributions of the fuel pin gap and the core temperature $P(T_\tau | w_\tau)$ within the τth fuel subassembly under consideration due to statistical variations of thermal and hydraulic parameters and structual design parameters are to be analyzed taking into consideration fuel pin deflection as well as subchannel coolant flow correlation

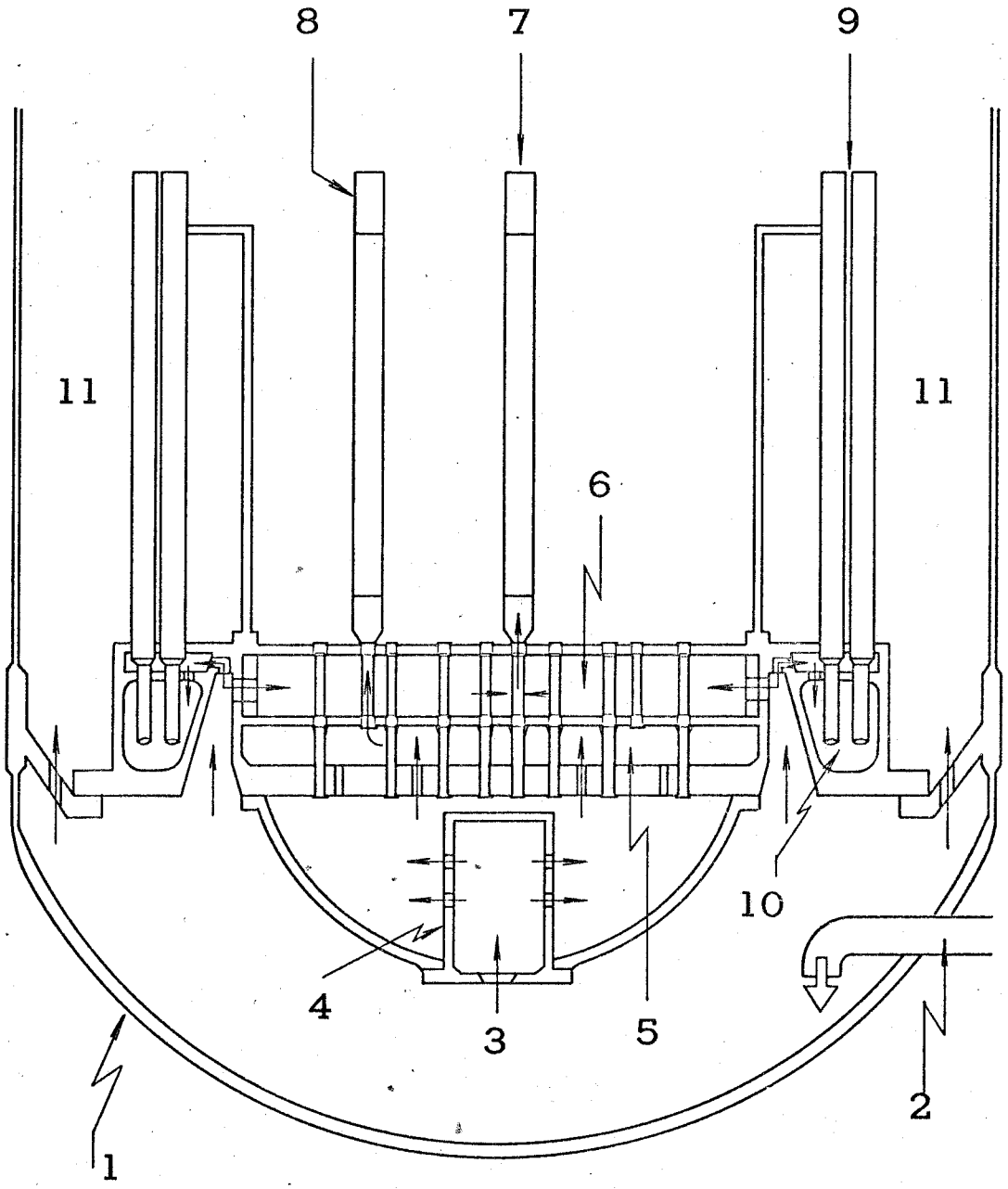

Fig. 1.1 Schematic representation of core-internal coolant flow channels. Key: 1, reactor vessel; 2, inlet nozzle; 3, inlet plenum; 4, depressurization mechanism; 5, low pressure plenum; 6, high pressure plenum; 7, core fuel subassembly; 8, blanket fuel subassembly; 9, spent fuel subassembly; 10, storage rack plenum; 11, side wall bulk plenum.

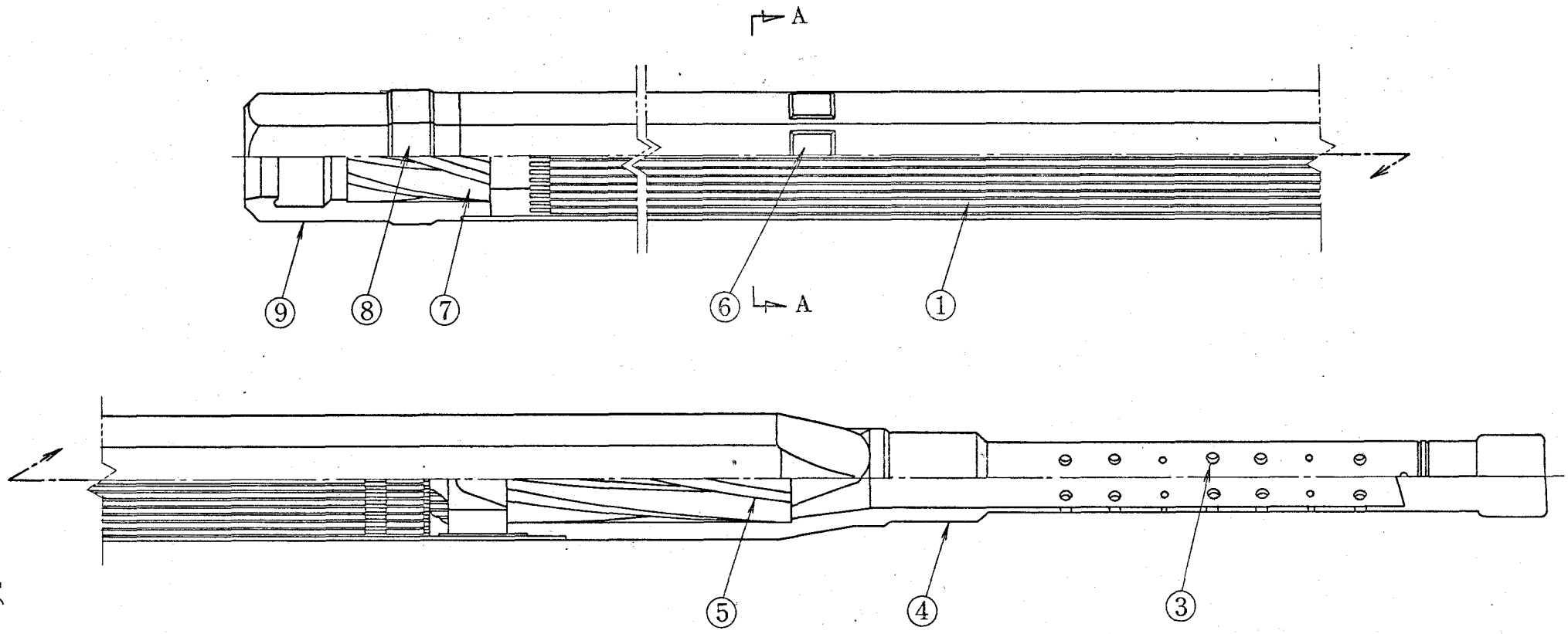

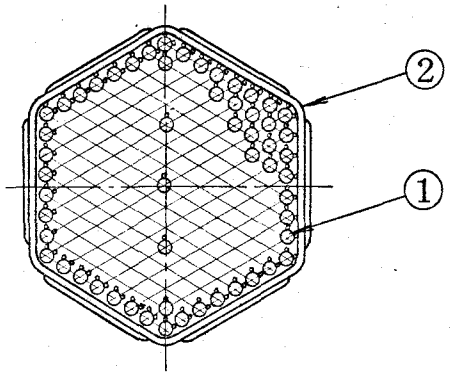

A-A cross section

① fuel pin
② wrapper tube
③ orificing hole
④ entrance nozzle
⑤ lower neutron shield
⑥ lower spacer pad
⑦ upper neutron shield
⑧ upper spacer pad
⑨ handling head

Fig. 1.2 Schematic representation of fuel subassembly internal structures

under the condition of constant subassembly coolant flow rate w_τ. These subjects will be discussed in chapter 3.

Block [2] includes the following analytical procedures.

Block [2.1]: For the nominal value of thermal and hydraulic parameters and core internal structual parameters, fuel subassembly coolant flow rate analyses and subassembly deflection analyses taking into consideration fuel subassembly coolant flow correlation as well as subassembly mechanical interactions under the constant coolant flow rate at a core inlet w^T are to be performed.

Block [2.2]: Conditional probabilistic distribution of τth fuel subassembly coolant flow rate $P(w_\tau | w^T)$ due to the statistical variations of thermal and hydraulic parameters and core structual design parameters are to be analyzed taking into consideration coolant flow correlation among coolant flow channels under the condition of constant coolant flow rate at a core inlet. The detailed discussion on Block [2.1] excluding the fuel subassembly deflection analyses and on Block [2.2] will be given in chapter 4.

Block [3] includes core thermal and hydraulics taking into consideration the mutual thermomechanical dependency of fuel pins within a fuel subasembly and of fuel subassemblies within a reactor core as follows:

Block [3.1]: Fuel subassembly deflection analyses are to be performed based on the temperature distribution within wrapper tubes based on fuel pin deflection modes within subassemblies and the effect of heat transfer through adjacent wrapper tube walls on fuel subassembly deflection.

Block [3.2]: Fuel pin deflection and subchannel temperature analyses within a fuel subassembly are to be performed based on the boundary conditions related to the fuel subassembly deflection modes.

Block [4] includes calculations on the probabilistic distribution of the core temperature based on the results in Block [1.2] and Block [2.2] as follows:

Block [4]: Based on the conditional probabilistic distribution of the core temperature within the τth fuel subassembly $P(T_\tau|w_\tau)$ under subassembly coolant flow rate w_τ and the conditional probabilistic distribution of coolant flow rate in the corresponding fuel subassembly $P(w_\tau|w^T)$ under the total coolant flow rate at a core inlet w^T, the probabilistic distribution of hot spot temperature $P(T_\tau|w^T)$ under the condition of constant coolant flow rate at a core inlet is to be computed according to addition and multiplication formulas in the theory of probability as follows:

$$P(T_\tau|w^T)=\int\cdots\int P(F_{\lambda_1})P(F_{\lambda_2})\cdots P(F_{\lambda_n})\sum_{w_\tau} P(T_\tau|w_\tau)P(w_\tau|w^T)dF_{\lambda_1}dF_{\lambda_2}\cdots dF_{\lambda_n} \tag{1-1}$$

where T_τ and w_τ are the hot spot temperature and the coolant flow rate in the τth fuel subassembly under consideration, respectively. w^T is the total coolant flow rate at a reactor core inlet and F_{λ_1}, $F_{\lambda_2}\cdots F_{\lambda_n}$ and $P(F_{\lambda_1})$, $P(F_{\lambda_2})\cdots$, $P(F_{\lambda_n})$ are uncertain parameters affecting core-wide inner-subassembly and inter-subassembly characteristics and the probabilistic distributions of the uncertain parameters, respectively.

Block [5] includes calculations on a hot spot factor H.S.F.(Λ) with confidence level Λ as follows:

Block [5]: Based on the probabilistic distribution of the hot spot core temperature $P(T_\tau|w^T)$ under w^T, the hot spot factor H.S.F. (Λ) with confidence level Λ for the τth fuel subassembly under consideration which corresponds to the probability that the core temperature does not exceed a given temperature $T_\tau^{H.S.}(\Lambda)$ is as follows:

$$\text{H.S.F.}(\Lambda) = 1 + \left\{\frac{T_\tau^{H.S.}(\Lambda) - T_\tau^N}{T_\tau^N - T_{in}}\right\}, \tag{1-2}$$

where $T_\tau^{H.S.}(\Lambda)$ is the temperature corresponding to the following definition as shown in Fig. 1.3,

$$\int_0^{T_\tau^{H.S.}(\Lambda)} P(T_\tau \mid w^T)\, dT_\tau = \Lambda \,. \qquad (1\text{-}3)$$

Usually, thermal and hydraulic design parameters are optimized that $T_\tau^{H.S.}(\Lambda)$ may be equal to the core temperature design criterion for a preassigned confidence level Λ. T_{in} corresponds to reactor inlet coolant temperature and T_τ^N corresponds to nominal temperature at the specified core point under consideration.

A method of fuel subassembly deflection analyses taking into consideration the mechanical interaction among subassemblies indicated in Block [2.1.3] has been developed[46], [47] and the analyses of thermal and hydraulic characteristics of a core taking into consideration the thermomechanical correlation listed in Block [3] turn out to be possible at present, however sample calculations shown in this paper do not include analyses corresponding to Block [2.1.3] and Block [3] in order to avoid redundant computations.

For the mutual hydrodynamical dependency of inner and inter-fuel subassembly hydraulics indicated in Block [1] and Block [2] on the core temperature through coolant flow correlation within a reactor core, the following expedient treatments are employed. Namely, the probabilistic distribution of hydraulic resistance across a fuel subassembly due to the variation in structual design parameters of a fuel subassembly is evaluated based on factory data as indicated in Block [1.2.3] and the resulting probabilistic distribution is introduced into evaluation on a probabilistic distribution of a fuel subassembly coolant flow rate indicated in Block [2.2.2]. Thus, the effect of the local variation in structual design parameters within a fuel subassembly on subassembly coolant flow rate and the core temperature is effectively taken into consideration.

The dependency of the conditional probabilistic distribution function $P(T_\tau \mid w_\tau)$ on w_τ, the deviation range of which is actually within $\pm 10\%$ to its

nominal value, is almost linear because of the week dependency of subchannel coolant flow rate ratios among subchannels and material properties through the core temperature on subassembly coolant flow rate w_τ. Based on the above-mentioned reasonings, it may be verified that the hot spot factor H.S.F.(A) corresponding to confidence level A defined by expression (1-2) may be expressed in terms of two hot spot subfactors covering core temperature variation due to inner-subassembly and inter-subassembly temperature correlations. The prime objective of the present study is to accomplish core design procedures explained in Table 1.3 to evaluate a hot spot factor of a core which corresponds to the specified confidence level taking into consideration the probabilistic contributions of design parameters with their mutual dependency to the core temperature.

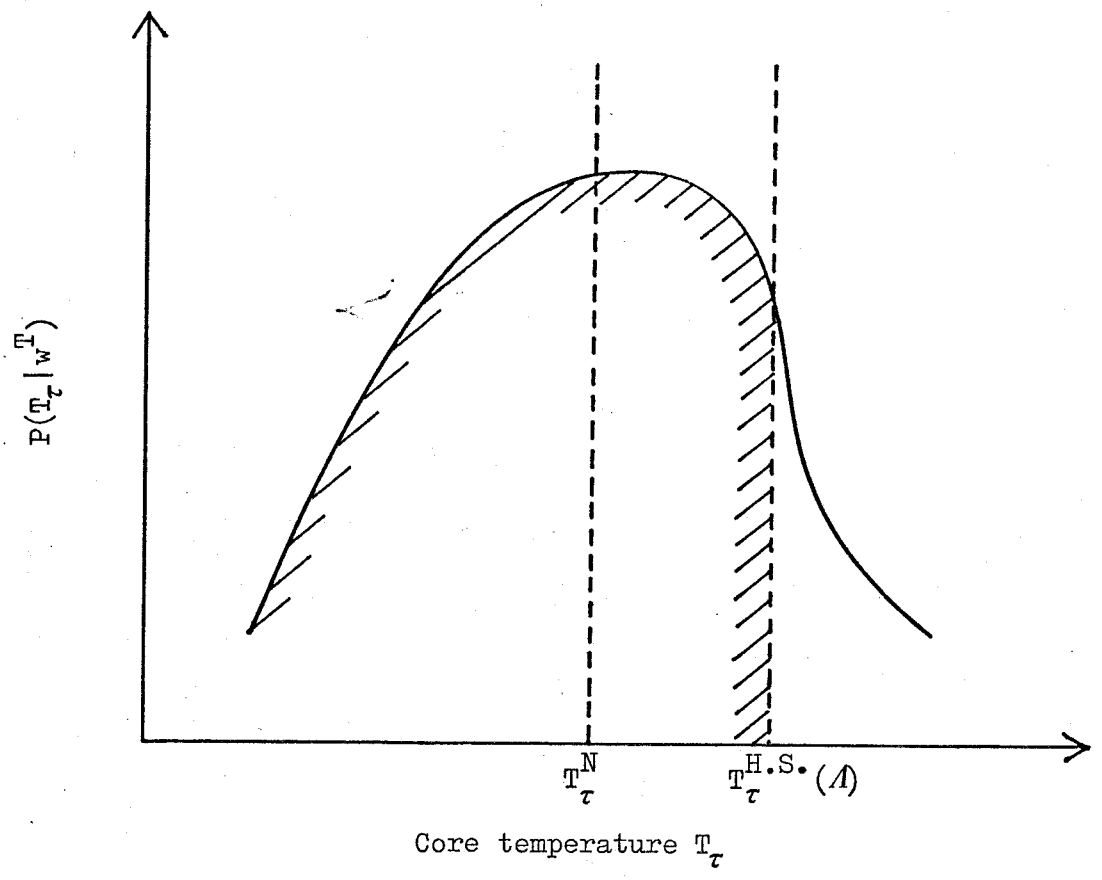

Fig. 1.3 Probabilistic distribution of the core temperature T_τ in the τth fuel subassembly.

Table 1.3 Procedures of hot spot factor analyses

Reactor thermal & hydraulics

[1] Inner-subassembly characteristics

[2] Inter-subassembly characteristics

[1.2] Evaluation of probabilistic variation in core design parameters

[1.1] Evaluation of nominal core design parameters

[2.1] Evaluation of nominal core design parameters

[2.2] Evaluation of probabilistic variation in core design parameters

[1.2.1] Probabilistic distributions of core design parameters
1) material properties
2) hydraulic parameters
3) structual design parameters

[1.2.2] Probabilistic distribution of fuel pin gaps taking into consideration fuel pin mutual interactions

[1.2.3] Probabilistic distribution of hydraulic resistance within a subassembly under constant subassembly coolant flow rate

[1.2.4] Probabilistic distribution of the core temperature under constant subassembly coolant flow rate

$P(T_\tau | w_\tau)$

[1.1.1] Nominal core design parameters
1) material properties
2) hydraulic parameters
3) structual design parameters

[1.1.2] Subchannel geometries taking into consideration fuel pin mutual interactions
1) fuel pin deflection
2) fuel pin gaps

[1.1.3] Thermal & hydraulics under constant subassembly coolant flow rate
1) core temperature distribution
2) subchannel coolant flow rate distribution
3) pressure distribution

[2.1.1] Nominal core design parameters
1) material properties
2) hydraulic parameters
3) structual design parameters

[2.1.2] Subassembly coolant flow rate taking into consideration core internal coolant channel geometries and mutual channel coolant flow correlations under constant reactor inlet coolant flow rate

[2.1.3] Subassembly deflection taking into consideration mutual subassembly interactions

[2.2.1] Probabilistic distribtions of core design parameters
1) material properties
2) hydraulic parameters
3) structual design parameters

[2.2.2] Probabilistic distribtion of subassembly coolant flow rate taking into consideration mutual channel coolant flow correlations under constant reactor inlet coolant flow rate

$P(w_\tau | w^T)$

[3] Thermal & hydraulics taking into consideration mutual thermomechanical interactions among inner-subassembly and inter-subassembly

[3.1] Subassembly deflection taking into consideration the heat transfer through wrapper tube walls and fuel pin deflection

[3.2] Fuel pin deflection and thermal & hydraulic characteristics taking into consideration subassembly deflection

[4] Probabilistic distribution taking into consideration coolant flow correlations among all channels under constant reactor inlet coolant flow rate

$$P(T_\tau | w^T) = \int \cdots \int P(F_{\lambda_1}) \cdots P(F_{\lambda_n}) \sum_{w_\tau} P(T_\tau | w_\tau) P(w_\tau | w^T) \cdot dF_{\lambda_1} \cdots dF_{\lambda_n}$$

where
$F_{\lambda_1} \cdots F_{\lambda_n}$: core-wide uncertainties affecting inner-subassembly and inter-subassembly characteristics

[5] Hot spot factor H.S.F.(Λ) with confidence level Λ

$$H.S.F.(\Lambda) = 1 + \left[\frac{T_\tau^{H.S}(\Lambda) - T_\tau^N}{T_\tau^N - T_{in}} \right]$$

Reference for Chapter 1

(1) B. W. Le Tourneau and R. E. Grimble, Engineering Hot Channel Factor for Nuclear Reactor Design, Nucl. Sci. Eng., 1 (1956) 359.

(2) P. A. Rude and A. C. Jr. Nelson, Statistical Analysis of Hot Channel Factors, Nucl. Sci. Eng., 1 (1960) 156.

(3) H. Chelemer and L. S. Tong, Engineering Hot Channel Factors for Open Lattice Cores, Nucleonics, 20 (9) (1962) 68.

(4) U. L. Businaro and G. P. Pozzi, A New Approach on Engineering Hot Channel and Hot Spot Statistical Analysis, EUR 1302 (1964).

(5) A. Amendola, A Statistical Method for Evaluation of Hot Channel Factors, EUR 3979 e (1968).

(6) A. Amendola, Advanced Statistical Hot Spot Analysis, KFK 1134-EUR 3687 (1970).

(7) F. D. Judge, A Study Concerning the Number of Effective Equally Limiting Hot Channel in a Reactor with a Cosine Power Distribution, Nucl. Sci. Eng., 31 (1968) 147.

(8) P. L. Arnsberger and M. Mazumdar, The Hot Channel Factor as Determined by the Permissible Number of Hot Channels in the Core, Nucl. Eng. Design, 47 (1972) 140.

(9) T. Inoue, F. Yoshino and A. Izumi, Consideration on Safety Margin in JOYO Thermal Design, N241 73-54, IAEA PANEL Nov. (1973).

(10) Kosoku Zoshyokuro MONJU Chyosei Sekkei (IV), PNC Report ZJ283 77-01-(A)-2, Mar. (1977) 2.1-1.

(11) Kosoku Zoshyoku Zisshoro Sekkei (II), PNC Report ZJ206 77-15, Mar. (1977) 3.2-88.

(12) M. Shaw, The Role of FFTF in the U.S. LMFBR Programme, Nucl. Eng. Int., Aug. (1972) 613.

(13) Preliminary Safety Analysis Report (Clinch River Breeder Reactor Project), Docket-50537-11, (1975).

(14) K. Sakai, Y. Okubo and H. Hishida, Preliminary Development of an Analytical Method for Evaluating Fuel Pin Deflection, Trans. of At. Energy Soc. Japan, Nov. (1975) E11.

(15) K. Sakai, Y. Okubo and H. Hishida, Development of a Computer Programme for Deflection Analysis of Wire-Wrapped Fuel Pin Bundle, PNC Report SJ206 76-17, July (1976).

(16) K. Sakai, et al., Evaluation of the Effect of Hydrodynamical Force on Fuel Pin Deflection, Trans. of At. Energy Soc. Japan, Oct. (1977) F58.

(17) K. Sakai, Y. Okubo and H. Hishida, Deflection of Wire-Spaced Fuel Pin Bundles, Trans. of A.N.S., 26 (1) (1977) 460.

(18) K. Sakai, Y. Okubo and H. Hishida, Three-Dimensional Deflection Analyses of Wire-Spaced Fuel Pin Bundles under Temperature and Hydrodynamical Force Fields with Irradiation Effects, Nucl. Eng. Design, 48 (1978) 595.

(19) K. Sakai, Y. Okubo and H. Hishida, Development of a Computational Method for Evaluating Fuel Pin Gaps in a FBR Fuel Subassembly, PNC Report SJ206 77-10, Mar. (1977).

(20) K. Sakai, Y. Okubo and H. Hishida, Preliminary Studies on a Probabilistic Distributions of Fuel Pin Gaps within a Wire-Spaced Fuel Subassembly, Trans. of At. Energy Soc. Japan, Oct. (1977) C53.

(21) K. Sakai, Y. Nakai and H. Hishida, Probabilistic Distributions of Pin Gaps within a Wire-Spaced Fuel Subassembly and Sensitivities of the Related Uncertainties to Pin Gaps, Nucl. Eng. Design, 48 (1978) 505.

(22) K. Sakai, et al., Development of a Computer Programme for Core-Internal Coolant Flow Distribution Analysis and Evaluation of Probabilistic

Coolant Flow Distribution, PNC Report SJ206 75-08, May (1975).

(23) K. Sakai, et al., An Evaluating Method of Core-Internal Coolant Flow Deviation with Correlation Among Fuel Subassemblies, Trans. of At. Energy Soc. Japan, Nov. (1975) E7.

(24) K. Sakai and H. Hishida, Probabilistic Evaluation of Core-Internal Coolant Flow Distribution, Trans. of A.N.S., 24 (1976) 337.

(25) K. Sakai and H. Hishida, Probabilistic Evaluation of Core-Internal Coolant Flow Distribution with Correlation Among Fuel Subassemblies, Nucl. Eng. Design, 44 (1977) 235.

(26) G. H. Golden, et al., Thermophysical Properties of Sodium, ANL-7323, Aug. (1967).

(27) P. Murray, Stainless Steel Cladding Development Quarterly Progress Report for the Period Ending June 30, 1970, WARD-4135-12, June (1970).

(28) R. F. Hilbert, et al., Evaluation of Material Property Correlations used in LIFE-II, GEAP-13967, June (1973).

(29) U. Asakawa, et al., Mechanical Engineering Handbook 6th ed., (1977).

(30) ASME Boiler and Pressure Vessel Code Sec III, Nuclear Power Plant Components, Division 1 Appendices, (1977) 67.

(31) R. D. Leggett, Plutonium Fuels for LMFBR - an Extrapolation, WHAN-SA-51, Oct. (1970).

(32) R. D. Leggett, et al., Linear Heat Rating for Incipient Fuel Melting in UO_2-PO_2 Fuel, Trans. of A.N.S., 15 (2) (1972) 752.

(33) W. A. Sangster, Calculation of Rod Bundle Pressure Loss, Heat Transfer Division of ASME, Dec. (1968).

(34) E. H. Novendstern, Turbulent Flow Pressure Drop Model for Fuel Rod Assemblies Utilizing a Helical Wire-Wrapped Spacer System, Nucl. Eng. Design, 22 (1972) 19.

(35) K. Rehme, Pressure Drop Correlation for Fuel Element Spacers, Nuclear Technology, 17 Jan. (1973) 15.

(36) T. Kido, Y. Fukumitsu and M. Kamiya, Fast Breeder Prototype Reactor Fuel Assembly Water Flow Test, PNC Report SJ242 73-02,Mar. (1973).

(37) T. Naganuma, M. Hayano, et al., Hydraulic Testing of a Single Nozzle Flow-Control Mechanism for Monju, PNC Report SJ201 74-05, Dec. (1973).

(38) T. Tamaoki, et al., Coolant Flow Study in a Reactor Model for a Prototype FBR, PNC Report SJ201 74-05, Dec. (1973).

(39) Y. Okamoto, M. Hishida and N. Akino, Hydraulic Performance in Rod Bundles of Fast Reactor Fuels - Pressure Drop, Vibration and Mixing Coefficient, IAEA-SM-130/15, Mar. (1970).

(40) K. Takahashi, E. Ishibashi and J. Takahashi, Mixing Test in Fuel Subassembly for Monju, PNC Report SN941 76-136, Dec. (1976).

(41) R. N. Lyon, Chem. Eng. Prog., 73 (1951) 803.

(42) O. E. Dwyer, A. I. Ch. E. Journal, 9 (2) (1963) 261.

(43) S. Aoki, Bulletin of the Tokyo Institute of Technology, 54 (1963) 63.

(44) H. Graber and M. Rieger, Experimental Study of Heat Transfer to Liquid Metals Flowing In-Line Through Tube Bundles, Euratom, Ispra (1971).

(45) Kosoku Zoshyoku Genkeiro MONJU Sekkei (II), PNC Report MP-22071 (30-PG-2026), Mar. (1972) 7-125.

(46) H. Kinjo, K. Sakai and H. Hishida, Three-Dimensional Core Deformation Analysis, Trans. of At. Energy Soc. Japan, Apr. (1977) C47.

(47) H. Hishida, et al., A Method for Three-Dimensional Analyses of Externally Constrained FBR Core under Temperature and Neutron Flux Fields with Clearance Effects at Lower Nozzle Sections, Nucl. Eng. Design, to be published (1978).

(48) H. Hishida, Effect of Temperature Dependence in Material Properties to Hot Spot Subfactors, IAEA Panel International Atomic Energy Agency,

Vienna at Karlsruhe (1973).

(49) K. Sakai, T. Koga and H. Hishida, Evaluation of Hot Spot Temperature by Monte Carlo Method, Trans. of At. Energy Soc. Japan, Oct. (1974) E22.

(50) M. Kazuyoshi and K. Inoue, A Monte Carlo Code for the Evaluation of the Thermal Design of a Nuclear Reactor Core, Nucl. Sci. Eng., 59 (1976) 161.

(51) H. Hishida, An Analytical Method of Evaluating the Effect of Rod Displacement on Circumferential Temperature and Heat Flux Distributions in Turbulent Flow Through Unbaffled Rod Bundles, Nucl. Eng. Design, 26 (1974) 408.

(52) K. Sakai, H. Hishida, et al., Circumferential Temperature Distribution on Fuel Cladding with Local Heat Transfer Depression, Trans. of At. Energy Soc. Japan, Oct. (1974) E21.

Chapter 2

Evaluation of fuel pin bundle deflection and its effect on the core temperature

2.1 Introduction

In this chapter, discussion on the inner-subassembly characteristics under nominal core design parameters described in section 1.3.3 will be given. Fuel pins in anLMFBR fuel subassembly are deflected from the nominal configuration under temperature gradient, hydrodynamical force exerted by coolant flow and thermal and irradiation induced creep and swelling. Especially in a case of a wire-spaced fuel pin bundle, which is usually packed loose to compensate for swelling of fuel pins, the deflection influences the subchannel coolant flow distribution and therefore the hot spot temperature[1] ~ [4], where the deviation in the edge flow coefficient[5], [6] from the nominal value takes a dominant role. In reactor operating condition, wire-spaced fuel pins are in contact with the adjacent pins or wrapper tube flats at variable locations with complicated deflection modes, which are governed by the equilibrium condition based on thermomechanical, hydrodynamical and irradiation effects[1] ~ [4].

In order to evaluate a hot spot factor associated with the core temperature rise in reactor core design, the equilibrium configuration of a fuel pin bundle with the corresponding subchannel coolant flow distribution should be known for fuel subassemblies in different flow zones. Some analytical methods have been published[7], [8], which may be applicable to the deflection analysis of a gridded fuel pin bundle, where the points of application of mechanical constraints and the number of constraints on a fuel pin are assumed to be previously known. However the application of those methods to a wire-spaced fuel pin bundle is considerably difficult since the points of application

of mechanical constraints due to fuel pin contact are not fixed. Further, the hydrodynamical force exerted on a deflected fuel pin is necessary to determine the equilibrium bundle configuration[1] ~ [4], the effect of which may usually be neglected for a gridded fuel pin bundle.

In this chapter, a method of evaluating the three-dimensional deflection of a wire-spaced fuel pin bundle and the corresponding deviation in hot spot subfactor is presented with boundary conditions of an arbitrarily bowed wrapper tube. Temperature gradient across a fuel subassembly, hydrodynamical force due to coolant flow and irradiation effect are taken into consideration in connection to the evaluation of deflected pin bundle configuration. The locations of fuel pin contact with adjacent fuel pins or a wrapper tube flat with or without an intervening wire spacer and the corresponding mechanical loads are consistently determined with generalized flexibility matrix based on the equilibrium conditions of a fuel pin bundle. In connection to evaluating the hydrodynamical drag force on a deflected fuel pin, experimental investigation on the drag coefficients for various types of wire-spaced fuel pins was carried out using a water loop facility simulating the hydrodynamical properties of sodium since the drag coefficient depends on the wrapping pitch and the diameter of spacer wire. A few experimental studies have ever been done for the drag coefficients for smooth tube[9], [10], however those for a wire-spaced fuel pin have not been reported yet. For calculating subchannel coolant flow rate and temperature distributions in a fuel subassembly, a lumped parameters technique similar to that employed in COBRA-IIIC[11] is iteratively coupled to the bundle deflection analysis.

2.2 Analytical formulation

2.2.1 Assumption underlying the pin bundle deflection analysis

The present fuel pin bundle deflection analysis is based on the following assumptions:

i) Non-uniform thermal expansion of a fuel pin due to circumferential temperature variation, hydrodynamical force acting on the periphery of a deflected fuel pin, thermal and irradiation induced creep and swelling, and the initial bowing of a fuel pin are the factors affecting fuel pin deflection.

ii) Mechanical behavior of a fuel pin is treated on a beam deflection model, the cross-sectional shape of which is invariant under the application of external forces at fuel pin contact points.

iii) A fuel pin is rigidly fixed at the lower end and is non-twistable. The upper end may either be free or fixed according to the design of a fuel pin bundle under consideration. In the current analysis, the upper end is kept free.

iv) Frictional force at pin contact is negligible with respect to the final pin bundle configuration.

v) A wrapper tube deflection which can be calculated with a method described in references (12) and (13) is considered as the boundary conditions for a fuel pin contact.

2.2.2 Equations governing fuel pin deflection

Under the beam deflection model, the general differential equations of elastic deflection are as follows:

$$\frac{\partial^2 u_i(z)}{\partial z^2} = -\frac{1}{E_i(z)I_i} M_{i,x}(z), \tag{2-1a}$$

$$\frac{\partial^2 v_i(z)}{\partial z^2} = -\frac{1}{E_i(z)I_i} M_{i,y}(z), \tag{2-1b}$$

where $u_i(z)$ and $v_i(z)$ are the x and the y coordinates of the central axis of the deflected fuel pin i at z. $M_{i,x}(z)$ and $M_{i,y}(z)$ are the x and the y

components of the bending moment and $E_i(z)$ is the modulus of elasticity of the fuel pin i at z respectively as illustrated in Fig. 2.1. $u_i(z)$ and $v_i(z)$ may be expressed in terms of the coordinates of the central axis of fuel pin i at $z = z_0$, i.e. $\{u_i(z_0), v_i(z_0)\}$ and its deflection x_i and y_i at z, namely

$$u_i(z) = u_i(z_0) + x_i(z), \tag{2-2a}$$

$$v_i(z) = v_i(z_0) + y_i(z). \tag{2-2b}$$

Based on the assumptions previously mentioned, bending moment $M_i(z)$ appeared in eq. (2-1) is apparently expressed as follows:

$$M_i(z) = M_i^T(z) + M_i^R(z) + M_i^H(z) + M_i^S(z) + M_i^C(z), \tag{2-3}$$

where $M_i^T(z)$, $M_i^R(z)$, $M_i^H(z)$, $M_i^S(z)$ and $M_i^C(z)$ are bending moments of the fuel pin i at z due to non-uniform circumferential temperature distribution, external loads acting at fuel pin contact points, hydrodynamical force acting on the periphery, non-uniform swelling and thermal and irradiation induced creep, respectively. $M_i^T(z)$, $M_i^S(z)$ and $M_i^C(z)$ may generally be expressed in terms of longitudinal strain $\varepsilon_i(x,y,z)$ as follows:

$$M_{i,x}^{T,S,C}(z) = \int_A x\, \varepsilon_i^{T,S,C}(x,y,z)\, E\,(T_i)\, dA, \tag{2-4a}$$

$$M_{i,y}^{T,S,C}(z) = \int_A y\, \varepsilon_i^{T,S,C}(x,y,z)\, E\,(T_i)\, dA, \tag{2-4b}$$

where integration is carried over the fuel pin cross section A,

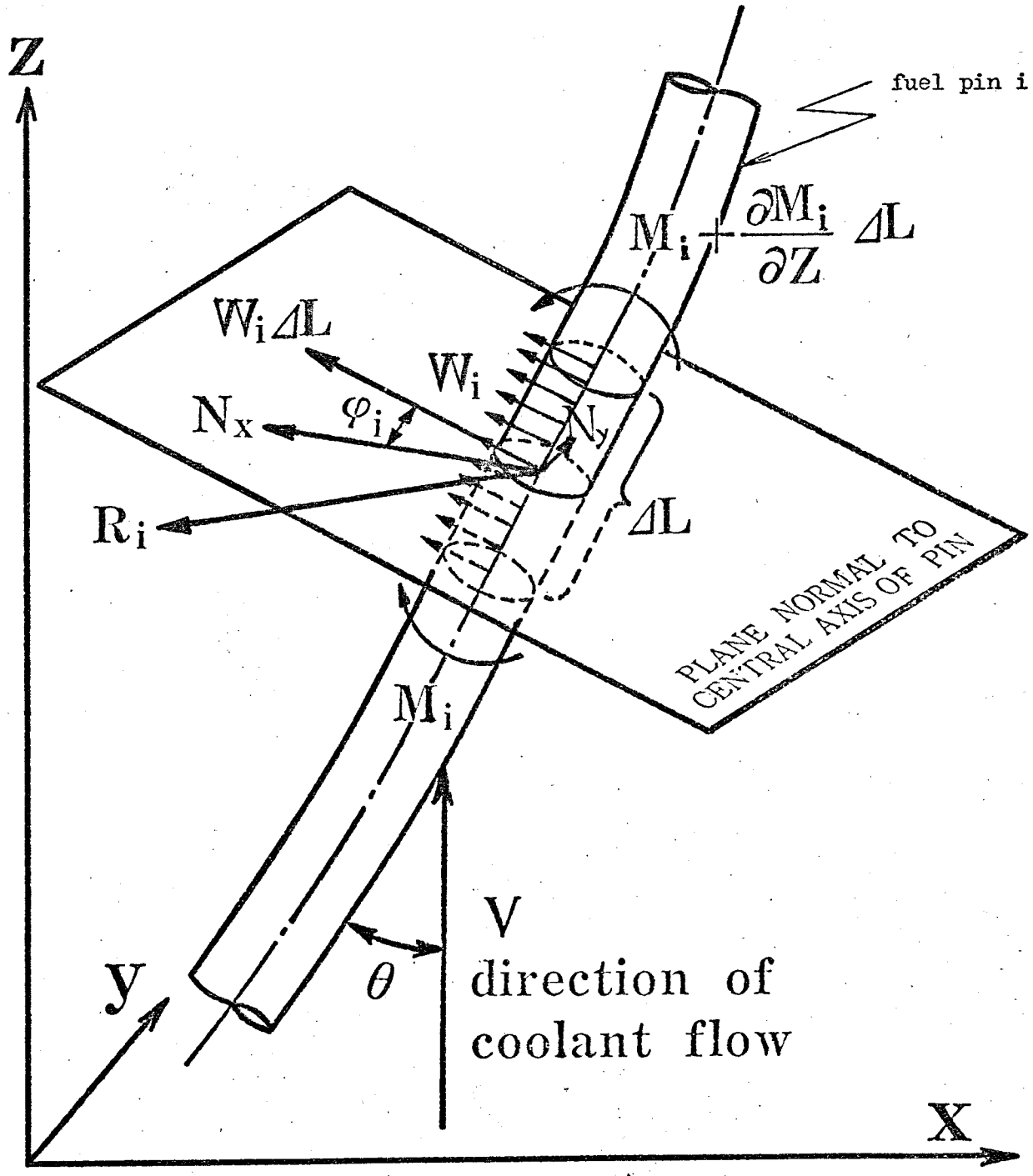

Fig. 2.1 Schematic representation of an external load and hydrodynamical force acting on a segment ΔL of a fuel pin.

R_i : load on fuel pin i due to pin contact

W_i : normal component of hydrodynamical force acting on a unit length of fuel pin i

M_i : bending moment on fuel pin i

$$\varepsilon_i^T(x,y,z) = \alpha(T_i)\, T_i(x,y,z), \tag{2-5}$$

$$\varepsilon_i^S(x,y,z) = f^S(T_i,\phi_i t), \tag{2-6a}$$

and

$$\varepsilon_i^C(x,y,z) = f^C(T_i,\phi_i t,\sigma_i). \tag{2-6b}$$

Here, $T_i(x,y,z)$ is computed using a lumped thermal-hydraulic subchannel analyses code explained in section 2.2.6 taking into consideration the feed back effects between the fuel pin bundle deflection and the fuel temperature iteratively. $\alpha(T_i)$ is the linear thermal expansion coefficient of the fuel pin i at (x,y,z) while $f^S(T_i,\phi_i t)$ and $f^C(T_i,\phi_i t,\sigma_i)$[14], [15] are strains at (x,y,z) due to swelling and creep under temperature T_i, neutron flux time $\phi_i t$ and stress σ_i. $M_i^R(z)$ and $M_i^H(z)$ are given by the following expressions:

$$M_{i,x}^R(z) = \sum_{k'=k}^{k_i^+} R_{i,k'}\, \gamma_i(z_{i,k'})(z_{i,k'}-z), \tag{2-7a}$$

$$M_{i,y}^R(z) = \sum_{k'=k}^{k_i^+} R_{i,k'}\, \delta_i(z_{i,k'})(z_{i,k'}-z), \tag{2-7b}$$

for

$$z\,\epsilon\,(z_{i,k-1} < z \leq z_{i,k}) \text{ with } k = 1,2,\cdots\cdots,\ k_i^+,$$

and

$$M_{i,x}^R(z) = 0, \tag{2-7a'}$$

$$M_{i,y}^R(z) = 0, \tag{2-7b'}$$

for

$$z > z_{i,k_i^+}$$

where $\gamma_i(z_{i,k})$ and $\delta_i(z_{i,k})$ are directional cosines defined such that if the intervening wire belongs to the fuel pin i,

$$\gamma_i(z_{i,k}) \equiv \cos\beta_j(z_{i,k}), \tag{2-8a}$$

$$\delta_i(z_{i,k}) \equiv \sin\beta_j(z_{i,k}), \tag{2-8b}$$

and if the intervening wire belongs to the fuel pin j which is in contact with the fuel pin i,

$$\gamma_i(z_{i,k}) \equiv -\cos\beta_i(z_{i,k}), \tag{2-8a'}$$

$$\delta_i(z_{i,k}) \equiv -\sin\beta_i(z_{i,k}), \tag{2-8b'}$$

as illustrated in Fig. 2.2.

$$M^H_{i,x}(z) = \int_z^{z^+} W_i(z'')\gamma^H_i(z'')(z''-z)dz'', \tag{2-9a}$$

$$M^H_{i,y}(z) = \int_z^{z^+} W_i(z'')\delta^H_i(z'')(z''-z)dz''. \tag{2-9b}$$

Here, $z_{i,k}$ is the z coordinate of the kth contact point from the lower end of the fuel pin i, $R_{i,k}$ is the load on the fuel pin i due to pin contact at $z_{i,k}$ and $W_i(z)$ is the normal component of the hydrodynamical force acting on a unit length of the fuel pin i at z. $\gamma^H_i(z)$ and $\delta^H_i(z)$ are directional cosines of $W_i(z)$ with respect to the normals N_x and N_y to the ith fuel pin at z lying on the planes normal to the axes y and x as illustrated in Fig. 2.1 and for small deflection i.e. $\theta \simeq 0$, $\gamma^H_i(z)$ and $\delta^H_i(z)$ may simply be expressed as follows:

$$\gamma_i^H(z) \simeq \cos\varphi_i(z), \tag{2-10a}$$

$$\delta_i^H(z) \simeq \sin\varphi_i(z). \tag{2-10b}$$

Experimental determination of $W_i(z)$ for a wire-spaced fuel pin will be reviewed in section 2.3.

It should be clear that $M_i^H(z)$ and $M_i^C(z)$ depend on the polar angle of the deflection and the internal stress $\sigma_i(z)$ of the fuel pin i and therefore eqs. (2-1a) and (2-1b) are nonlinear. However, in the present analyses, these equations are linearized by the usual iterative means by using the up-to-date values, which will be explained in detail in section 2.2.6.

2.2.3 Boundary conditions

In the present analyses, the following boundary conditions are employed. However, the supporting conditions for a fuel pin bundle at both ends are arbitrary and their alternation does not affect the proposed analytical procedures.

a) Pin bundle supporting conditions:

A fuel pin bundle is rigidly supported at the lower end i.e.

$$x_i(z_0) = y_i(z_0) = 0, \tag{2-11a}$$

$$\frac{dx_i(z_0)}{dz} = \frac{dy_i(z_0)}{dz} = 0, \tag{2-11b}$$

and is free at the upper end, which is already taken into consideration through deriving expressions (2-7a'), (2-7b'), (2-9a) and (2-9b).

b) Fuel pin contact conditions:

A fuel pin may contact with the adjacent fuel pins or a wrapper tube flat with or without an intervening wire spacer depending on which layer the fuel pin under consideration belongs to and which direction it is deflected to. In a case of the fuel pin i making contact with the adjacent fuel pin j

with an intervening wire spacer illustrated in Fig. 2.2, the following contact condition should be satisfied. Let $q(z)$ be a center to center distance of the fuel pins i and j at z, and $z_{i,j,\ell}$ be the z coordinate of the ℓth contact point between the fuel pins i and j from their lower ends, then

$$q^2(z_0) = \{u_i(z_0) - u_j(z_0)\}^2 + \{v_i(z_0) - v_j(z_0)\}^2, \tag{2-12}$$

and

$$\begin{aligned} q^2(z_{i,j,\ell}) &= \{u_i(z_{i,j,\ell}) - u_j(z_{i,j,\ell})\}^2 + \{v_i(z_{i,j,\ell}) - v_j(z_{i,j,\ell})\}^2 \\ &= \{r_i(z_{i,j,\ell}) + r_w\}^2 + \{r_j(z_{i,j,\ell}) + r_w\}^2 \\ &\quad -2\{r_i(z_{i,j,\ell}) + r_w\}\{r_j(z_{i,j,\ell}) + r_w\} \cdot \\ &\quad \cos\{\beta_j(z_{i,j,\ell}) - \beta_i(z_{i,j,\ell})\}, \end{aligned} \tag{2-13}$$

where $\beta_i(z_{i,j,\ell})$ and $\beta_j(z_{i,j,\ell})$ are the directional angles of the fuel pins i and j with respect to the center of intervening wire spacer at $z = z_{i,j,\ell}$, respectively as illustrated in Fig. 2.2. r_w and r_i are the radii of the intervening wire spacer and the fuel pin i. Deflection of the fuel pins i and j may be correlated to $q(z_0)$ and $q(z_{i,j,\ell})$ as follows:

$$\begin{aligned} &\{x_i(z_{i,j,\ell}) - x_j(z_{i,j,\ell})\}^2 + \{y_i(z_{i,j,\ell}) - y_j(z_{i,j,\ell})\}^2 \\ &= q^2(z_0) + q^2(z_{i,j,\ell}) - 2q(z_0)q(z_{i,j,\ell})\cos\{\lambda_i(z_{i,j,\ell}) - \lambda_i(z_0)\}, \end{aligned} \tag{2-14}$$

where $\lambda_i(z_{i,j,\ell})$ is defined such that

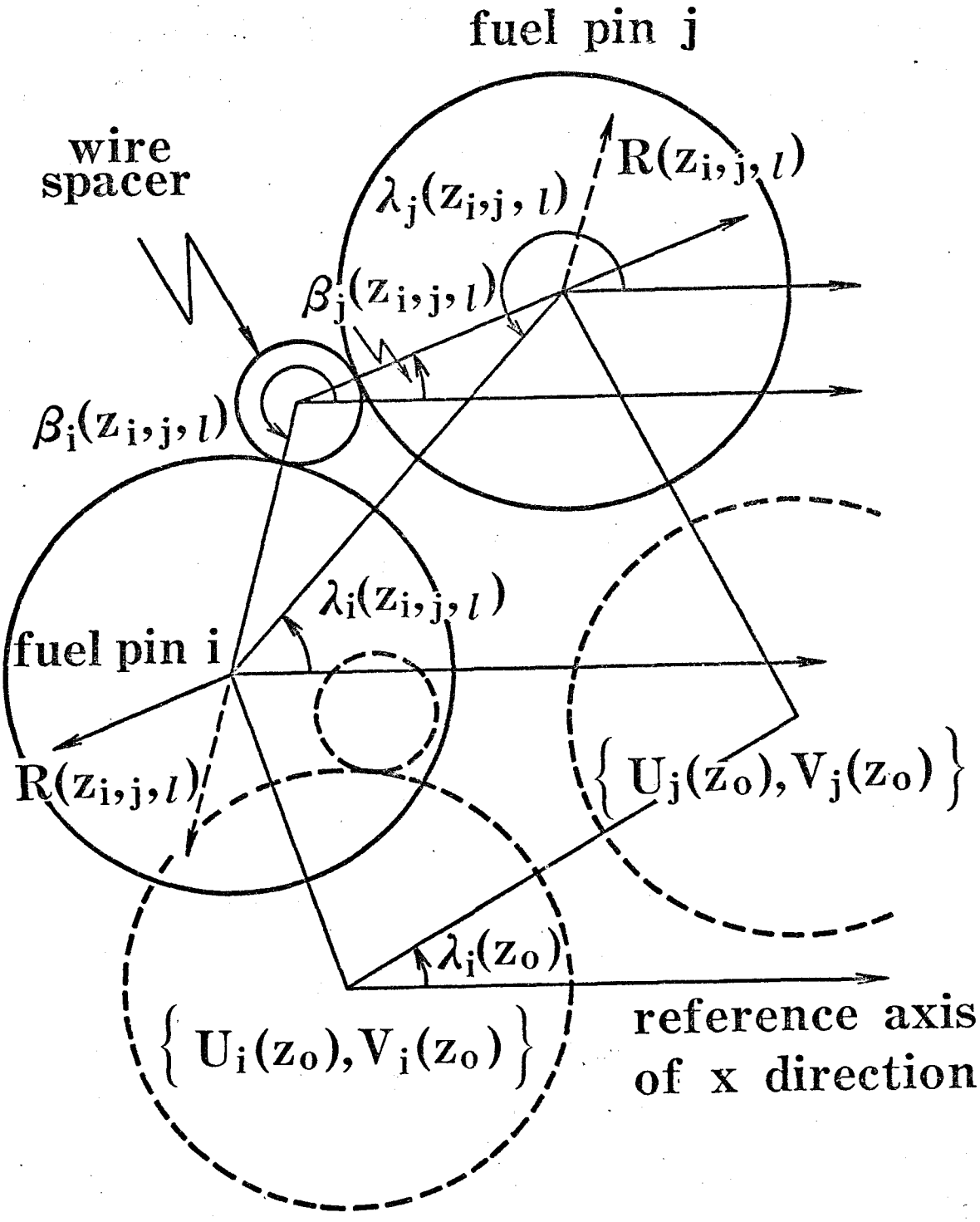

Fig. 2.2 Geometrical correlation between a pair of fuel pins in contact with an intervening wire spacer. Solid and broken arrows indicating load R correspond to fuel pin contact with the intervening wire spacer belonging to the fuel pin i and j, respectively.

$$\lambda_i(z_{i,j,\ell})$$

$$= \cos^{-1}\left[\frac{\{r_j(z_{i,j,\ell})+r_w\}\cos\beta_j(z_{i,j,\ell})-\{r_i(z_{i,j,\ell})+r_w\}\cos\beta_i(z_{i,j,\ell})}{q(z_{i,j,\ell})}\right]. \tag{2-15}$$

Substituting expressions (2-12) and (2-13) into (2-14), the following boundary condition for fuel pin contact may be derived, which is linear in deflection of the both fuel pins:

$$\{u_i(z_0) - u_j(z_0)\}\{x_i(z_{i,j,\ell}) - x_j(z_{i,j,\ell})\}$$

$$+\{v_i(z_0) - v_j(z_0)\}\{y_i(z_{i,j,\ell}) - y_j(z_{i,j,\ell})\}$$

$$= q(z_0)[q(z_{i,j,\ell})\cos\{\lambda_i(z_{i,j,\ell}) - \lambda_i(z_0)\} - q(z_0)]. \tag{2-16}$$

In expressions (2-13) and (2-15), either $\beta_i(z_{i,j,\ell})$ or $\beta_j(z_{i,j,\ell})$ is known depending on whose wire spacer is intervening. The rest is to be determined in a course of contact search as is explained in section 2.2.6.

For pin contact without an intervening wire spacer, the contact condition (2-16) is general when r_w is set to be zero in expressions (2-13) and (2-15).

In a case of the fuel pin i in contact with the inner flat of a wrapper tube, let

$$u_e(z) + a_e(z)v_e(z) + b_e(z) = 0 \tag{2-17}$$

be a general equation for the inner boundary of the hexagonal cross section of a wrapper tube at z, where $u_e(z)$ and $v_e(z)$ are x and y coordinates and

$a_e(z)$ and $b_e(z)$ are previously known constants, then the boundary condition of fuel pin contact on a wrapper tube flat at $z = z_{i,e,\ell}$ with an intervening wire spacer may be expressed as follows:

$$u_i(z_{i,e,\ell})-\{r_i(z_{i,e,\ell})+r_w\}\cos\beta_i(z_{i,e,\ell})+r_w\cos\beta_e(z_{i,e,\ell})$$

$$+ a_e(z_{i,e,\ell})[v_i(z_{i,e,\ell})-\{r_i(z_{i,e,\ell})+r_w\}\sin\beta_i(z_{i,e,\ell}) +$$

$$+ r_w\sin\beta_e(z_{i,e,\ell})]+ b_e(z_{i,e,\ell}) = 0. \qquad (2\text{-}18)$$

In the above eq. (2-17), $z_{i,e,\ell}$ is the z coordinate of the ℓth contact point between the fuel pin i and the side e of the hexagon from the lower end and $\beta_e(z)$ is the directional angle from the center of the intervening wire spacer to the inner flat of the wrapper tube in contact.

For pin to wrapper tube contact without an intervening wire spacer, the contact condition (2-18) is general when r_w is set to be zero.

2.2.4 General solution of the deflection equation

Solutions of eqs. (2-1a) and (2-1b) which satisfy the boundary conditions (2-11a) and (2-11b) may generally be written as follows:

$$x_i(z) = x_i^M(z) + x_i^R(z) + x_i^I(z), \qquad (2\text{-}19a)$$

and

$$y_i(z) = y_i^M(z) + y_i^R(z) + y_i^I(z), \qquad (2\text{-}19b)$$

where

$$x_i^M(z) \equiv -\int_0^z \int_0^{z''} \frac{\{M_{i,x}^T(z''')+M_{i,x}^H(z''')+M_{i,x}^S(z''')+M_{i,x}^C(z''')\}dz''dz'''}{E(T_i)I_i}, \qquad (2\text{-}20a)$$

$$y_i^M(z) \equiv -\int_0^z \int_0^{z''} \frac{\{M_{i,x}^T(z''')+M_{i,x}^H(z''')+M_{i,x}^S(z''')+M_{i,x}^C(z''')\}dz''dz'''}{E(T_i)I_i}, \qquad (2\text{-}20b)$$

and

$$x_i^R(z) \equiv \sum_{k'=1}^{k-1} (\tfrac{1}{3}z_{i,k'}-z)z_{i,k'}^2 \frac{\gamma_i(z_{i,k'})}{2E(\bar{T}_i)I_i} R_{i,k'}$$

$$+ \sum_{k'=k}^{k_i^+} (\tfrac{1}{3}z - z_{i,k'})z^2 \frac{\gamma_i(z_{i,k'})}{2E(\bar{T}_i)I_i} R_{i,k'}, \qquad (2\text{-}21a)$$

$$y_i^R(z) \equiv \sum_{k'=1}^{k-1} (\tfrac{1}{3}z_{i,k'}-z)z_{i,k'}^2 \frac{\delta_i(z_{i,k'})}{2E(\bar{T}_i)I_i} R_{i,k'}$$

$$+ \sum_{k'=k}^{k_i^+} (\tfrac{1}{3}z - z_{i,k'})z^2 \frac{\delta_i(z_{i,k'})}{2E(\bar{T}_i)I_i} R_{i,k'}, \qquad (2\text{-}21b)$$

for

$$z\varepsilon(z_{i,k-1} < z \leq z_{i,k}) \text{ with } k = 1, 2, \cdots\cdots, k_i^+$$

and

$$x_i^R \equiv \sum_{k'=1}^{k_i^+} (\tfrac{1}{3}z_{i,k'} - z)z_{i,k'}^2 \frac{\gamma_i(z_{i,k'})}{2E(\bar{T}_i)I_i} R_{i,k'}, \qquad (2\text{-}21c)$$

$$y_i^R \equiv \sum_{k'=1}^{k_i^+} (\tfrac{1}{3}z_{i,k'} - z)z_{i,k'}^2 \frac{\delta_i(z_{i,k'})}{2E(\bar{T}_i)I_i} R_{i,k'}, \qquad (2\text{-}21d)$$

for

$$z > z_{i,k_i^+}.$$

$x_i^I(z)$ and $y_i^I(z)$ are the x and y coordinates of the initially deflected central axis of the fuel pin i.

It should be remarked that the dependency of the modulus of elasticity of a fuel pin on temperature in the range of current interest is negligible with respect to the final fuel pin deflection in engineering point of view and in deriving $x_i^R(z)$ and $y_i^R(z)$, $E(T_i)$ is kept constant $E(\overline{T}_i)$ for simplicity. However, in a case that the dependency considerably reflects on the evaluation of fuel pin deflection, the interval of z is subdivided into a reasonable number of subintervals in which the dependency may be negligible and solutions corresponding to these subintervals should be analytically connected to give $x_i^R(z)$ and $y_i^R(z)$[12], [13].

2.2.5 Equilibrium matrix equation for fuel pin bundle deflection

So far, general solutions for three-dimensional fuel pin deflection (2-19a) and (2-19b) and contact conditions for fuel pin to fuel pin (2-16) and fuel pin onto wrapper tube flat (2-18) have been derived. Hence, once contact points in a fuel subassembly are established, the corresponding algebraic equations satisfying contact conditions may simultaneously be solved for loads and the equilibrium deflection modes of all fuel pins in a subassembly are subsequently determined. Procedures for searching contact points are to be explained in section 2.2.6.

In expressions (2-16) and (2-18) representing the geometrical correlations of a pair of fuel pins or a fuel pin and its adjacent wrapper tube flat, subscripts (i,j,ℓ) are employed while in expressions (2-19a) and (2-19b) including the elastic deflection of a fuel pin due to loads distributed along the axial direction, subscripts (i,k) are practical. However, to avoid the complexity associated with those subscripts, we define a pair number p to every pair of adjacent fuel pins and every pair of a peripheral fuel pin and its adjacent wrapper tube flat. Then, load $R_{i,k}$ may be rewritten in terms

of a pair number p as $R_{p,\ell}$, where ℓ indicates the ℓth contact point from the lower ends of the pair p as before.

Suppose a set of n^+ contact points to be started with are temporarily presumed through contact search as indicated in steps 4 and 5 of Table 2.1, then for each contact point $z = z_{p,\ell}$ substitution of solutions (2-19a) and (2-19b) with definitions (2-20a), (2-20b), (2-21a) and (2-21b) or (2-21c) and (2-21d) instead of (2-21a) and (2-21b), which represent the correlations between the x and the y displacements of fuel pin i or j and unknown loads on pin i or j due to contacts, into a contact condition (2-16) or (2-18) results in a linear algebraic equation in loads $R_{p,\ell}$ which are acting on a fuel pin pair p(i,j). For n^+ contact points in a whole fuel subassembly, n^+ simultaneous algebraic equations in $R_{p,\ell}$ corresponding to all preset contact points are derived which are expressed through straightforward rearrangement of equations in terms of an matrix equation of the following form:

$$\mathbb{M}\ \mathbb{R} = \mathbb{D} \tag{2-22}$$

where $\mathbb{R} \equiv (R_n)$ is a column vector whose element $R_n (\equiv R_{p,\ell})$ is a load corresponding to the $\left(\sum_{p'=1}^{p-1} \ell_{p'}^+ + \ell\right)$th contact point in a subassembly provided that ℓ_p^+ is the total number of loads in the pair p and $n = \sum_{p'=1}^{p-1} \ell_{p'}^+ + \ell$.

Suppose the mth row of the flexibility matrix $\mathbb{M}$ corresponds to the ℓth contact point from the lower ends of the fuel pins i and j and let $m = \sum_{p'=1}^{p-1} \ell_{p'}^+ + \ell$ and p(i,j) be the pair number associated with those fuel pins, then loads coming into the mth equilibrium equation are related to pair numbers p(i,j), $p(i,c_3)$, $p(i,c_4)$, $p(i,c_5)$, $p(i,c_6)$, $p(i,c_7)$, $p(j,c_1)$, $p(j,c_2)$, $p(j,c_3)$, $p(j,c_7)$ and $p(j,c_8)$ where c_1, c_2, ..., c_8 are the pin numbers of eight fuel pins surrounding the fuel pins i and j as shown in Fig. 2.3. In a case that one or both of the fuel pins i and j belong to the peripheral

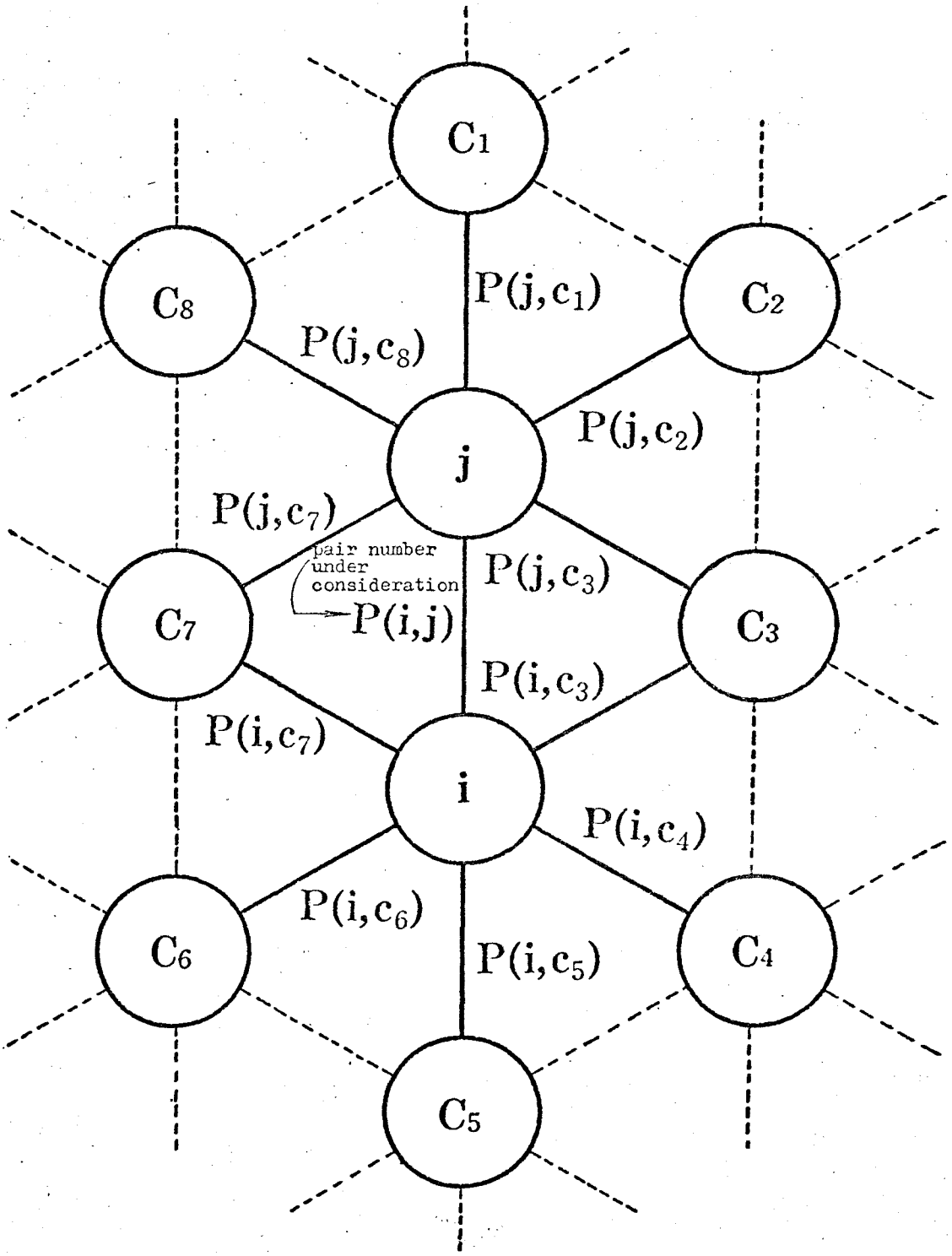

Fig. 2.3 Fuel pins and the corresponding pair numbers related to the fuel pin contact between i and j.
Solid lines and broken lines correspond to pair numbers related to the fuel pin contact between pin i and pin j, and not related to the contact under consideration, respectively.

layer of a fuel subassembly, c may stands for one of the six flats of a wrapper tube and the number of pairs involved in the equilibrium equation diminishes from the geometry of a fuel subassembly. The numerical order of the above listed eleven pair numbers differs according to which fuel pins in a subassembly i and j refer to, nevertheless all the pair numbers are fixed. Therefore to facilitate discussion, let the above listed eleven pair numbers be represented by $p(\xi_1,\eta_1)$, $p(\xi_2,\eta_2)$, $\cdots\cdots$, $p(\xi_{10},\eta_{10})$ and $p(\xi_{11},\eta_{11})$ such that

$$p(\xi_1,\eta_1) < p(\xi_2,\eta_2) < \cdots\cdots < p(\xi_{10},\eta_{10}) < p(\xi_{11},\eta_{11}), \tag{2-23}$$

then the elements $M_{m,n}$ in the mth row of the flexibility matrix $\mathbb{M}$ are expressed as follows (see Appendix 2A):

1) for $1 \le n \le \sum_{p'=1}^{p(\xi_1,\eta_1)-1} \ell^+_{p'}$,

$$M_{m,n} = 0, \tag{2-24}$$

2) for $\sum_{p'=1}^{p(\xi,\eta)-1} \ell^+_{p'} + 1 \le n \le \sum_{p'=1}^{p(\xi,\eta)-1} \ell^+_{p'} + \ell^*\{p(i,j),\ell|p(\xi,\eta)\}$,

if $(\xi,\eta) \neq (i,j)$(namely, when $\xi=i$, $\eta=c_3$, c_4, $\cdots c_7$ and when $\xi=j$, $\eta=c_1$, c_2, c_3, c_7 and c_8)

$$M_{m,n} = G_u\{p(i,j),\ell;\ p(\xi,\eta),\zeta\} + G_v\{p(i,j),\ell;\ p(\xi,\eta),\zeta\}, \tag{2-25a}$$

and if $(\xi,\eta) = (i,j)$

$$\begin{aligned} M_{m,n} = {} & G_u\{p(i,j),\ell;\ p(i,j),\zeta\} + G_v\{p(i,j),\ell;\ p(i,j),\zeta\} \\ & + G_u\{p(i,j),\ell;\ p(j,i),\zeta\} + G_v\{p(i,j),\ell;\ p(j,i),\zeta\}, \end{aligned} \tag{2-25b}$$

where

$$\zeta \equiv n - \sum_{p'=1}^{p(\xi,\eta)-1} \ell_{p'}^{+}, \tag{2-26}$$

3) for $\sum_{p'=1}^{p(\xi,\eta)-1} \ell_{p'}^{+} + \overset{*}{\ell}\{(p(i,j),\ell|p(\xi,\eta)\} + 1 \leq n \leq \sum_{p'=1}^{p(\xi,\eta)} \ell_{p'}^{+}$,

if $(\xi,\eta) \neq (i,j)$,

$$M_{m,n} = H_u\{p(i,j),\ell;\ p(\xi,\eta),\zeta\} + H_v\{p(i,j),\ell;\ p(\xi,\eta),\zeta\}, \tag{2-27a}$$

and if $(\xi,\eta) = (i,j)$,

$$\begin{aligned} M_{m,n} = {} & H_u\{p(i,j),\ell;\ p(i,j),\zeta\} + H_v\{p(i,j),\ell;\ p(i,j),\zeta\} \\ & + H_u\{p(i,j),\ell;\ p(j,i),\zeta\} + H_v\{p(i,j),\ell;\ p(j,i),\zeta\}, \end{aligned} \tag{2-27b}$$

4) for $\sum_{p'=1}^{p(\xi,\eta)} \ell_{p'}^{+} + 1 \leq n \leq \sum_{p'=1}^{p(\xi^*,\eta^*)-1} \ell_{p'}^{+}$,

$$M_{m,n} = 0 \tag{2-28}$$

for all (ξ,η) such that

$$(\xi,\eta) = (\xi_1,\eta_1),\ (\xi_2,\eta_2),\ \cdots\cdots,\ (\xi_{11},\eta_{11}), \tag{2-29}$$

where $p(\xi^*,\eta^*)$ is the next larger pair number to $p(\xi,\eta)$ in the ordered set (2-23) and if $p(\xi,\eta) = p(\xi_{11},\eta_{11})$, the interval of n in 4) should be replaced by $\sum_{p'=1}^{p(\xi_{11},\eta_{11})} \ell_{p'}^{+} + 1 \leq n$.

$\mathbb{D} \equiv (D_m)$ in eq. (2-22) is a column vector whose element D_m is

$$D_m = q(z_0)[q(z_{p(i,j),\ell}) \cos\{\lambda_i(z_{p(i,j),\ell}) - \lambda_i(z_0)\} - q(z_0)] - \{u_i(z_0) - u_j(z_0)\} \cdot$$

$$\cdot \{x_i^M(z_{p(i,j),\ell}) + x_i^I(z_{p(i,j),\ell}) - x_j^M(z_{p(i,j),\ell}) - x_j^I(z_{p(i,j),\ell})\}$$

$$- \{v_i(z_0) - v_j(z_0)\} \cdot$$

$$\cdot \{y_i^M(z_{p(i,j),\ell}) + y_i^I(z_{p(i,j),\ell}) - y_j^M(z_{p(i,j),\ell}) - y_j^I(z_{p(i,j),\ell})\} \qquad (2\text{-}30)$$

Functions $G\{p(i,j),\ell;\ p(\xi,\eta),\zeta\}$ and $H\{p(i,j),\ell;\ p(\xi,\eta),\zeta\}$ in terms of which the matrix elements $M_{m,n}$ are expressed are defined such that

$$G_u\{p(i,j),\ell;\ p(\xi,\eta),\zeta\}$$

$$\equiv \{u_i(z_0) - u_j(z_0)\}\{\tfrac{1}{3} z_{p(\xi,\eta),\zeta} - z_{p(i,j),\ell}\} \cdot$$

$$\cdot z^2_{p(\xi,\eta),\zeta} \frac{\gamma_\xi\{z_{p(\xi,\eta),\zeta}\}\Omega(\xi)}{2E\ (\overline{T}_\xi)\ I_\xi}, \qquad (2\text{-}30a)$$

$$G_v\{p(i,j),\ell;\ p(\xi,\eta),\zeta\}$$

$$\equiv \{v_i(z_0) - v_j(z_0)\}\{\tfrac{1}{3} z_{p(\xi,\eta),\zeta} - z_{p(i,j),\ell}\} \cdot$$

$$\cdot z^2_{p(\xi,\eta),\zeta} \frac{\delta_\xi\{z_{p(\xi,\eta),\zeta}\}\Omega(\xi)}{2E\ (\overline{T}_\xi)\ I_\xi}, \qquad (2\text{-}30b)$$

$$H_u\{p(i,j),\ell;\ p(\xi,\eta),\zeta\}$$

$$\equiv \{u_i(z_0) - u_j(z_0)\}\{\tfrac{1}{3} z_{p(i,j),\ell} - z_{p(\xi,\eta),\zeta}\} \cdot$$

$$\cdot z^2_{p(i,j),\ell} \frac{\gamma_\xi\{z_{p(\xi,\eta),\zeta}\}\Omega(\xi)}{2E\ (\overline{T}_\xi)\ I_\xi}, \qquad (2\text{-}31a)$$

and

$$H_v\{p(i,j),\ell;\ p(\xi,\eta),\zeta\}$$

$$\equiv\{v_i(z_0) - v_j(z_0)\}\left\{\frac{1}{3} z_{p(i,j),\ell} - z_{p(\xi,\eta),\zeta}\right\}\cdot$$

$$\cdot z^2_{p(i,j),\ell}\frac{\delta_\xi\{z_{p(\xi,\eta),\zeta}\}\,\Omega(\xi)}{2E\,(\overline{T}_\xi)\,I_\xi}, \qquad (2\text{-}31b)$$

where

$$\Omega(\xi) = 1 \quad \text{if } \xi = i,$$
$$= -1 \quad \text{if } \xi = j. \qquad (2\text{-}32)$$

$\ell^*\{p(i,j),\ell|\,p(\xi,\eta)\}$ represents the number of all loads $R_{p(\xi,\eta),\zeta}$'s associated with the pair $p(\xi,\eta)$ whose points of application $z_{p(\xi,\eta),\zeta}$'s satisfy $z_{p(\xi,\eta),\zeta} \leq z_{p(i,j),\ell}$, as shown in Fig. 2.4.

In a case that the mth row of the flexibility matrix M corresponds to the ℓth contact point from the lower end of the fuel pin in contact with the wrapper tube flat e, five pair numbers are concerned with expressing the equilibrium condition as is clear from the configuration of a fuel subassembly. From contact condition (2-18) and solutions for fuel pin deflection (2-19a) and (2-19b), the matrix elements $M_{m,n}$ are expressed as follows:

1) for $1 \leq n \leq \sum_{p'=1}^{p(\xi_1,\eta_1)-1} \ell^+_{p'}$,

$$M_{m,n} = 0, \qquad (2\text{-}33)$$

2) for $\sum_{p'=1}^{p(\xi,\eta)-1} \ell_{p'}^{+} + 1 \leq n \leq \sum_{p'=1}^{p(\xi,\eta)-1} \ell_{p'}^{+} + \ell^{*}\{p(i,e),\ell|p(\xi,\eta)\}$,

$$M_{m,n} = G_u\{p(i,e),\ell;\ p(\xi,\eta),\zeta\} + a_e(z_{p(i,e)},\ell)G_v\{p(i,e),\ell;\ p(\xi,\eta),\zeta\}, \tag{2-34}$$

3) for $\sum_{p'=1}^{p(\xi,\eta)-1} \ell_{p'}^{+} + \ell^{*}\{p(i,e),\ell|p(\xi,\eta)\} + 1 \leq n \leq \sum_{p'=1}^{p(\xi,\eta)} \ell_{p'}^{+}$,

$$M_{m,n} = H_u\{p(i,e),\ell;\ p(\xi,\eta)\zeta\} + a_e(z_{p(i,e)},\ell)H_v\{p(i,e),\ell;\ p(\xi,\eta),\zeta\}, \tag{2-35}$$

4) for $\sum_{p'=1}^{p(\xi,\eta)} \ell_{p'}^{+} + 1 \leq n \leq \sum_{p'=1}^{p(\xi^{*},\eta^{*})-1} \ell_{p'}^{+}$,

$$M_{m,n} = 0 \tag{2-36}$$

for all (ξ,η) such that

$$(\xi,\eta) = (\xi_1,\eta_1),\ (\xi_2,\eta_2),\cdots\cdots,\ (\xi_5,\eta_5), \tag{2-37}$$

where $p(\xi^{*},\eta^{*})$ is the next larger pair number to $p(\xi,\eta)$ in the ordered set (2-35) and if $p(\xi,\eta) = p(\xi_5,\eta_5)$, the interval of n in 4) should be replaced by $\sum_{p'=1}^{p(\xi_5,\eta_5)} \ell_{p'}^{+} + 1 \leq n$.

The element D_m for this case is

$$D_m = -u_i(z_0) - x_i^M(z_{p(i,e),\ell}) - x_i^I(z_{p(i,e),\ell})$$
$$+ \{r_i(z_{p(i,e),\ell}) + r_w\} \cos\beta_i(z_{p(i,e),\ell}) - r_w \cos\beta_e(z_{p(i,e),\ell})$$
$$+ a_e(z_{p(i,e),\ell})[-v_i(z_0) - y_i^M(z_{p(i,e),\ell}) - y_i^I(z_{p(i,e),\ell})$$
$$+ \{r_i(z_{p(i,e),\ell}) + r_w\}\sin\beta_i(z_{p(i,e),\ell}) - r_w \sin\beta_e(z_{p(i,e),\ell})]$$
$$- b_e(z_{p(i,e),\ell}). \qquad (2\text{-}38)$$

Once, matrix elements $M_{m,n}$ and column vector D_m are obtained, eq. (2-22) is analytically solved and the equilibrium defection modes of all the fuel pins in a subassembly under operating condition may be found.

If any of the preset contact points are not realistic or any actual contact points are missing in the preset contact points, we have negative loads as solutions of eq. (2-22) or the resulting deflected configurations of a pair of fuel pins intersect each other. Then a set of contact points are corrected based on the up-to-date fuel pin bundle configuration and the computations are to be restarted, since the external boundary conditions for a fuel pin bundle associated with wrapper tube walls may restrain the freedom of fuel pin displacement. In a case that a row of fuel pins are bridged by wrapper tube walls from the both sides, the order of matrix $(M_{m,n})$ in eq. (2-22) is to be reduced by eliminating a contact condition. In an actual fuel pin bundle, fuel pins are usually packed loose to compensate thermal expansion and irradiation-induced swelling of pins and wire-spacers are wrapped in the same phase, linear and circumferential bridgings of fuel pins hardly occur.

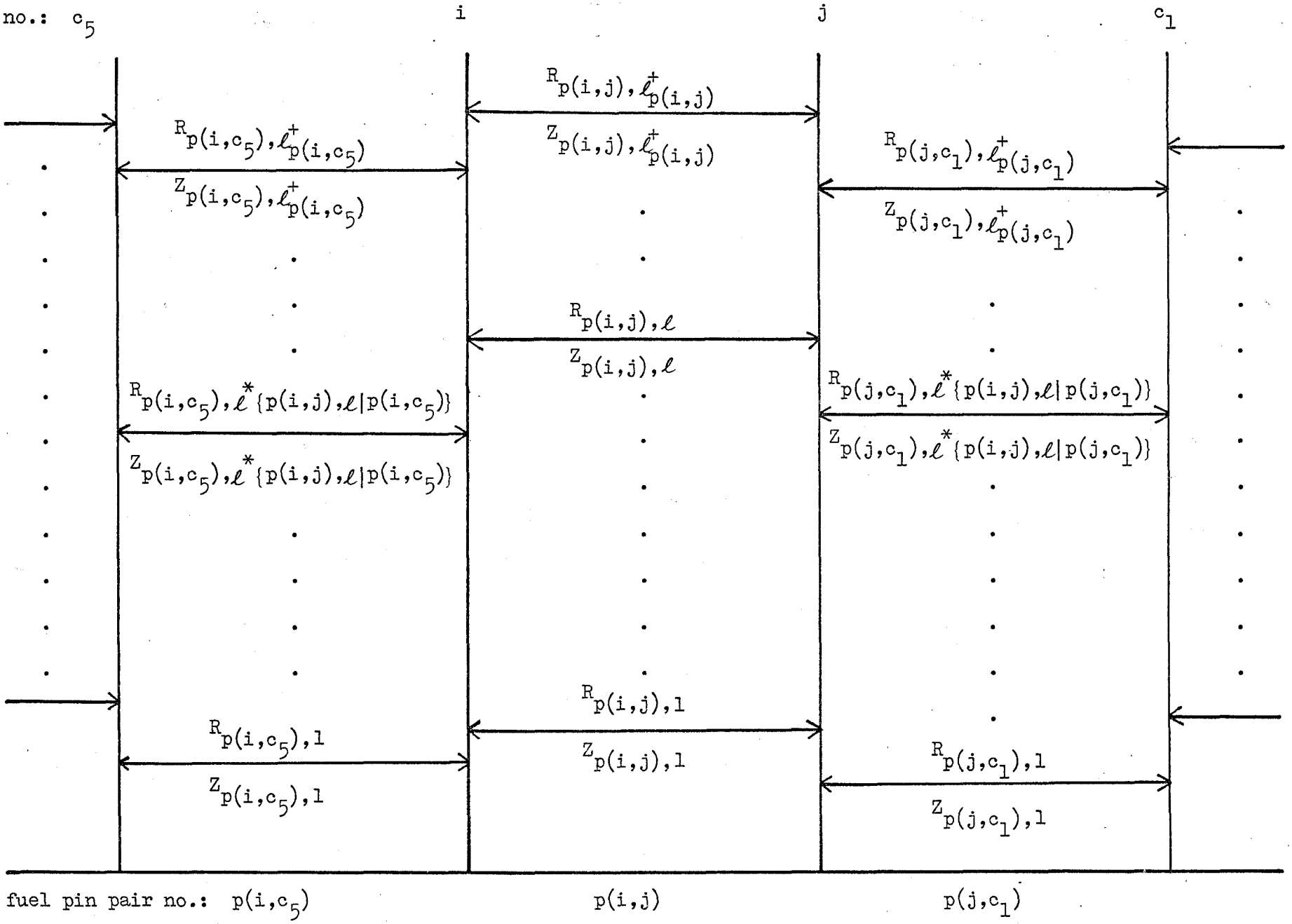

Fig. 2.4 Contact load $R_{p,\zeta}$ and contact location $Z_{p,\zeta}$ among fuel pins c_5, i, j and c_1 illustrated in Fig. 2.3

2.2.6 Subchannel analysis method in a fuel subassembly

In calculating subchannel coolant flow rates and temperature distributions in a fuel subassembly, a computer code MIX-II based on a lamped parameters technique similar to that employed in COBRA-IIIC[11] is iteratively coupled to bundle deflection analyses. This lamped parameters method considers a fuel pin bundle to be an interconnected set of parallel flow subchannels defined by fuel pin walls and the narrow gaps among fuel pins. The conservation equations of mass, energy and momentum are solved numerically by using a finite difference method under the boundary condition of uniform pressure at the bundle outlet, and the initial conditions of subassembly coolant flow rate, temperature and pressure distributions of subchannels at the bundle inlet. Consequently, coolant flow rate and coolant temperature in the subchannels of a fuel pin bundle as well as cladding and fuel temperature are determined under the assumption of uniform heat flux.

One of the important experimental parameters in the subchannel analysis method is turbulent mixing coefficient ε_H for which the following best fit of sodium experimental data for a prototype LMFBR fuel subassembly[16] was derived by author, et al.,

$$\varepsilon_H = 0.2\, \nu_v\, Re^{0.8} \qquad (2\text{-}39)$$

where ν_v is kinematic viscosity and Re is Reynolds number of sodium coolant.

2.2.7 Computational scheme

A computer program MULTIBOW-3D which computes the three-dimensional equilibrium fuel pin bundle configuration under operating condition, the magnitudes and the points of application of constraint forces due to pin contact and the subchannel coolant temperature and flow velocity distributions as well as the hot channel factor for a given fuel subassembly has been

completed based on hitherto developed analytical procedures. The brief computational scheme is explained in Table 2.1.

2.3 Experimental investigation on lateral drag coefficients of a fuel pin

2.3.1 Introduction

In connection to evaluating the hydrodynamical drag force on a deflected fuel pin which is necessary to determine a fuel pin bundle equilibrium configuration in a reactor operating condition, experimental investigation on lateral drag coefficients for several different types of wire-spaced fuel pins was carried out using a water loop facility. A few experimental studies have been done on this subject for a smooth tube[9], [10], however those for a wire-wrapped fuel pin have not been reported yet.

2.3.2 Experimental facilities and methods

1) Facilities

Experiments were performed using a 270 m^3/h water loop, the flow diagram and the side view of which are shown in Fig. 2.5 and Fig. 2.6, respectively. The test section was designed so that the angle of a test pin to the flow direction could continuously be varied. Three windows with reinforced glass covering were provided in the test section to allow visual observation at a test pin during test operation. Side view of the test section and its schematic representation are shown in Fig. 2.7 and Fig. 2.8, respectively. Flow straightners were placed in the upper stream of the test section in order to eliminate the secondary flow. Incoming flow was regulated at an arbitrary rate (50 $m^3/h \sim$ 270 m^3/h) through a valve V-4 in Fig. 2.5.

2) Test pins

Test pins employed in the present experimental investigation were of equivalent quality to prototype FBR fuel pins currently under design studies. In the test section, a test pin was clamped at the upstream end with the down stream end free and was set at an oblique angle varying $3° \sim 7°$ to the flow

Table 2.1 Flow diagram illustrating brief computational scheme of MULTIBOW-3D.

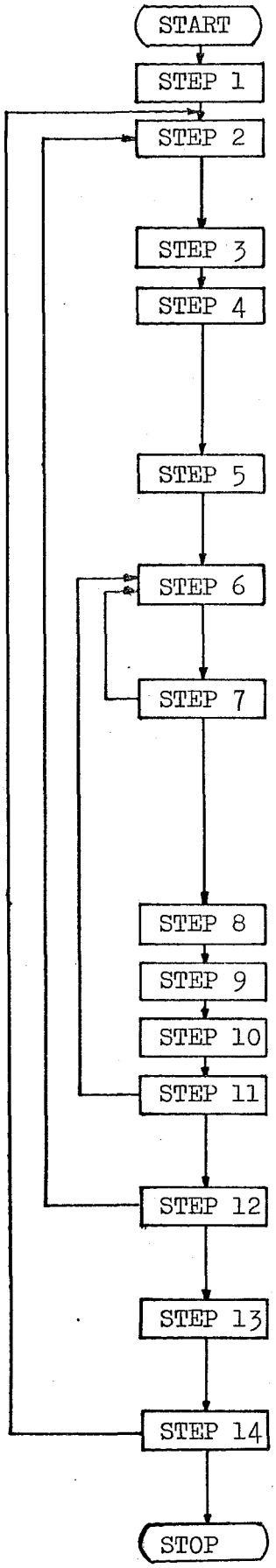

Set nominal parameters.

Compute thermal and hydraulic characteristics of each subchannel based on the up-to-date data.

Compute $\{x_i^M(z),\ y_i^M(z)\}$ for each fuel pin.

Define depressed free deflection $\{[x_i^M(z)],[y_i^M(z)]\}$ such that for $N_0 > 1$ ($x_i^M = x_i^{T+H+S+C}$, $y_i^M = y_i^{T+H+S+C}$) $[x_i^M(z)] \equiv x_i^M(z)/N_0$, $[y_i^M(z)] \equiv y_i^M(z)/N_0$.

Search temporary sets of contact points $z_{p(i,j),\ell}$ and either $\beta_i(z_{p(i,j),\ell})$ or $\beta_j(z_{p(i,j),\ell})$ using $\{[x_i^M(z)],[y_i^M(z)]\}$.

Compute matrix elements $M_{m,n}$ and D_m based on the up-to-date contact points, β's and $\{x_i^M(z),\ y_i^M(z)\}$.

Solve $\mathbb{M}\mathbb{R} = \mathbb{D}$ for R_n.

If R_n is negative, the corresponding contact point is eliminated and go to Step 6. If all R_n's are positive, go to Step 8.

Compute $\{x_i(z),\ y_i(z)\}$ based on (R_n) and $\{x_i^M(z),\ y_i^M(z)\}$.

Search new contact points based on $\{x_i(z),\ y_i(z)\}$.

Adjust sets of contact points and β's.

Go to Step 6 if contact points set is not converged, otherwise to Step 12.

Go to Step 2 if fuel pin configuration is not converged, otherwise to Step 13.

Write final pin bundle configuration, loads at contact points and subchannel temperature characteristics.

Proceed to the next time step. If the final time step is reached, stop the computation.

direction. The diameter of wrapping wire was 1.0 ~ 1.3 mm and the wrapping pitch was 200 ~ 306 mm. Two kinds of test pins with and without dummy pellets were brought into experiments. Dimensions and a side view of the test pins are shown in Fig. 2.9 and Fig. 2.10, respectively.

3) Instrumentations

Deflection of a test pin due to the lateral drag force was measured by an optical profilo-meter through the glass windows in the test section and by means of five strain gauges mounted on the outer surface of a test pin. An optical profilo-meter consists of a T.V. monitoring camera with a special 300 mm telescopic lenz and a remote focus control system, a screen control box, and a videomonitor to record and repeat the screens. A side view of a T.V. monitoring camera and an optical profilo-meter are shown in Fig. 2.11 and Fig. 2.12, respectively. On-line recording of the deflection data was performed by a videomonitor connected to the optical profilo-meter and strains due to pin deflection at five axial locations on a test pin were recorded simultaneously by a data loger.

4) Test procedures

Before hydraulic tests, the moment of inertia of test pins was investigated. At the beginning of each test, the position of a test pin under the zero-flow rate condition was adjusted so that the effect of buoyancy and gravity on the displacement of a test pin could be identified and eliminated. Setting the axis of a test pin at several oblique angles to the flow direction, magnitudes of displacement and strain were measured with an optical profilometer and strain gauges for various flow rates.

2.3.3 Data analyses and results

1) Investigation on moment of inertia

To evaluate the effect of a wrapping wire and dummy fuel pellets on the stiffness of a test pin, moments of inertia of several different types of

wire-wrapped test pins were investigated by bending tests. The results are shown in Fig. 2.13 for various types of test pins. From these results, wrapping wires and dummy fuel pellets hardly influence the effective moment of inertia for a small deflection range of fuel pins in a reactor operating condition. The value of moment of inertia shows good agreement with a theoretically predicted value of 39.35 mm^4. The accuracy of these experimental results was estimated to be of $\pm$ 5 % based on the fabrication tolerances of the test pins and the error inherent in the measurement of test pin displacement and external loads.

2) Investigation on lateral drag coefficients

Forces acting on a single rod set obliquely to a stream of fluid were discussed by Taylor[9]. For a rough cylinder with the roughness consisting of thin disks and plates, he proposed the following expression

$$W = \frac{1}{2g} \rho d V^2 \, C_d \, \sin^2\theta, \qquad (2\text{-}40)$$

where W represents the normal component of force acting on a unit length of a cylinder, θ is an oblique angle of a cylinder with respect to the flow direction and d, ρ and V are the diameter of the cylinder, the density and the velosity of the fluid, respectively and C_d is a drag coefficient. A wire-wrapped fuel pin has a strong resemblance to a cylinder with roughness of thin disks and plates. Thus, expression (2-40) was employed for the current data analyses.

Analytical model for pin deflection due to hydrodynamical force in axial coolant flow is shown in Fig. 2.14, where G_b and G_g are buoyancy and gravity acting on a unit length of a test pin, respectively. Then, the sum of the normal component of forces $\Phi(z')$ acting on a unit length of a test pin at an axial location z' is expressed as follows:

$$\Phi(z') = \frac{1}{2g}\rho d V^2 C_d \sin^2\theta' + (G_b - G_g)\sin\theta', \qquad (2\text{-}41)$$

where θ' is the angle between the coolant flow direction and the tangential direction of a test pin at an axial location z'. Since the oblique angle θ set at the upstream end is small and the deflection of a test pin $\Delta(z')$ from its zero-flow position is considerably small, θ' is nearly equal to θ and $\Phi(z')$ may be treated uniform over a whole length of a test pin. Then, bending moment M(z') and the deflection $\Delta(z')$ at z' are as follows:

$$M(z') = \int_{z'}^{z'^+} \Phi(z')(z'' - z')\, dz'' \qquad (2\text{-}42a)$$

$$\cong \Phi_0 \{\frac{1}{2}(z'^+)^2 - z'^+z' + \frac{1}{2}z'^2\}, \qquad (2\text{-}42b)$$

$$\Delta(z') \cong -\frac{\Phi_0}{EI}\{\frac{1}{4}(z'^+)^2 z'^2 - \frac{1}{6}z'^+z'^3 + \frac{1}{24}z'^4\}, \qquad (2\text{-}43)$$

where Φ_0 corresponds to expression (2-41) with θ' replaced by θ. Based on the measured displacement $\Psi'(z')$ due to buoyancy and gravity at zero-flow condition and the measured displacement $\Psi(z')$ due to the total force $\Phi(z')$ in flowing fluid, drag coefficient C_d was calculated by the following expression according to expressions (2-41) and (2-43):

$$C_d = \left(\frac{2EIg}{d\rho V^2 \sin^2\theta}\right) \frac{[\Psi(z') - \Psi'(z')]}{\{\frac{1}{4}(z'^+)^2 z'^2 - \frac{1}{6}z'^+ z'^3 + \frac{1}{24}z'^4\}}. \qquad (2\text{-}44)$$

Drag coefficient C_d was hardly dependent upon the oblique angle θ for the range of $3° \sim 7°$ in the experiments. The results are shown for several different types of wire-wrapped test pins in Fig. 2.15 where types of the test pins are common in Figures 2.13 and 2.15. C_d gradually increases due to friction force as the velocity of fluid flow decreases and is almost constant at high

velosity, which shows the similar trend exhibited in fig. 1 of reference (9) for smooth tubes. Value of C_d for the test pins without wrapping wire is about 1.0 for the velosity range of 5 m/s ~ 6 m/s which corresponds to the reactor operating condition for a prototype LMFBR and values of C_d for the wire-wrapped test pins are larger by 20 % ~ 50 % than those for the test pins without wrapping wire.

Experimental error was due to material properties of fluid, dimensions of test pins, and inaccuracy in measurements of displacement and oblique angle of a test pin and fluid velosity. These factors connected to experimental error were treated statistically or cummulatively according to their natures, and the resulting inaccuracy of drag coefficient C_d obtained through present experiments was estimated to be of $\pm$ 18 %.

2.4 Numerical results and discussion

Several cases of sample calculation have been performed using MULTIBOW-3D code to verify the effects of 1) hydrodynamical force exerted on fuel pin by coolant, 2) bowing of a wrapper tube and 3) swelling and creep of a fuel subassembly on pin bundle deflection as well as the deviation in engineering hot channel factor, and to demonstrate the applicability of MULTIBOW-3D to a prototype LMFBR fuel subassembly. Parameters employed in sample calculations are listed in Table 2.2. A solid line and a broken line appeared in Figs. 2. 16, 18, 19 and 20 indicate the central axes of a fuel pin in deflected and nominal configurations, respectively. A long arrow corresponds to a contact point between a pair of adjacent fuel pins in the displayed plane, while a short arrow corresponds to a contact point between a fuel pin displayed and an adjacent fuel pin not in the displayed plane. The feed back effects between the fuel pin bundle deflection and the fuel thermal-hydraulic behavior are considered in these analyses.

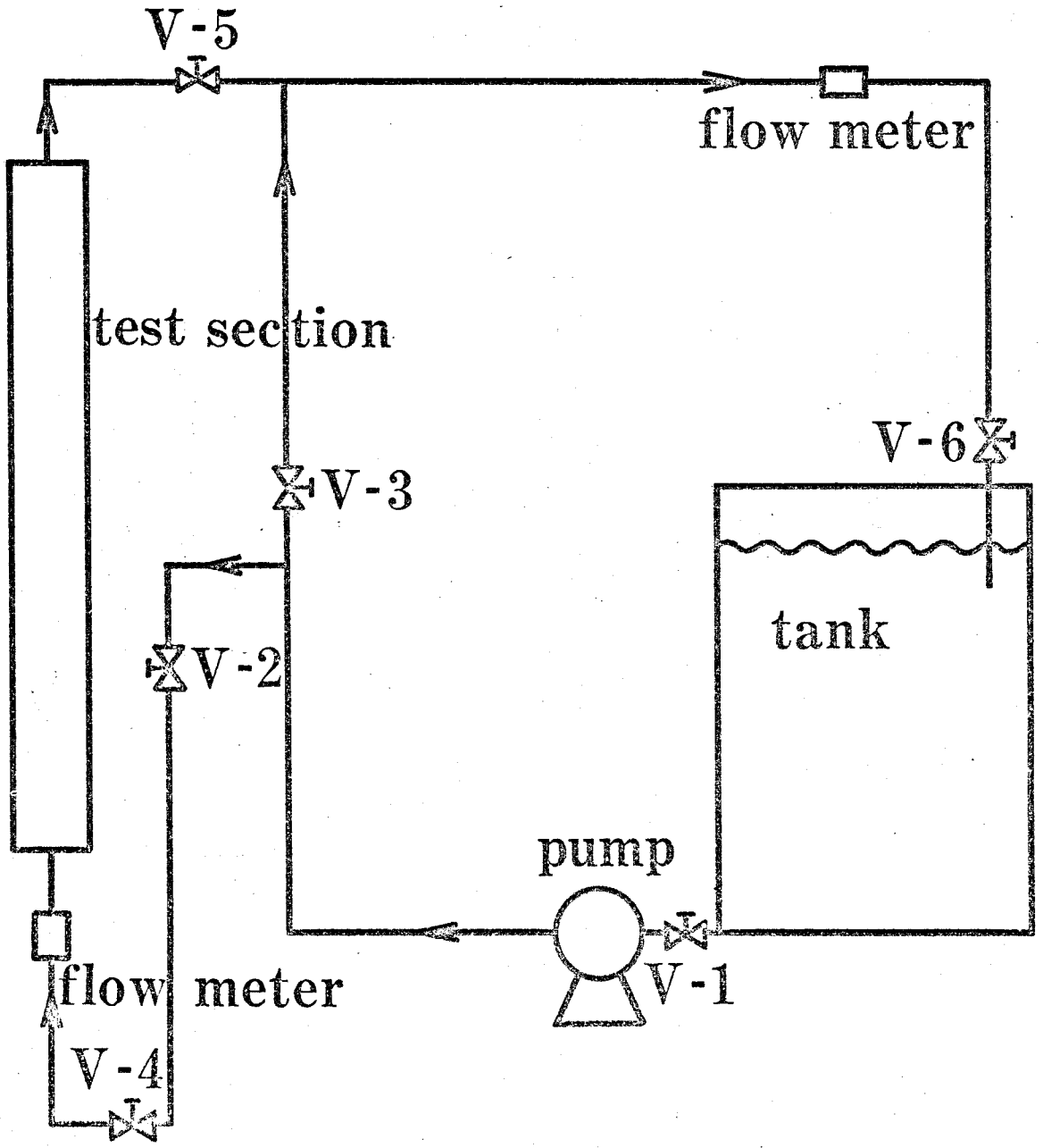

Fig. 2.5 Flow diagram of the test loop.

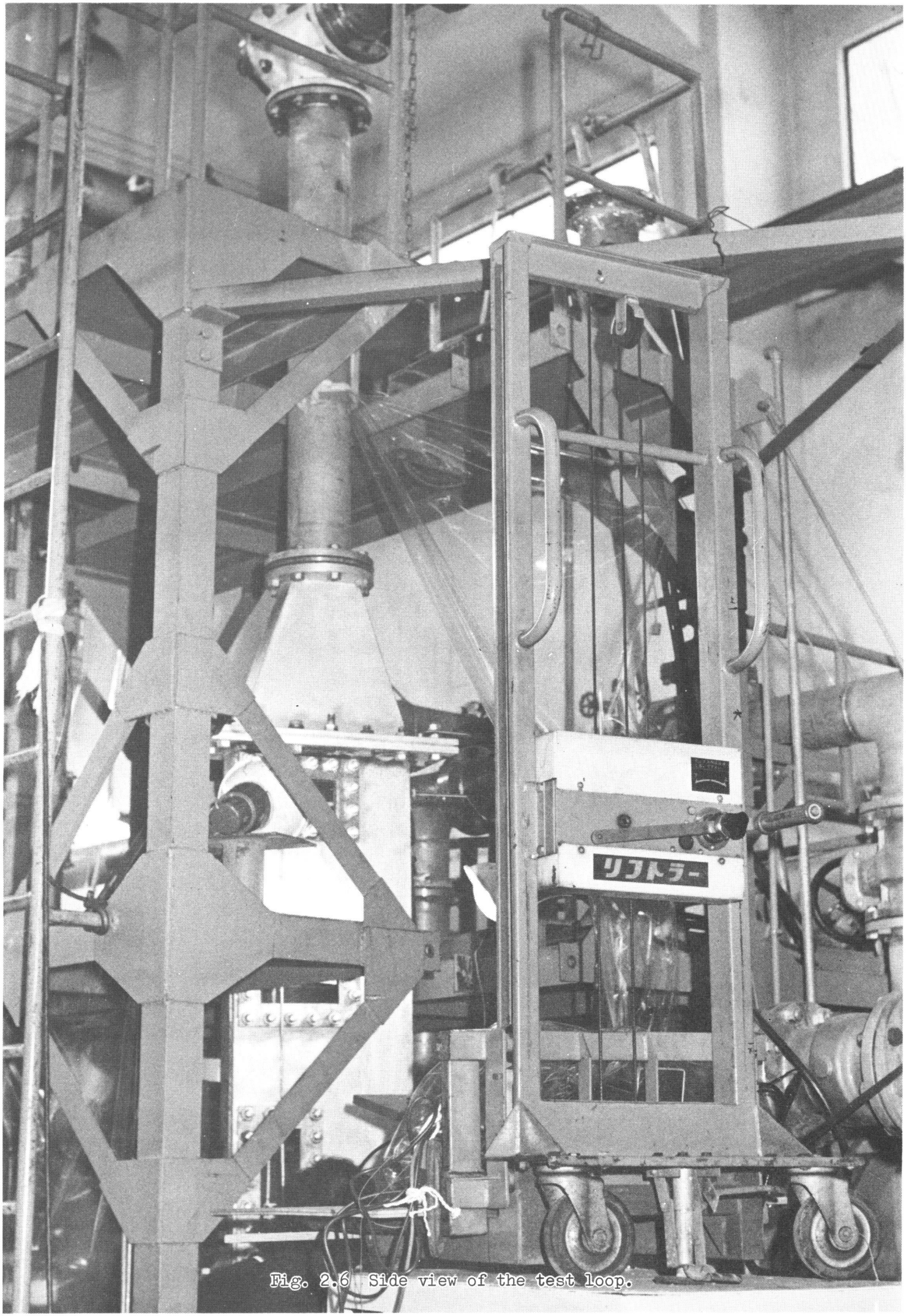

Fig. 2.6 Side view of the test loop.

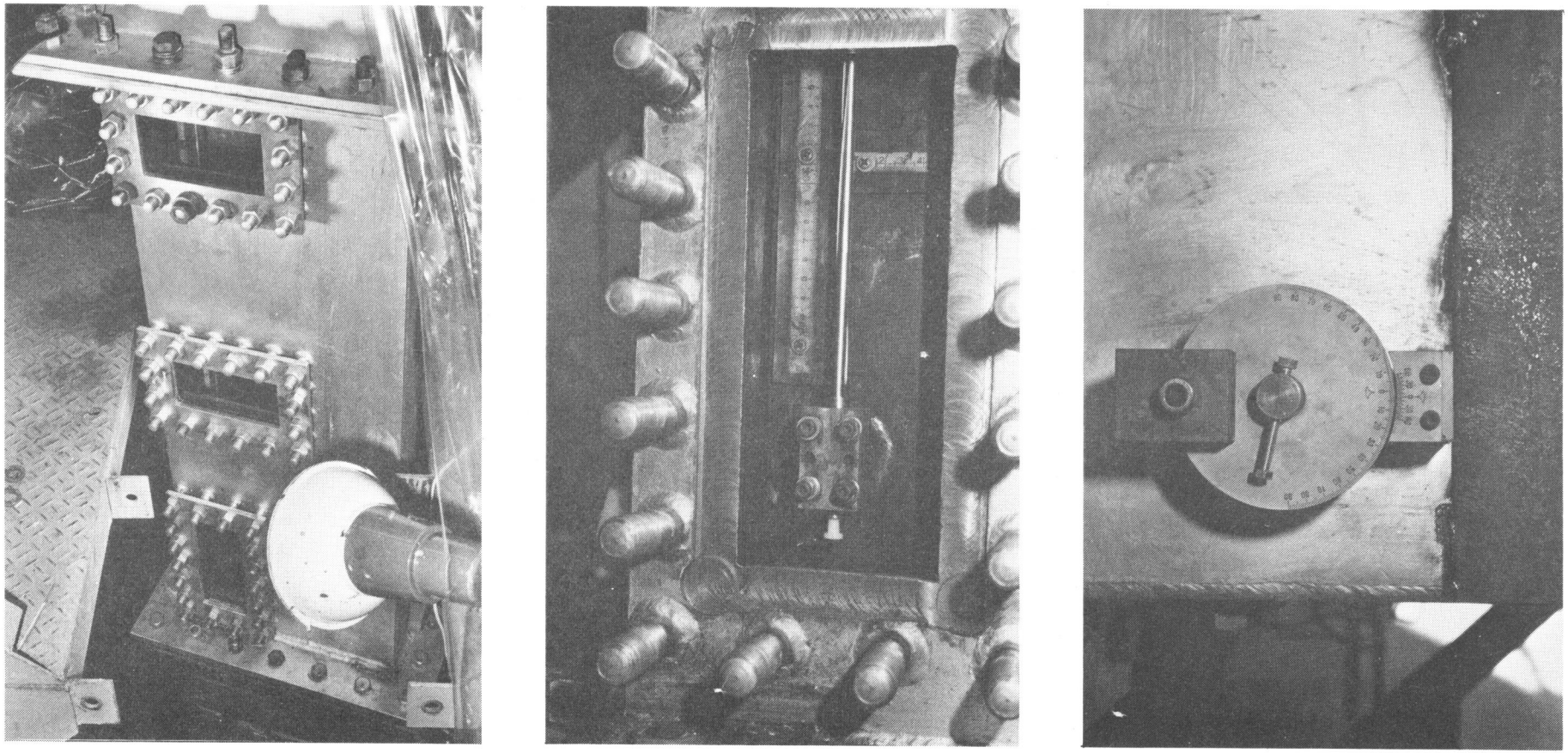

A B C

Fig. 2.7 Side views of the test section (A: a whole view, B: a pin supporting section at the lower end, C: a test pin angle adjusting mechanism).

Keys

① test pin
② test column
③ flow straightening section
④ reducer
⑤ test pin angle adjusting and supporting mechanism
⑥ window with reinforced glass covering

unit in mm

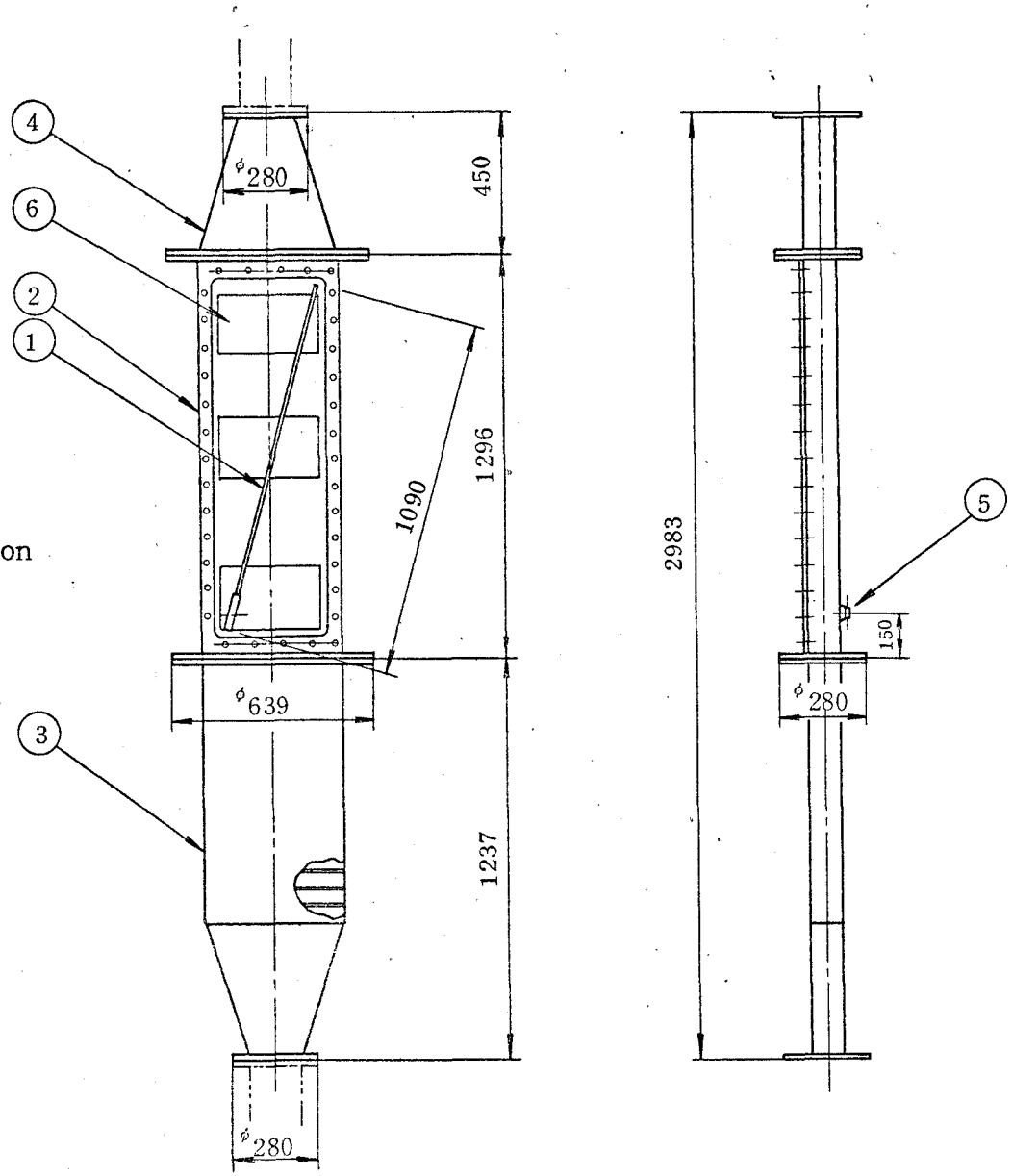

Fig. 2.8 Schematic representation of the test section.

Keys

① cladding tube (SUS316)
② lower end plug (SUS304)
③ upper end plug (SUS304)
④ wrapping wire (SUS316)

unit in mm

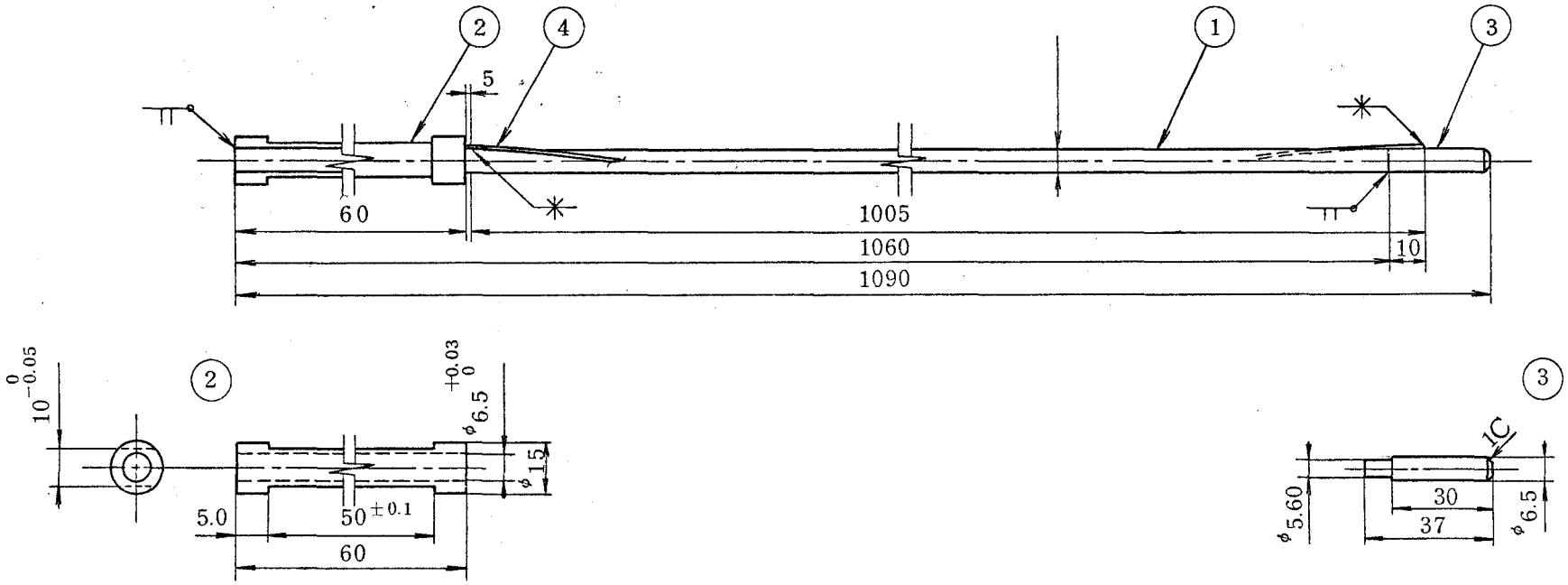

Fig. 2.9 Schematic representation of the test pin.

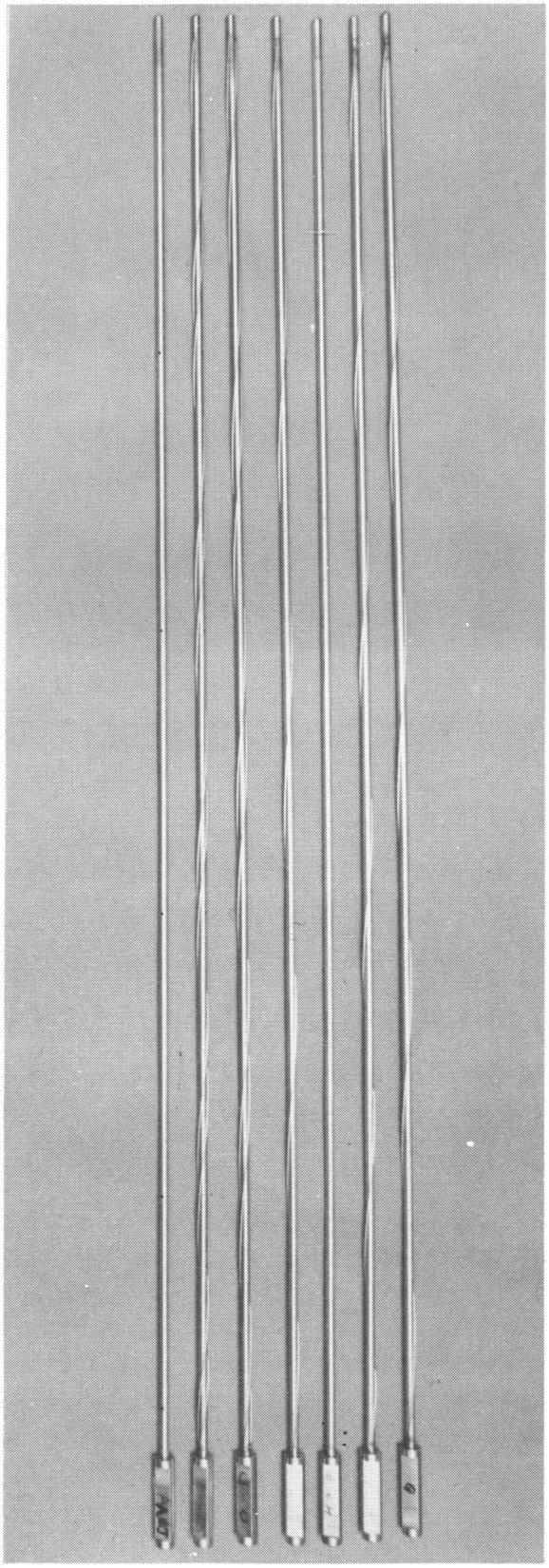

A

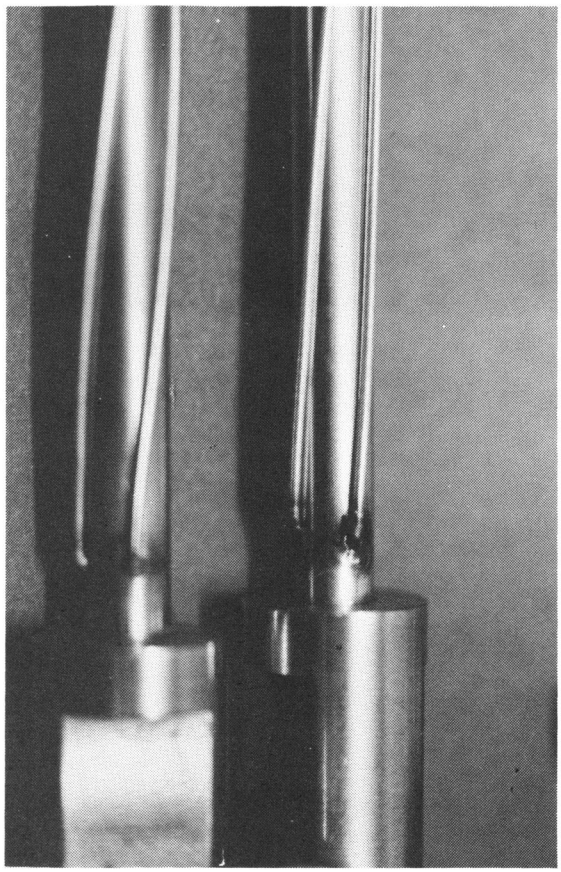

B

Fig. 2.10 Side views of the test pins (A: test pins, B: pin supporting section)

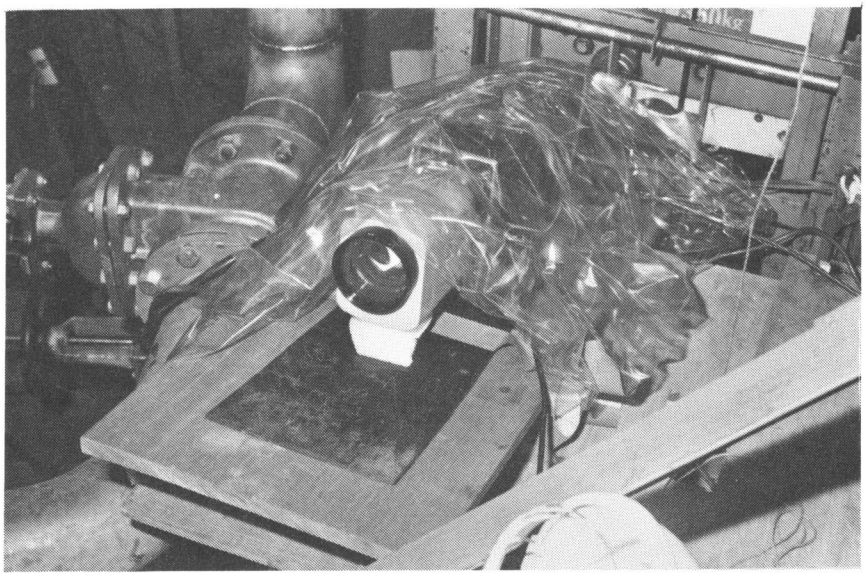

Fig. 2.11 Side view of a T.V. monitoring camera.

Fig. 2.12 Side view of an optical profilo-meter.

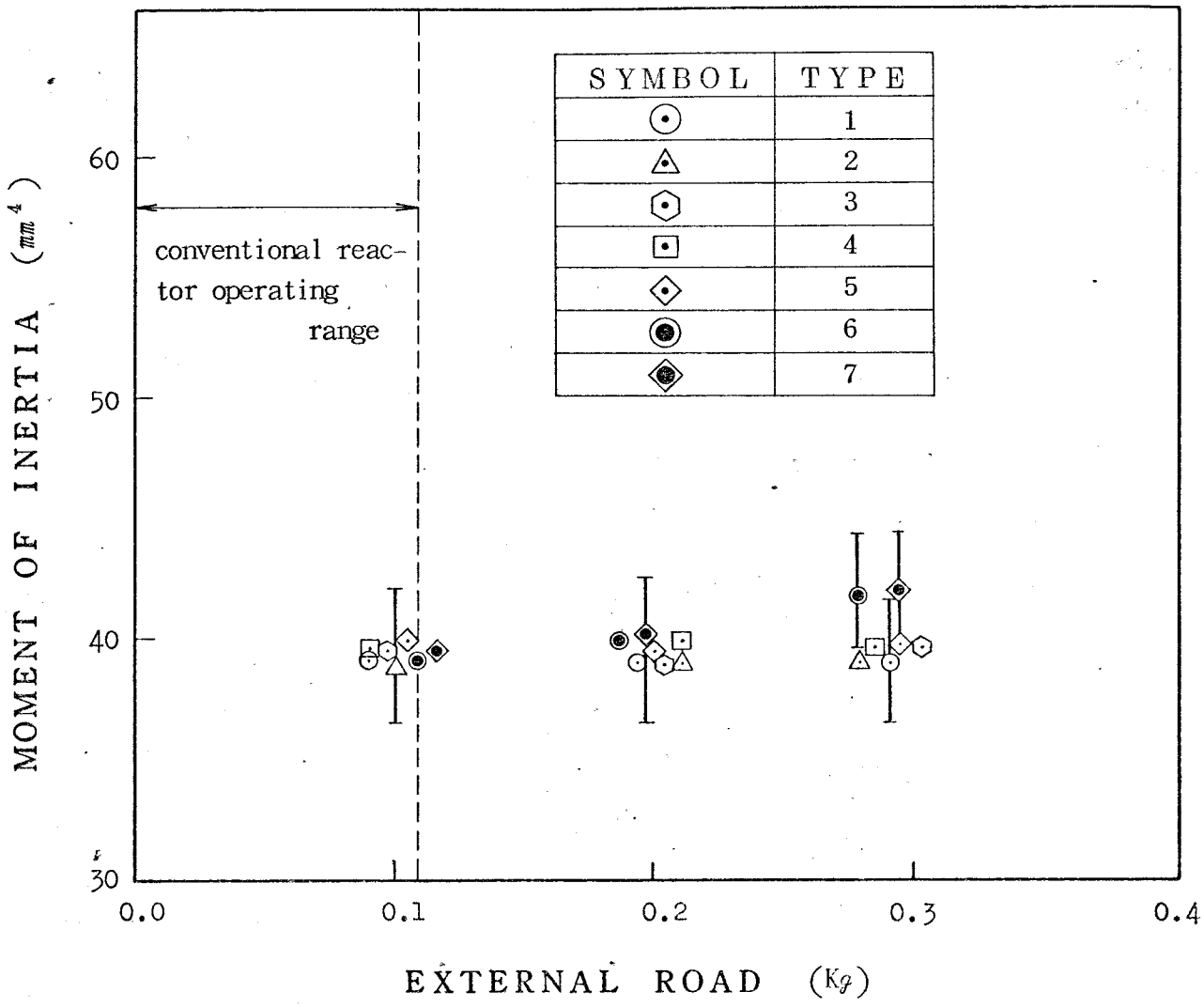

Fig. 2.13 Measured moment of inertia for different types of the test pin.

note: type 1, 2, 3, 4 and 5 are without dummy pellets, and type 6 and 7 are with dummy pellets.
type 1 corresponds to a fuel pin without a wire spacer, type 2 with single wire spacer of 1.3 mm in diameter and 306 mm in wrapping pitch, type 3 with double wire spacer of 1.0 mm in diameter and 306 mm in wrapping pitch, type 4 with single wire spacer of 1.3 mm in diameter and 200 mm in wrapping pitch, type 5 with double wire spacer of 1.0 mm in diameter and 200 mm in wrapping pitch, type 6 without a wire spacer and type 7 with wire spacers of the same diameter and wrapping pitch as type 5.

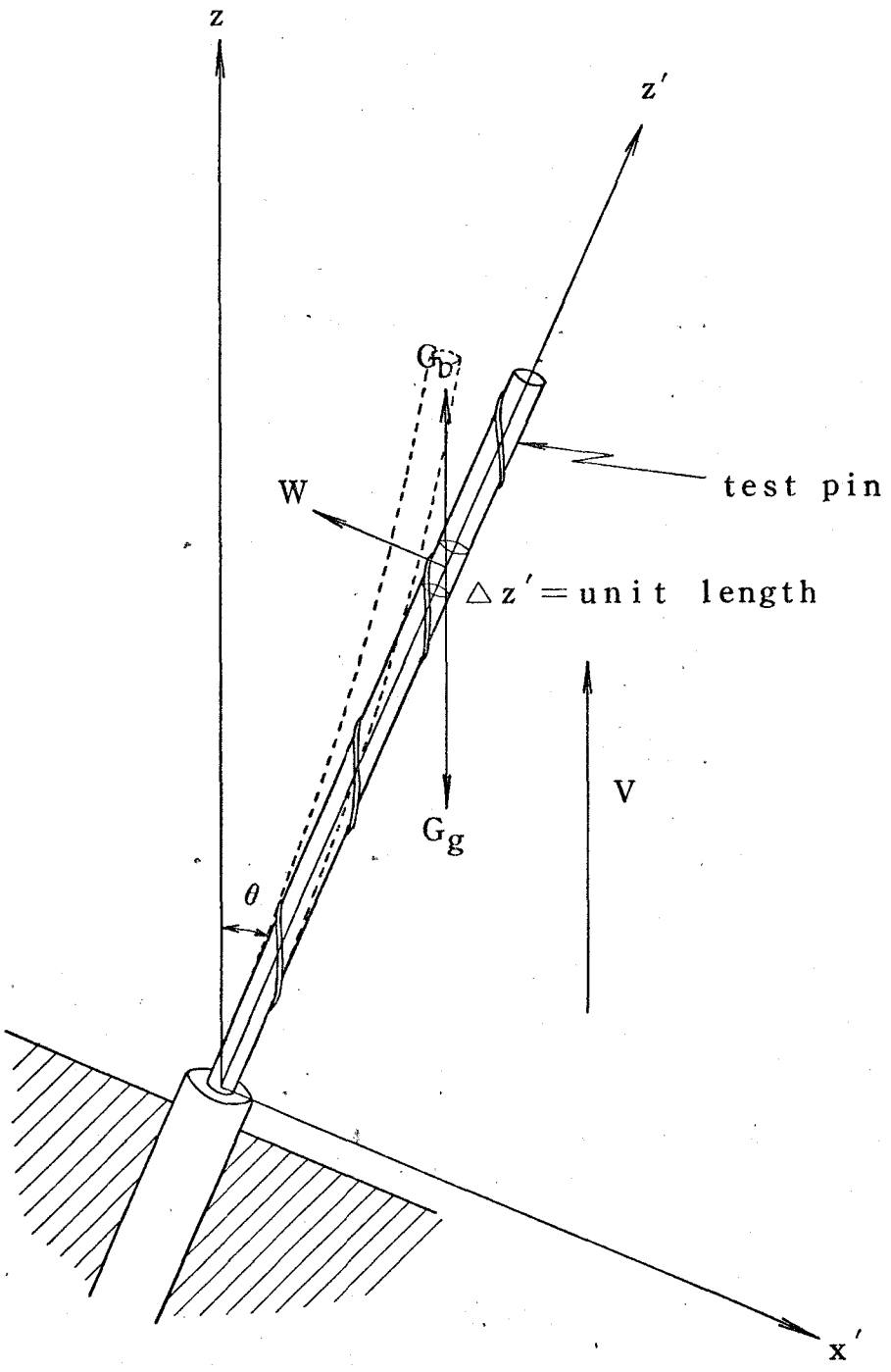

Fig. 2.14 Analytical model for pin deflection due to hydrodynamical force in flowing fluid. W, G_b and G_g are hydrodynamical force, buoyancy and gravity acting on an unit length of a test pin, respectively. Broken line shows a deflected fuel pin.

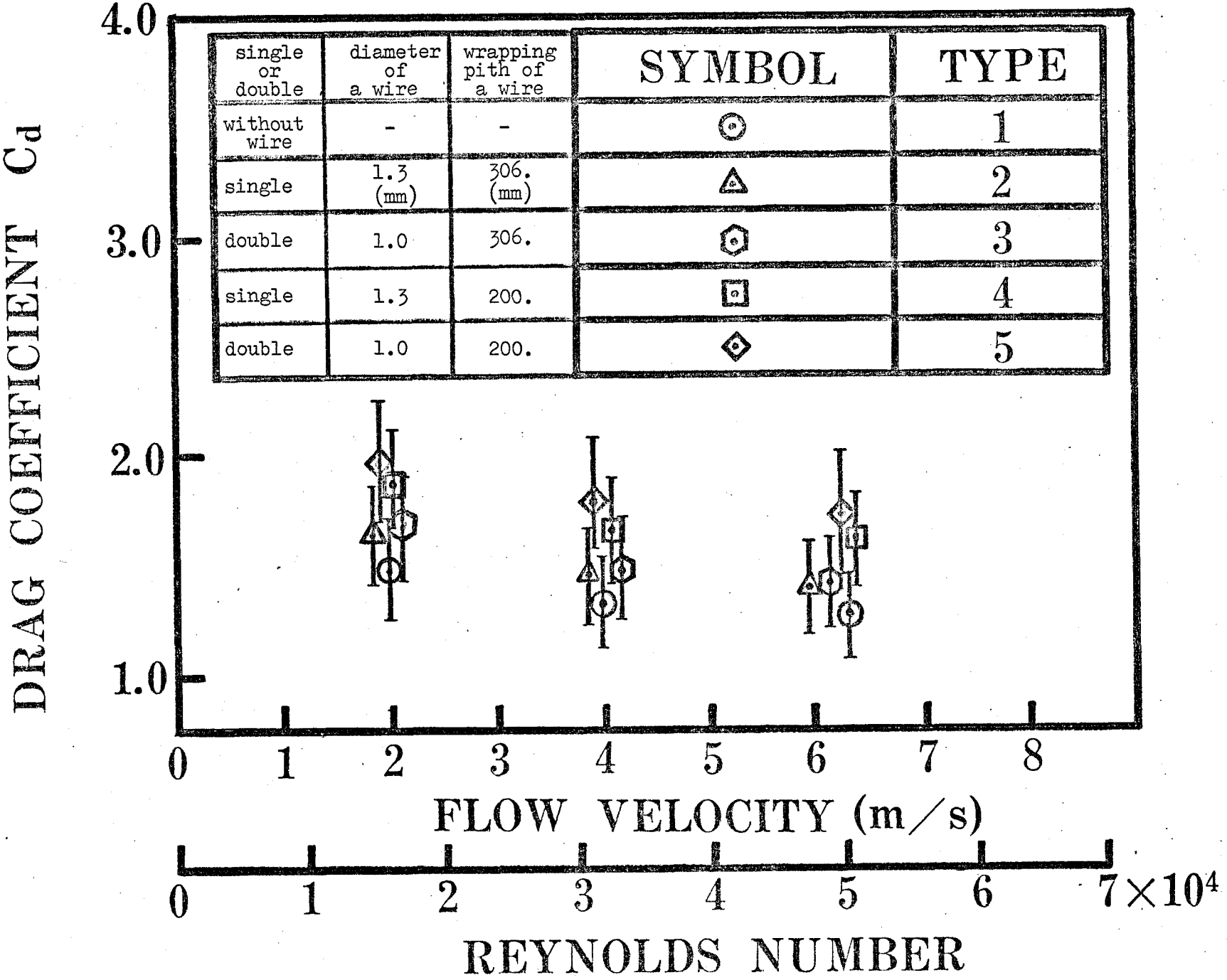

single or double	diameter of a wire	wrapping pith of a wire	SYMBOL	TYPE
without wire	-	-	◎	1
single	1.3 (mm)	306. (mm)	△	2
double	1.0	306.	⬡	3
single	1.3	200.	□	4
double	1.0	200.	◇	5

Fig. 2.15 Experimentally determined drag coefficients.

Sample calculation 1

Deflection of a 7 fuel pin bundle in a hexagonal lattice was investigated with and without taking into consideration the hydrodynamical effect. Figure 2.16 shows the equilibrium deflection modes of fuel pins standing in a corner to corner line with the hydrodynamical effect.

Comparison between the two cases shows that the inward deflection of the corner fuel pins at the upper core region is suppressed by 0.05 mm due to the hydrodynamical effect, which corresponds to the decrease in engineering hot spot subfactor by about 0.4 %.

Sample calculation 2

Deflection analysis of a prototype LMFBR fuel bundle consisting of 169 fuel pins assembled in a hexagonal lattice was performed with respect to a sector of 30 degree symmetry. The symmetry condition does not hold in a strict sense considering the wrapping phase of spacer wire, however it was employed for simplicity. The peripheral fuel pins were double wire-spaced to improve the edge flow effect and the wrapper tube was assumed to be straight.

The corresponding equilibrium deflection modes are displayed in Figs. 2. 17, 18 and 19. Variation in subchannel area is of the order of $^{-10}_{+2}$ % except for the peripheral subchannels where about 14～50 % increase is observed in the regions of the upper core and the upper blanket. Accordingly, the edge flow effect becomes locally exaggerated resulting in the increase in engineering hot spot subfactor by 3.5 %. The maximum load is 0.52 kg at the upper end of a fuel pin in contact with a wrapper tube.

Sample calculation 3

Deformation analysis of a similar fuel pin bundle with a wrapper tube bowed to the flat to flat direction was performed and the equilibrium deflection modes of fuel pins in two adjacent rows including the center pin and parallel to the direction of bowing are displayed in Fig. 2.20 where only the

contact points between pairs of fuel pins displayed are indicated. The displacement at the upper end of a wrapper tube due to bowing was assumed to be 2.64 mm which may actually be a case of a fuel subassembly in the vicinity of a control rod subassembly[12], [13]. Comparison of the results with those for a straight wrapper tube shows that the increase in engineering hot spot subfactor and the maximum load are 0.45 % and 0.11 kg,respectively.

Sample calculation 4

To evaluate the effect of swelling and creep of a fuel subassembly[14], [15] on engineering hot spot subfactor through the deflection of a fuel pin bundle as well as a wrapper tube, Fig. 2.21 shows the deflection modes of two adjacent rows of fuel pins including the center pin and parallel to the flat to flat direction. Solid lines and broken lines correspond to fuel pins at zero and after 500 day irradiation,respectively.

Owing to higher temperature and neutron flux distributions, swelling is dominant in the core region, where deflection of fuel pins is quite appreciable. At zero irradiation, the increase in engineering hot spot subfactor due to fuel pin deflection is 2.3 %, which is smaller than that in the case of flat power distribution considered in sample calculation 2. It is partly because the deflection of peripheral fuel pins due to edge flow effect is considerably compensated by the power gradient.

After 500 day irradiation, the total increase in engineering hot spot subfactor is 4.5 % and the maximum load is appeared to be 1.31 kg in the inner core region, which is 2.5 times as large as that appeared at zero irradiation at the upper end of a peripheral fuel pin. However, no direct fuel pin contact without intervening wire spacer is observed.

2.5 Conclusions

Some of the conclusions obtained through the present studies with respect to a prototype LMFBR fuel subassembly are as follows:

1) The engineering hot spot subfactor accounting for the fuel pin bundle deflection is around 1.023 ~ 1.035 at zero irradiation depending upon the power gradient within a fuel subassembly and further increases up to 1.045 at 500 day irradiation.

2) The variation of the peripheral subchannel area after 500 day irradiation is considerably large and the edge flow effect is exaggerated resulting in the increase in engineering hot spot subfactor.

3) At zero irradiation, the maximum load is 0.52 kg at the upper end of a peripheral fuel pin in contact with a straight wrapper tube, however after 500 day irradiation it increases by the factor of about 2.5 depending upon the power gradient and that the maximum loaded point moves to the inner core region.

4) The decrease in engineering hot spot subfactor due to hydrodynamical effect is around 0.3 % at zero irradiation, however the effect becomes more appreciable as irradiation progresses.

5) The drag coefficient for a wire wrapped fuel pin is experimentally determined as in Fig. 2.15.

However, in deriving the above conclusions, the time-variation in subassembly power generation rate is not taken into consideration in evaluating subassembly characteristics after 500 day irradiation, as is clear from Table 2.2.

Table 2.2 Parameters employed in the sample calculations.

Sample Calculation	1	2	3	4
Geometry				
outer diameter of fuel pin (mm)	6.5	6.5	6.5	6.5
diameter of wire spacer (mm)				
inner fuel pin	1.3	1.3	1.3	1.3
peripheral fuel pin	1.0	1.0	1.0	1.0
length of fuel pin (mm)				
lower blanket region	350	350	350	350
core region	930	930	930	930
upper blanket region	300	300	300	300
number of pins per subassembly	7	169	169	169
number of wire spacer per pin				
inner fuel pin	single	single	single	single
peripheral fuel pin	double	double	double	double
wrapping pitch of wire spacer (mm)	306	306	306	306
flat to flat distance of wrapper tube (mm)	22.5	104.6	104.6	104.6
Subassembly Thermal and Hydraulic Data				
peak to ave. power distribution				
radial	flat	flat	flat	1.17
axial	1.2	1.2	1.2	1.2
heat generation rate (MW)	0.19	4.6	4.6	4.6
Na-coolant flow rate (kg/sec)	0.85	20.2	20.2	20.2
inlet coolant temperature (°C)	397	397	397	397
Initial Bowing				
wrapper tube	straight	straight	bowed	straight
fuel pin	straight	straight	straight	straight
Cause of Deflection				
1. thermal 2. hydrodynamical 3. swelling, creep	1/1,2	1,2	1,2	1,2,3

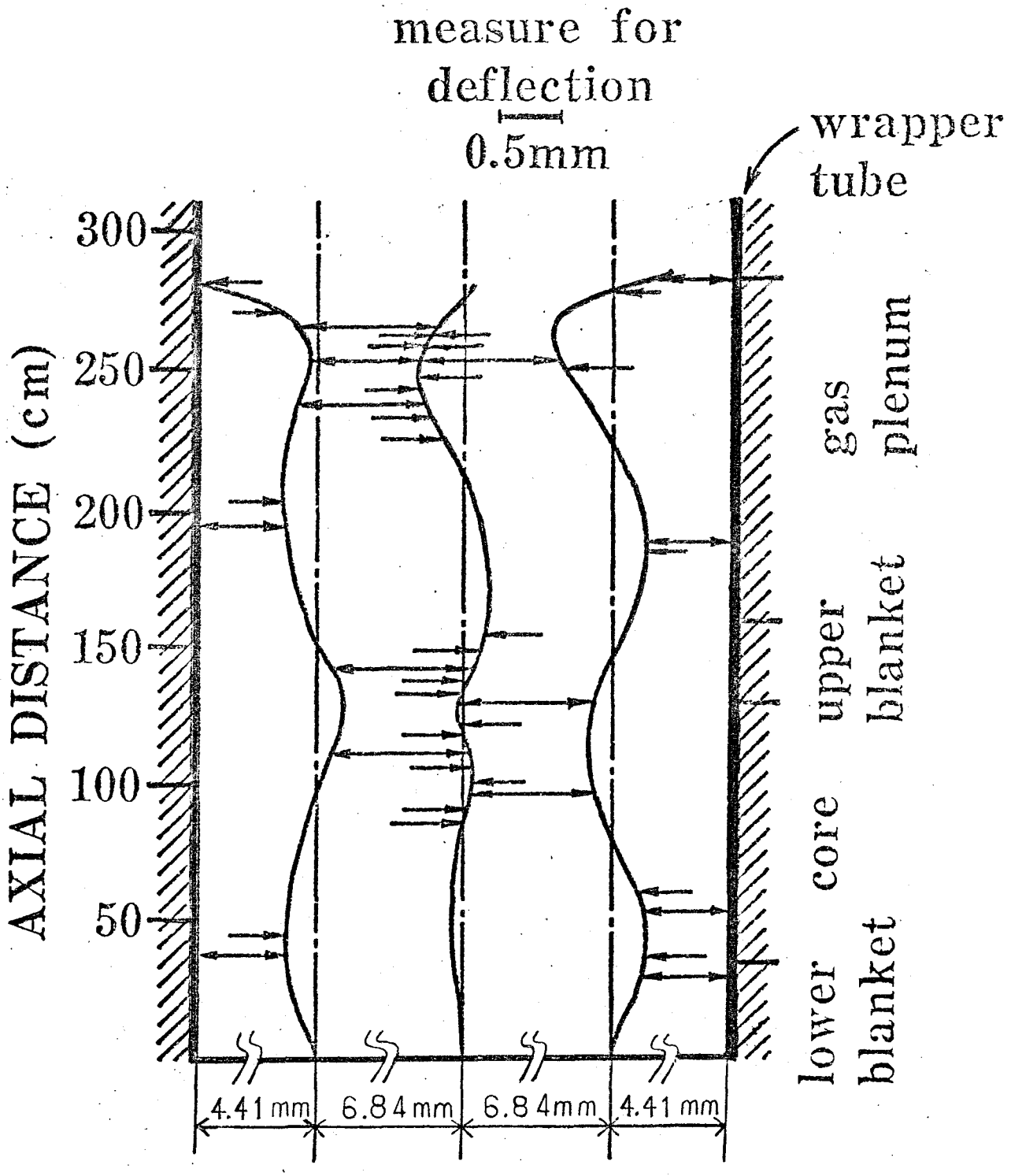

Fig. 2.16 Equilibrium deflection modes and contact points of fuel pins standing in a corner to corner line of a 7 pin subassembly with the hydrodynamical effect.

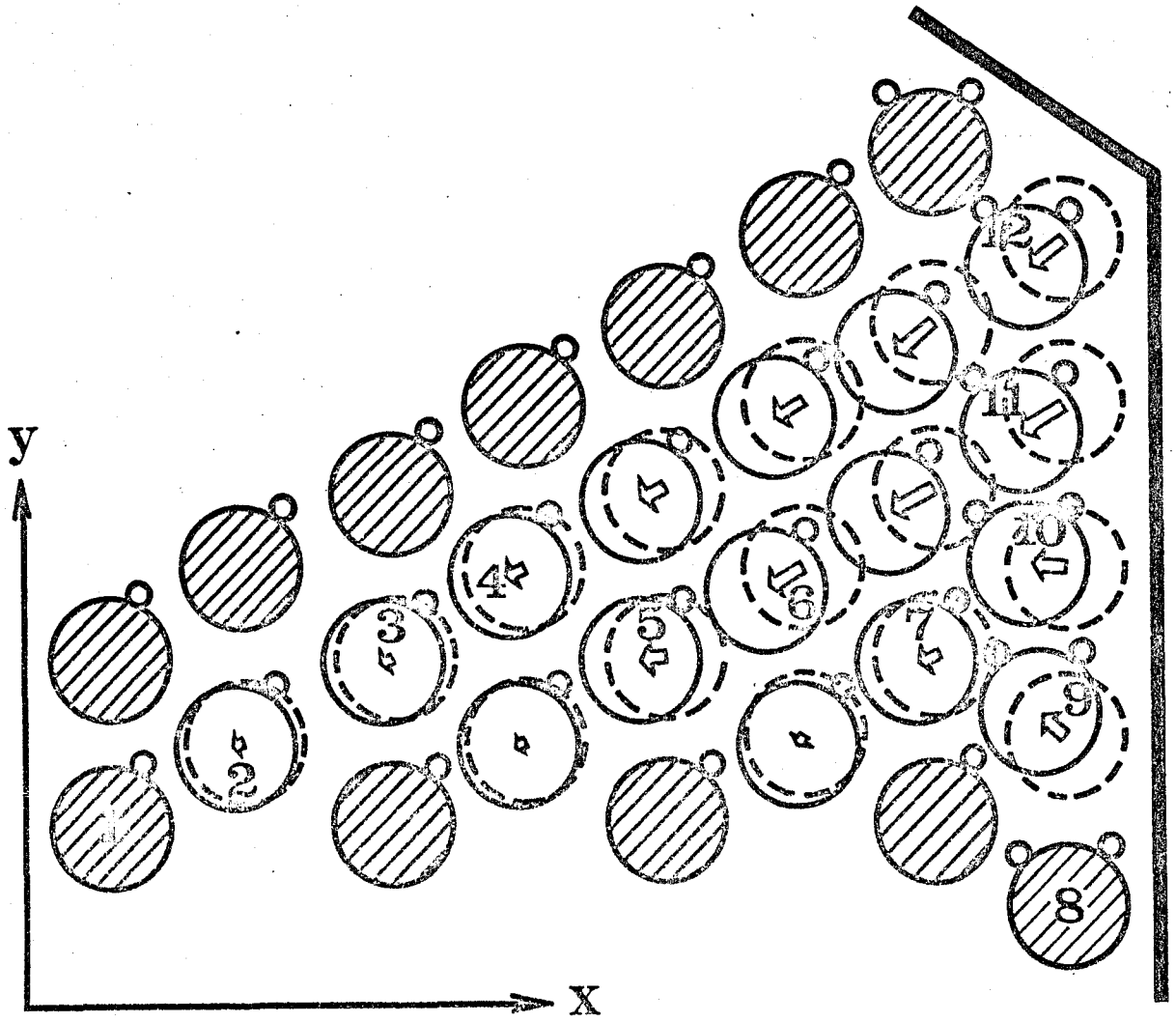

Fig. 2.17 Fuel pin deflection of a 169 pin subassembly in the horizontal plane at z = 129.5 cm. An arrow indicates the direction of fuel pin deflection.

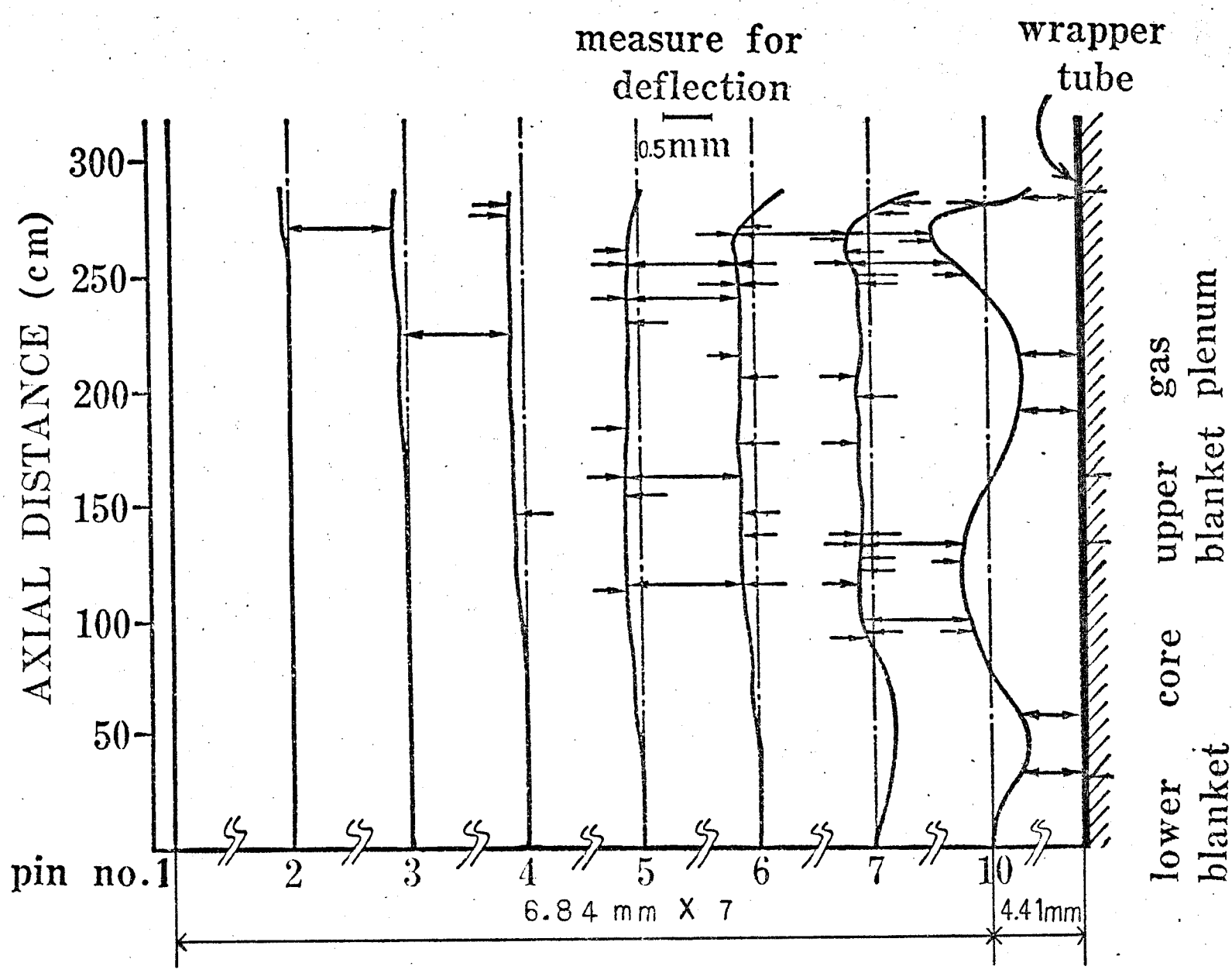

Fig. 2.18 Equilibrium deflection modes and contact points of fuel pins standing in the x direction. Double arrows and single arrows indicate contact points between pairs of fuel pins displayed and not displayed, respectively.

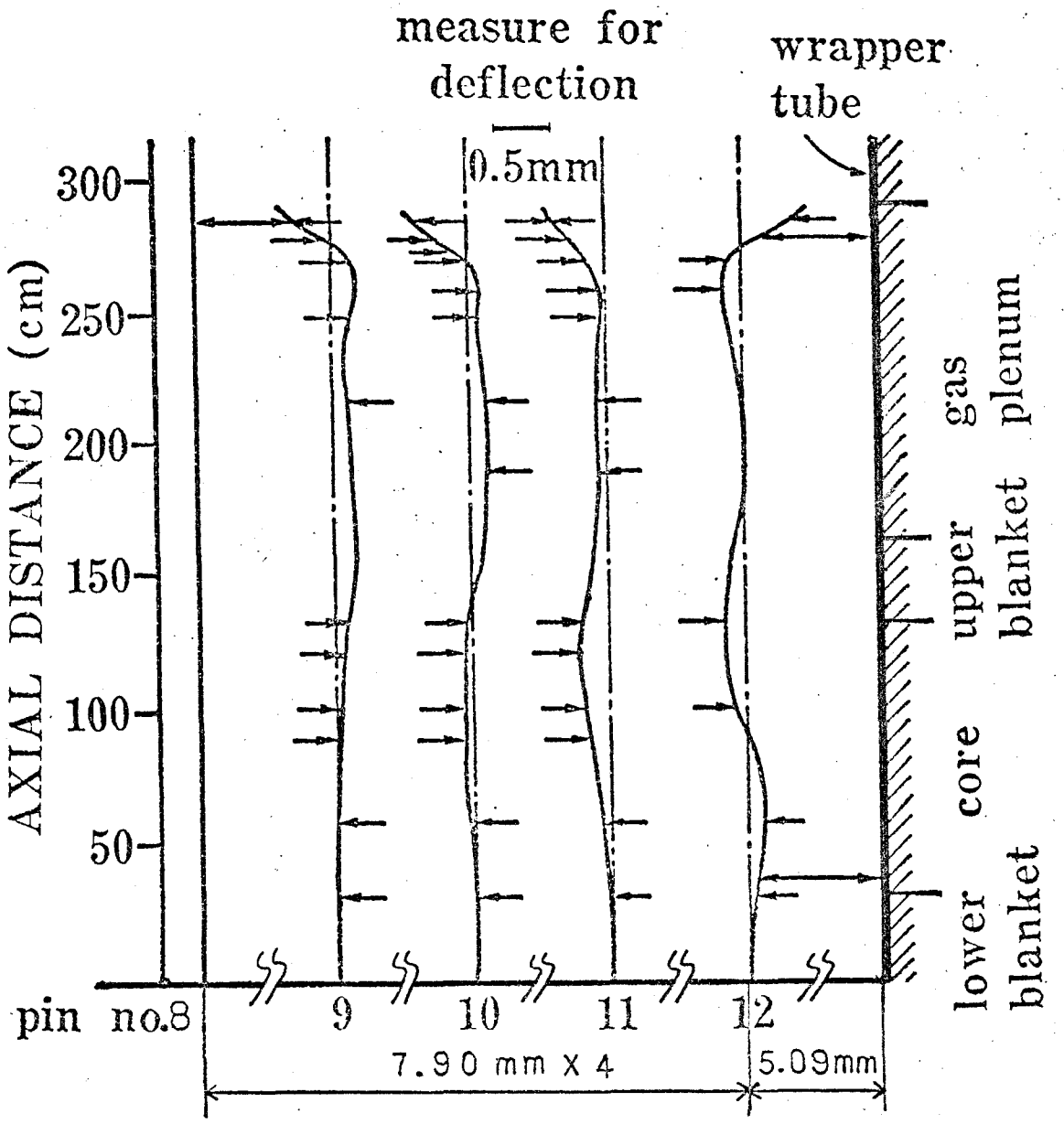

Fig. 2.19 Equilibrium deflection modes and contact points of fuel pins standing in the y direction.

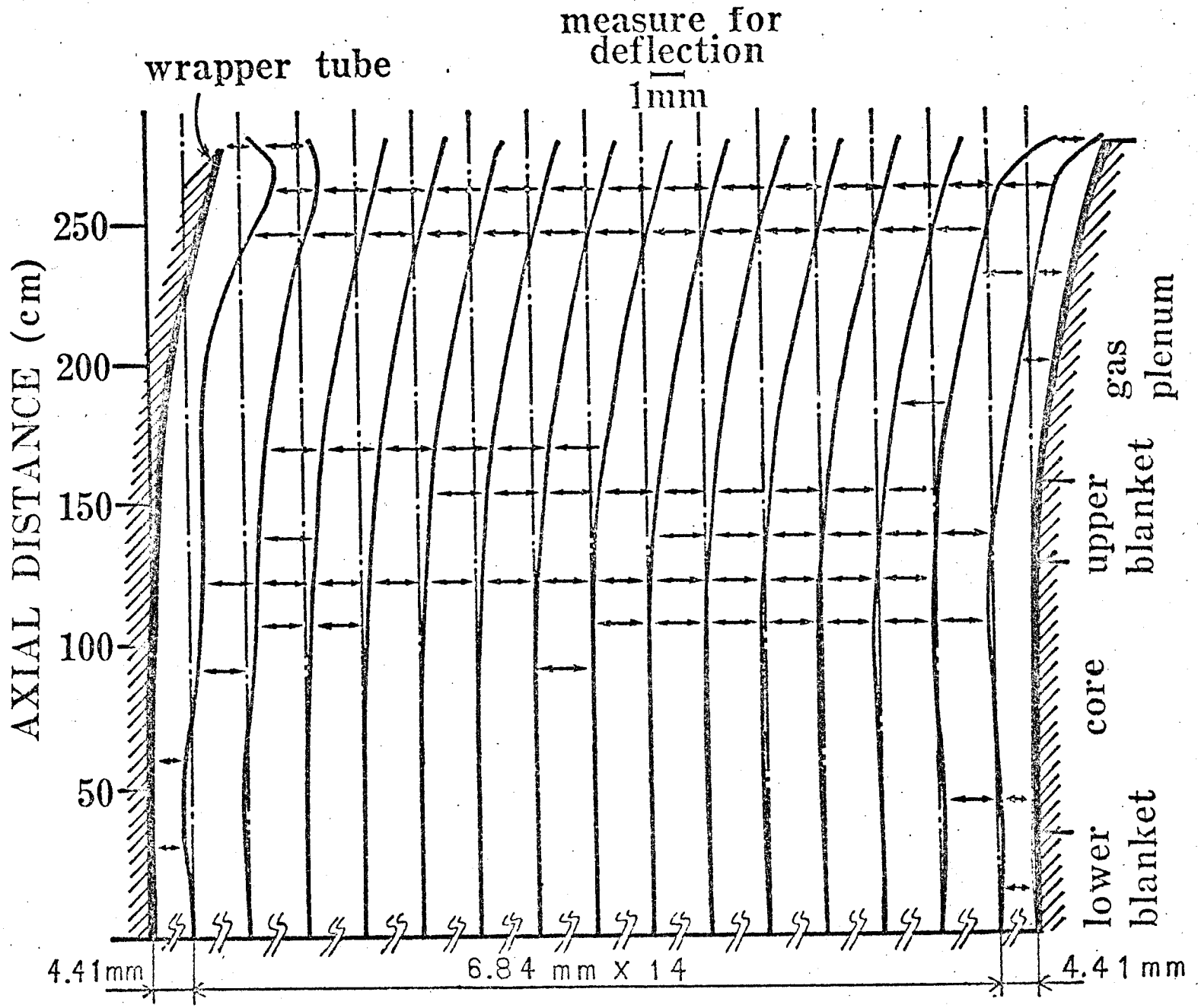

Fig. 2.20 Equilibrium deflection modes and contact points of fuel pins with a bowed wrapper tube. Arrows indicate contact points between pairs of fuel pins displayed.

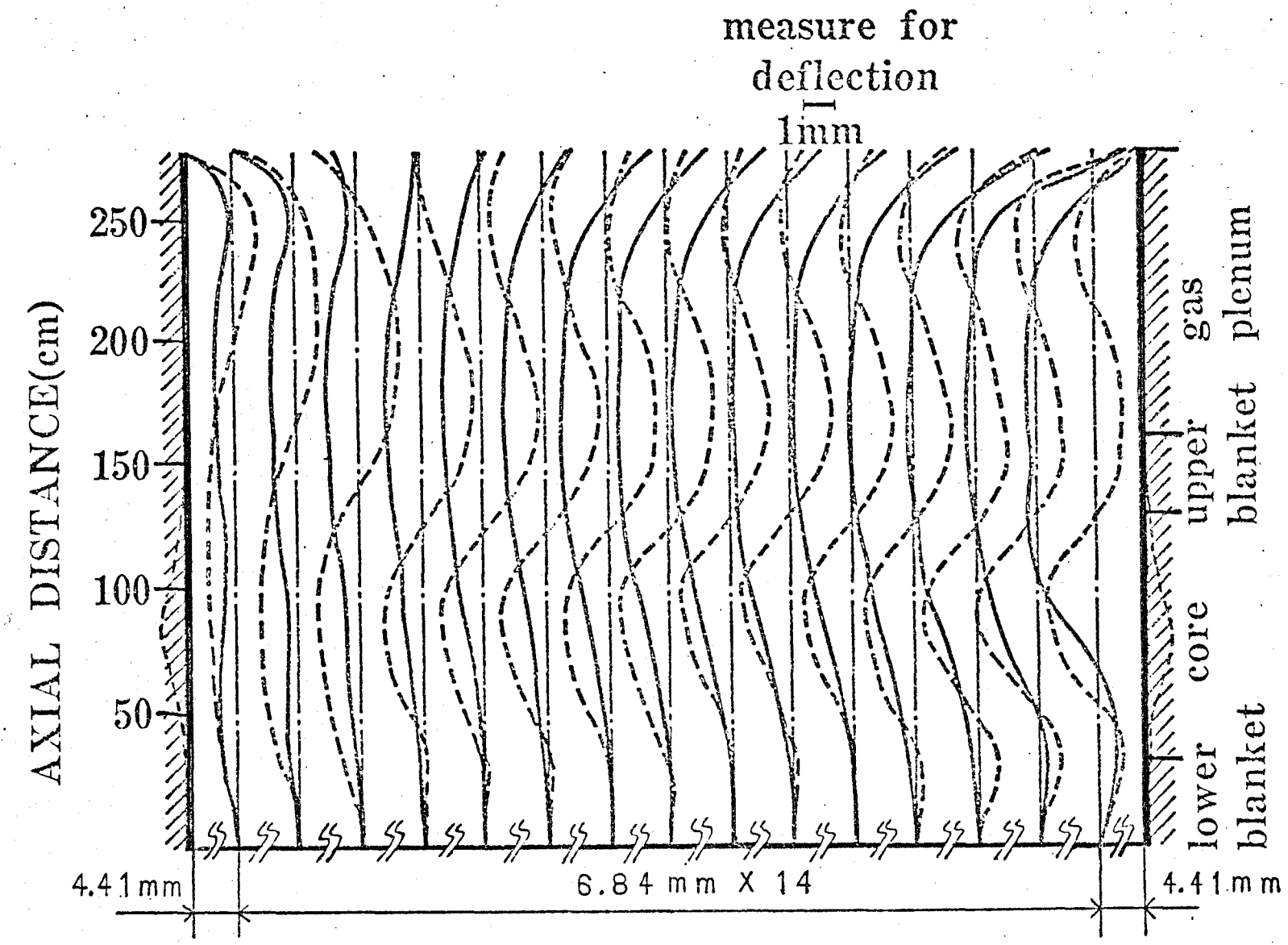

Fig. 2.21 Equilibrium deflection modes of fuel pins at zero and 500 day irradiation levels. Solid lines and broken lines correspond to fuel pins at zero and 500 day irradiation levels, respectively.

Appendix 2A

Derivation of the expressions (2-24) $\sim$ (2-30) for the elements $M_{m,n}$ in the mth row of the flexibility matrix M will be shown as follows: We consider the boundary condition (2-16) corresponding to fuel pin contact between fuel pins i and j at $z = z_{p(i,j),\ell}$. The eight fuel pins surrounding the fuel pins i and j and the corresponding eleven pair numbers are shown in fig. 2.3. Rewriting the general solutions (2-20a), (2-20b), (2-21a) and (2-21b) with respect to external loads $R_{p,\ell}$ at contact points, substitution of solutions (2-19a) and (2-19b) for $x_i(z)$ and $y_i(z)$ with definitions (2-20a), (2-20b), (2-21a) and (2-21b) into the contact condition (2-16) results in the following one of the n^+ simultaneous algebraic equations.

$$\{u_i(z_0) - u_j(z_0)\}A + \{v_i(z_0) - v_j(z_0)\}B$$

$$= q(z_0)[q(z_{p(i,j),\ell}) \cos\{\lambda_i(z_{p(i,j),\ell}) - \lambda_i(z_0)\} - q(z_0)], \qquad (2A\text{-}1)$$

where A and B are defined as follows:

$$A \equiv x_i^M(z_{p(i,j),\ell}) + x_i^I(z_{p(i,j),\ell}) - x_j^M(z_{p(i,j),\ell}) - x_j^I(z_{p(i,j),\ell})$$

$$\left.\begin{aligned}
&+ \sum_{\zeta=1}^{\ell-1} \left[\left(\tfrac{1}{3} z_{p(i,j),\zeta} - z_{p(i,j),\ell}\right) z_{p(i,j),\zeta}^2 \frac{\gamma_i\{z_{p(i,j),\zeta}\}}{2E(\overline{T}_i)I_i}\right. \\
&\left. - \left(\tfrac{1}{3} z_{p(i,j),\zeta} - z_{p(i,j),\ell}\right) z_{p(i,j),\zeta}^2 \frac{\gamma_j\{z_{p(i,j),\zeta}\}}{2E(\overline{T}_j)I_j}\right] R_{p(i,j),\zeta} \\
&+ \sum_{\zeta=\ell}^{\ell_{p(i,j)}^+} \left[\left(\tfrac{1}{3} z_{p(i,j),\ell} - z_{p(i,j),\zeta}\right) z_{p(i,j),\ell}^2 \frac{\gamma_i\{z_{p(i,j),\zeta}\}}{2E(\overline{T}_i)I_i}\right. \\
&\left. - \left(\tfrac{1}{3} z_{p(i,j),\ell} - z_{p(i,j),\zeta}\right) z_{p(i,j),\ell}^2 \frac{\gamma_j\{z_{p(i,j),\zeta}\}}{2E(\overline{T}_j)I_j}\right] R_{p(i,j),\zeta}
\end{aligned}\right\} \text{interaction between pins i and j}$$

(expression to be continued to the next page)

$$
\left.
\begin{aligned}
&\ell^{*}\{p(i,j),\ell|p(i,c_3)\}-1 \\
&+\sum_{\zeta=1}^{\ell^{*}\{p(i,j),\ell|p(i,c_3)\}-1}\left(\tfrac{1}{3}z_{p(i,c_3),\zeta}-z_{p(i,j),\ell}\right)z^{2}_{p(i,c_3),\zeta}\,\frac{\gamma_i\{z_{p(i,c_3),\zeta}\}}{2E(\overline{T}_i)I_i}\,R_{p(i,c_3),\zeta} \\
&+\sum_{\zeta=\ell^{*}\{p(i,j),\ell|p(i,c_3)\}}^{\ell^{+}_{p(i,c_3)}}\left(\tfrac{1}{3}z_{p(i,j),\ell}-z_{p(i,c_3),\zeta}\right)z^{2}_{p(i,j),\ell}\,\frac{\gamma_i\{z_{p(i,c_3),\zeta}\}}{2E(\overline{T}_i)I_i}\,R_{p(i,c_3),\zeta}
\end{aligned}
\right\}\ \text{interaction between pins i and } c_3
$$

$$
\left.
\begin{aligned}
&\ell^{*}\{p(i,j),\ell|p(i,c_4)\}-1 \\
&+\sum_{\zeta=1}^{\ell^{*}\{p(i,j),\ell|p(i,c_4)\}-1}\left(\tfrac{1}{3}z_{p(i,c_4),\zeta}-z_{p(i,j),\ell}\right)z^{2}_{p(i,c_4),\zeta}\,\frac{\gamma_i\{z_{p(i,c_4),\zeta}\}}{2E(\overline{T}_i)I_i}\,R_{p(i,c_4),\zeta} \\
&+\sum_{\zeta=\ell^{*}\{p(i,j),\ell|p(i,c_4)\}}^{\ell^{+}_{p(i,c_4)}}\left(\tfrac{1}{3}z_{p(i,j),\ell}-z_{p(i,c_4),\zeta}\right)z^{2}_{p(i,j),\ell}\,\frac{\gamma_i\{z_{p(i,c_4),\zeta}\}}{2E(\overline{T}_i)I_i}\,R_{p(i,c_4),\zeta}
\end{aligned}
\right\}\ \text{interaction between pins i and } c_4
$$

$$
\left.
\begin{aligned}
&\ell^{*}\{p(i,j),\ell|p(i,c_5)\}-1 \\
&+\sum_{\zeta=1}^{\ell^{*}\{p(i,j),\ell|p(i,c_5)\}-1}\left(\tfrac{1}{3}z_{p(i,c_5),\zeta}-z_{p(i,j),\ell}\right)z^{2}_{p(i,c_5),\zeta}\,\frac{\gamma_i\{z_{p(i,c_5),\zeta}\}}{2E(\overline{T}_i)I_i}\,R_{p(i,c_5),\zeta} \\
&+\sum_{\zeta=\ell^{*}\{p(i,j),\ell|p(i,c_5)\}}^{\ell^{+}_{p(i,c_5)}}\left(\tfrac{1}{3}z_{p(i,j),\ell}-z_{p(i,c_5),\zeta}\right)z^{2}_{p(i,j),\ell}\,\frac{\gamma_i\{z_{p(i,c_5),\zeta}\}}{2E(\overline{T}_i)I_i}\,R_{p(i,c_5),\zeta}
\end{aligned}
\right\}\ \text{interaction between pins i and } c_5
$$

$$
\left.
\begin{aligned}
&\ell^{*}\{p(i,j),\ell|p(i,c_6)\}-1 \\
&+\sum_{\zeta=1}^{\ell^{*}\{p(i,j),\ell|p(i,c_6)\}-1}\left(\tfrac{1}{3}z_{p(i,c_6),\zeta}-z_{p(i,j),\ell}\right)z^{2}_{p(i,c_6),\zeta}\,\frac{\gamma_i\{z_{p(i,c_6),\zeta}\}}{2E(\overline{T}_i)I_i}\,R_{p(i,c_6),\zeta} \\
&+\sum_{\zeta=\ell^{*}\{p(i,j),\ell|p(i,c_6)\}}^{\ell_{p(i,c_6)}}\left(\tfrac{1}{3}z_{p(i,j),\ell}-z_{p(i,c_6),\zeta}\right)z^{2}_{p(i,j),\ell}\,\frac{\gamma_i\{z_{p(i,c_6),\zeta}\}}{2E(\overline{T}_i)I_i}\,R_{p(i,c_6),\zeta}
\end{aligned}
\right\}\ \text{interaction between pins i and } c_6
$$

$$
\left.
\begin{aligned}
&\ell^{*}\{p(i,j),\ell|p(i,c_7)\}-1 \\
&+\sum_{\zeta=1}^{\ell^{*}\{p(i,j),\ell|p(i,c_7)\}-1}\left(\tfrac{1}{3}z_{p(i,c_7),\zeta}-z_{p(i,j),\ell}\right)z^{2}_{p(i,c_7),\zeta}\,\frac{\gamma_i\{z_{p(i,c_7),\zeta}\}}{2E(\overline{T}_i)I_i}\,R_{p(i,c_7),\zeta} \\
&+\sum_{\zeta=\ell^{*}\{p(i,j),\ell|p(i,c_7)\}}^{\ell^{+}_{p(i,c_7)}}\left(\tfrac{1}{3}z_{p(i,j),\ell}-z_{p(i,c_7),\zeta}\right)z^{2}_{p(i,j),\ell}\,\frac{\gamma_i\{z_{p(i,c_7),\zeta}\}}{2E(\overline{T}_i)I_i}\,R_{p(i,c_7),\zeta}
\end{aligned}
\right\}\ \text{interaction between pins i and } c_7
$$

(expression to be continued to the next pate)

$$
\left.
\begin{aligned}
&\ell^{*}\{p(i,j),\ell|p(j,c_1)\}-1\\
&-\sum_{\zeta=1}^{\ell^{*}\{p(i,j),\ell|p(j,c_1)\}-1}\left(\tfrac{1}{3}\,z_{p(j,c_1),\zeta}-z_{p(i,j),\ell}\right)z^{2}_{p(j,c_1),\zeta}\,\frac{\gamma_j\{z_{p(j,c_1),\zeta}\}}{2E(\overline{T}_j)I_j}\,R_{p(j,c_1),\zeta}\\
&\ell^{+}_{p(j,c_1)}\\
&-\sum_{\zeta=\ell^{*}\{p(i,j),\ell|p(j,c_1)\}}^{\ell^{+}_{p(j,c_1)}}\left(\tfrac{1}{3}\,z_{p(i,j),\ell}-z_{p(j,c_1),\zeta}\right)z^{2}_{p(i,j),\ell}\,\frac{\gamma_j\{z_{p(j,c_1),\zeta}\}}{2E(\overline{T}_j)I_j}\,R_{p(j,c_1),\zeta}
\end{aligned}
\right\}\text{interaction between pins j and } c_1
$$

$$
\left.
\begin{aligned}
&\ell^{*}\{p(i,j),\ell|p(j,c_2)\}-1\\
&-\sum_{\zeta=1}^{\ell^{*}\{p(i,j),\ell|p(j,c_2)\}-1}\left(\tfrac{1}{3}\,z_{p(j,c_2),\zeta}-z_{p(i,j),\ell}\right)z^{2}_{p(j,c_2),\zeta}\,\frac{\gamma_j\{z_{p(j,c_2),\zeta}\}}{2E(\overline{T}_j)I_j}\,R_{p(j,c_2),\zeta}\\
&\ell^{+}_{p(j,c_2)}\\
&-\sum_{\zeta=\ell^{*}\{p(i,j),\ell|p(j,c_2)\}}^{\ell^{+}_{p(j,c_2)}}\left(\tfrac{1}{3}\,z_{p(i,j),\ell}-z_{p(j,c_2),\zeta}\right)z^{2}_{p(i,j),\ell}\,\frac{\gamma_j\{z_{p(j,c_2),\zeta}\}}{2E(\overline{T}_j)I_j}\,R_{p(j,c_2),\zeta}
\end{aligned}
\right\}\text{interaction between pins j and } c_2
$$

$$
\left.
\begin{aligned}
&\ell^{*}\{p(i,j),\ell|p(j,c_3)\}-1\\
&-\sum_{\zeta=1}^{\ell^{*}\{p(i,j),\ell|p(j,c_3)\}-1}\left(\tfrac{1}{3}\,z_{p(j,c_3),\zeta}-z_{p(i,j),\ell}\right)z^{2}_{p(j,c_3),\zeta}\,\frac{\gamma_j\{z_{p(j,c_3),\zeta}\}}{2E(\overline{T}_j)I_j}\,R_{p(j,c_3),\zeta}\\
&\ell^{+}_{p(j,c_3)}\\
&-\sum_{\zeta=\ell^{*}\{p(i,j),\ell|p(j,c_3)\}}^{\ell^{+}_{p(j,c_3)}}\left(\tfrac{1}{3}\,z_{p(i,j),\ell}-z_{p(j,c_3),\zeta}\right)z^{2}_{p_{(i,j),\ell}}\,\frac{\gamma_j\{z_{p(j,c_3),\zeta}\}}{2E(\overline{T}_j)I_j}\,R_{p(j,c_3),\zeta}
\end{aligned}
\right\}\text{interaction between pins j and } c_3
$$

$$
\left.
\begin{aligned}
&\ell^{*}\{p(i,j),\ell|p(j,c_7)\}-1\\
&-\sum_{\zeta=1}^{\ell^{*}\{p(i,j),\ell|p(j,c_7)\}-1}\left(\tfrac{1}{3}\,z_{p(j,c_7),\zeta}-z_{p(i,j),\ell}\right)z^{2}_{p(i,c_7),\zeta}\,\frac{\gamma_i\{z_{p(j,c_7),\zeta}\}}{2E(\overline{T}_j)I_j}\,R_{p(j,c_7),\zeta}\\
&\ell^{+}_{p(j,c_7)}\\
&-\sum_{\zeta=\ell^{*}\{p(i,j),\ell|p(j,c_7)\}}^{\ell^{+}_{p(j,c_7)}}\left(\tfrac{1}{3}\,z_{p(i,j),\ell}-z_{p(j,c_7),\zeta}\right)z^{2}_{p(i,j),\ell}\,\frac{\gamma_j\{z_{p(j,c_7),\zeta}\}}{2E(\overline{T}_j)I_j}\,R_{p(j,c_7),\zeta}
\end{aligned}
\right\}\text{interaction between pins j and } c_7
$$

$$
\left.
\begin{aligned}
&\ell^{*}\{p(i,j),\ell|p(j,c_8)\}-1\\
&-\sum_{\zeta=1}^{\ell^{*}\{p(i,j),\ell|p(j,c_8)\}-1}\left(\tfrac{1}{3}\,z_{p(j,c_8),\zeta}-z_{p(i,j),\ell}\right)z^{2}_{p(j,c_8),\zeta}\,\frac{\gamma_j\{z_{p(j,c_8),\zeta}\}}{2E(\overline{T}_j)I_j}\,R_{p(j,c_8),\zeta}\\
&\ell^{+}_{p(j,c_8)}\\
&-\sum_{\zeta=\ell^{*}\{p(i,j),\ell|p(j,c_8)\}}^{\ell^{+}_{p(j,c_8)}}\left(\tfrac{1}{3}\,z_{p(i,j),\ell}-z_{p(j,c_8),\zeta}\right)z^{2}_{p(i,j),\ell}\,\frac{\gamma_j\{z_{p(j,c_8),\zeta}\}}{2E(\overline{T}_j)I_j}\,R_{p(j,c_8),\zeta}
\end{aligned}
\right\}\text{interaction between pins j and } c_8
$$

. (2A-2)

B is expressed by replacing x_i^M, x_i^I, x_j^M and x_j^I in the expression (2A-2) for A by y_i^M, y_i^I, y_j^M and y_j^I, and γ in A by δ, respectively. Let the above eleven pair numbers illustrated in Fig. 2.3 be represented by $p(\xi_1, \eta_1)$, $p(\xi_2, \eta_2)$, ..., $p(\xi_{10}, \eta_{10})$ and $p(\xi_{11}, \eta_{11})$ such that $p(\xi_1, \eta_1) < p(\xi_2, \eta_2) < \cdots\cdots < p(\xi_{10}, \eta_{10}) < p(\xi_{11}, \eta_{11})$, then we get the matrix elements $M_{m,n}$ represented in expressions (2-24)~(2-30).

References for Chapter 2

(1) K. Sakai, Y. Okubo and H. Hishida, Preliminary Development of an Analytical Method for Evaluating Fuel Pin Deflection, Trans. of At. Energy Soc. Japan, Nov. (1975) E11.

(2) K. Sakai, Y. Okubo and H. Hishida, Deflection of Wire-Spaced Fuel Pin Bundles, Trans. of ANS, 26 (1) (1977) 460.

(3) K. Sakai, et al., Evaluating of the Effect of Hydrodynamical Force on Fuel Pin Deflection, Trans. of At. Energy Soc. Japan, Oct. (1977) F58.

(4) K. Sakai, Y. Okubo and H. Hishida, Three-Dimensional Deflection Analysis of Wire-Spaced Fuel Pin Bundles under Temperature and Hydrodynamical Force Fields with Irradiation Effects, Nucl. Eng. Design, 48 (1978) 595.

(5) K. Sakai and H. Hishida, Probabilistic Evaluation of Core-Internal Coolant Flow Distribution, Trans. of ANS, 24 (1976) 337.

(6) K. Sakai and H. Hishida, Probabilistic Evaluation of Core-Internal Coolant Flow Distribution with Correlation among Fuel Subassemblies, Nucl. Eng. Design, 44 (1977) 235.

(7) D. A. Kucera and D. Mohr, BOW-V, a CDC-3600 Program to Calculate the Equilibrium Configurations of a Thermally Bowed Reactor Core, ANL/EBR-014 (1970).

(8) K. Ohmae, A. Morino, N. Nakao and S. Hirao, Channel Deformation Analysis for Fast Reactor Fuel Assemblies Undergoing Swelling and Thermal Bowing, Nucl. Eng. Design, 23 (1972) 309.

(9) G. Taylor, Analysis of the Swimming of Long and Narrow Animals, Proc. Roy. Soc. A, 214 (1952) 158.

(10) E. F. Relf and C. H. Powell, Rep. Memor. Aero. Res. Comm., Lond., 307 (1917).

(11) D. S. Rowe, COBRA IIIC: A Digital Computer Program for Steady State and Transient Thermal-Hydraulic Analysis of Rod Bundle Nuclear Fuel Element, NBWL-1695 (1973).

(12) H. Kinjo, K. Sakai and H. Hishida, Three-Dimensional Core Deformation Analysis, Trans. of At. Energy Soc. Japan, Apr. (1977) C47.

(13) H. Hishida, et al., A Method for Three-Dimensional Analyses of Externally Constrained FBR Core under Temperature and Nuetron Flux Fields with Clearance Effects at Lower Nozzle Sections, Nucl. Eng. Design, to be published (1978).

(14) T. T. Claudson, Irradiation Induced Swelling and Creep in Fast Reactor Materials, NBWL-SA-3283 (1970).

(15) R. D. Legett, Plutonium Fuels for LMFBR-an Extrapolation, WHAN-SA-51, Oct. (1970).

(16) K. Takahashi, E. Ishibashi and J. Takahashi, Mixing Test in Fuel Subassembly for "Monju", PNC Report SN941 76-136, Dec. (1976).

Chapter 3

Probabilistic evaluation of fuel pin gaps due to the variation of core design parameters

3.1 Introduction

In this chapter, discussion on the inner-subassembly characteristics under the probabilistic variation of core design parameters described in section 1.3.3 will be given. Evaluation of the effect of probabilistic deviation in fuel pin gaps of a FBR fuel subassembly due to manufacturing and assembling tolerances on thermal and hydraulic characteristics of a core plays an important role in connection to the safety assurance of a reactor performance through a full core life[1]~[4]. In a case of a gridded fuel pin bundle, where fuel pins are supported with elastic dimples inside grid spacers, fuel pin gap distributions in a reactor operating condition may be evaluated in terms of the corresponding measured fuel pin gap distributions at a factory site[5], [6]. However, wire-spaced fuel pin gap distributions in a reactor operating condition differ considerably from those at an assembling site since wire-spaced fuel pins are usually packed loose in a bundle to compensate for fuel pin swelling and are deflected with complicated modes under a reactor operating condition due to temperature gradient across a fuel pin bundle, hydrodynamical force exerted by coolant, irradiation-induced swelling and creep[7], [8]. Recently, a computer code PACT is reported which takes into consideration several uncertainties in mixing constants, inlet temperature, power level, fabrication and material properties which are to be sampled at the beginning of thermal and hydraulic subchannel analyses[9].

In this chapter, the sensitivity of uncertainties due to manufacturing and assembling tolerances of a fuel subassembly to the deviation in wire-spaced fuel pin gaps is discussed based on the method for three-dimensional

fuel pin deflection analyses explained in section 2.2. A fuel pin gap between an arbitrary pin pair at any axial distance within an equilibrium fuel pin bundle in a reactor operating condition is expressed in terms of a set of reference values of all the related uncertainties and their deviations with the corresponding sensitivity functions which correlate the deviations to a fuel pin gap under consideration. Then, the probabilistic distribution of a local fuel pin gap may be obtained through taking all the possible combinations of the values of uncertainties within their ranges of deviation. Uncertainties due to local and global tolerances are classified into three categories according to the scope of their influence[10], [11].

Sample calculations were performed on the sensitivity of uncertainties to probable fuel pin gap distributions of a typical FBR core based on the currently available factory data of fuel subassemblies for test production[12] and the results for the fuel pin pair corresponding to the cladding hot spot of a center fuel subassembly are discussed.

3.2 Analytical formulation

3.2.1 Assumptions underlying the probabilistic evaluation of fuel pin gaps

Present probabilistic evaluation of wire-spaced fuel pin gaps within a FBR fuel subassembly in a reactor operating condition is valid under the assumptions employed in the previous section 2.2.1 with the following additional assumption:

(i) Uncertainties listed in Table 3.1 are the factors affecting wire-spaced fuel pin gap distributions.

3.2.2 Probabilistic variation in fuel pin gaps

1) Classification of uncertainties

We consider in the preceeding sections the probabilistic variation in a fuel pin gap due to the related uncertainties including manufacturing and assembling tolerances of a fuel subassembly as well as the ambiguity in

material properties and experimental data. These uncertainties are classified into three categories according to the scope of their influence as listed in Table 3.1.

Table 3.1 Classification of uncertainties related to fuel pin gaps.

Category	Symbol	Specifications of Uncertainty
core and subassembly uncertainties	$F^s(1)$	modulus of fuel pin elasticity
	$F^s(2)$	fuel pin drag coefficient
	$F^s(3)$	fuel pin linear thermal expansion coefficient
	$F^s(4)$	flat to flat distance of a wrapper tube
fuel pin uncertainties	$F^f(i;1)$	diameter of fuel pin i
	$F^f(i;2)$	wire spacer diameter of fuel pin i
	$F^f(i;3)$	pitch of fuel pin i at the end supporting matrix
	$F^f(i;4)$	welding angle at the lower end plug of fuel pin i
	$F^f(i;5)$	end support tube installation angle of fuel pin i
local uncertainties	$F^\ell(i,h;1)$	wire spacer wrapping pitch of fuel pin i at z_h
	$F^\ell(i,h;2)$	initial bowing amplitude of fuel pin i at z_h

We define a normalized uncertainty $F(i;\lambda)$ such that

$$F(i;\lambda) \equiv \frac{\xi(i;\lambda)}{\tilde{\xi}(i;\lambda)} , \qquad (3\text{-}1)$$

where $\tilde{\xi}(i;\lambda)$ is the nominal value of the λth uncertainty in the ith category and $\xi(i;\lambda)$ is a deviated value of the uncertainty in the vicinity of $\tilde{\xi}(i;\lambda)$. A welding angle of an end plug of a fuel pin i, $F^f(i;4)$ and an installation angle of an end support tube for a fuel pin i, $F^f(i;5)$ are illustrated in Fig. 3.1. Basically, diameters of a fuel pin and a wire spacer vary locally

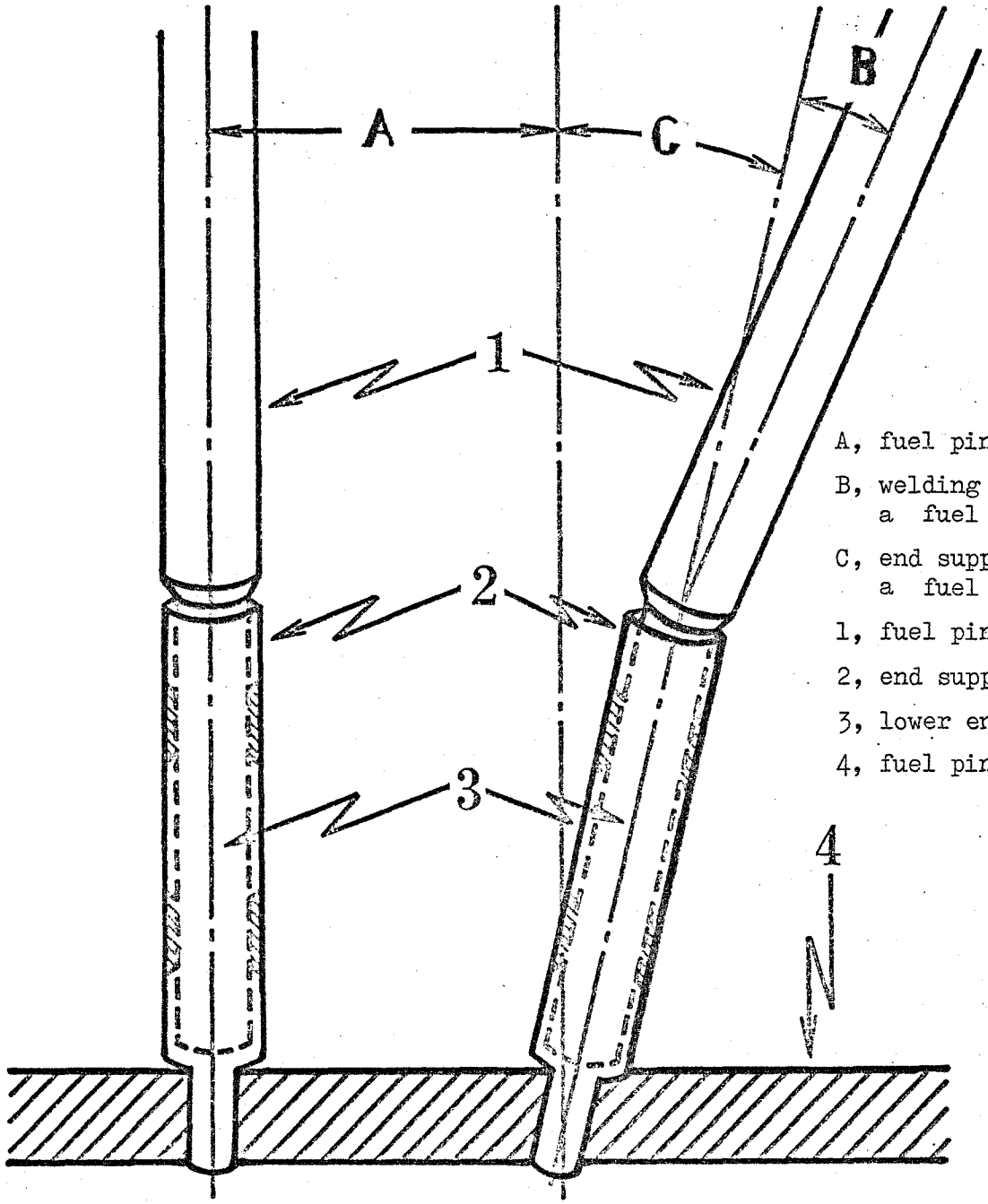

Keys

A, fuel pin pitch: $F^f(i;3)$

B, welding angle at the lower end plug of a fuel pin: $F^f(i;4)$

C, end support tube installation angle of a fuel pin: $F^f(i;5)$

1, fuel pin

2, end support tube

3, lower end plug

4, fuel pin support plate

Fig. 3.1 Schematic representation of a fuel pin end support

along the axial pin direction. However the local variations are considered to be negligibly small according to the currently available factory data[12] and these uncertainties are classified into the category of fuel pin uncertainties. Wire-spaced fuel pins are usually bowed spirally with the period of a wire-wrapping pitch due to the tension of a wire spacer[12] and therefore the amplitude of the initial bowing of a fuel pin and the wrapping pitch of a wire spacer are treated as local uncertainties.

2) Sensitivity functions associated with uncertainties

In order to discuss a probabilistic distribution of the mth fuel pin gap $g_m(z, \{F_\lambda\})$ at z under a set of all the related uncertainties $\{F_\lambda\}$ in a fuel subassembly, let $P(g_m, z)$ be the probabilistic density such that the pin gap $g_m(z, \{F_\lambda\})$ is included in the interval (g_m, g_m+dg_m). Then, since $g_m(z, \{F_\lambda\})$ is to be determined through mechanical and geometrical correlations among all the fuel pins in a subassembly with temperature and neutron flux fields and hydrodynamical influence due to coolant flow, $P(g_m,z)$ may generally be expressed in terms of the product of probabilistic density functions of all uncertainties as follows:

$$P(g_m,z) = \int_{on\Omega} \cdots \int \prod_{\lambda_s} P^s(\lambda_s) dF^s(\lambda_s) \prod_i \prod_{\lambda_f} P^f(i;\lambda_f) dF^f(i;\lambda_f) \cdot$$

$$\cdot \prod_h \prod_{\lambda_\ell} P^\ell(i,h;\lambda_\ell) dF^\ell(i,h;\lambda_\ell). \qquad (3\text{-}2)$$

In expression (3-2), $F^s(\lambda_s)$, $F^f(i;\lambda_f)$ and $F^\ell(i,h;\lambda_\ell)$ represent a normalized subassembly uncertainty of the λ_sth kind, a normalized fuel pin uncertainty of the λ_fth kind belonging to the fuel pin i and a normalized local uncertainty of the λ_ℓth kind belonging to the fuel pin i at z_h and $P^s(\lambda_s)$, $P^f(i;\lambda_f)$ and $P^\ell(i,h;\lambda_\ell)$ are probabilistic density functions of normalized uncertainties $F^s(\lambda_s)$, $F^f(i;\lambda_f)$ and $F^\ell(i,h;\lambda_\ell)$, respectively. Indices i, h, λ_s, λ_f and λ_ℓ vary so as to cover all the uncertainties related to an equilibrium fuel pin bundle configuration. Ω indicates that the integration should

conditionally be carried out on F^s, F^f and F^ℓ such that the mth fuel pin gap at z is included in $(g_m,\ g_m+dg_m)$.

However, in carrying through the integration conditionally on Ω, computational difficulties are involved since a set of simultaneous equations for an equilibrium configuration of a fuel pin bundle should be solved once for every possible combination of the values of uncertainties to assure whether the integrating condition is satisfied. For avoiding such computational difficulties, we expand $g_m(z,\{F_\lambda\})$ into Taylor's series at $\{\hat{F}_\lambda\}$ as follows:

$$\begin{aligned} g_m(z,\{F_\lambda\}) = g_m(z,\{\hat{F}_\lambda\})\Big[1 &+ \sum_{\lambda_s}\rho_{m;\lambda_s}(z,\{\hat{F}_\lambda\})\{F^s(\lambda_s)-\hat{F}^s(\lambda_s)\} \\ &+ \sum_i\sum_{\lambda_f}\rho_{m,i;\lambda_f}(z,\{\hat{F}_\lambda\})\{F^f(i;\lambda_f)-\hat{F}^f(i;\lambda_f)\} \\ &+ \sum_i\sum_h\sum_{\lambda_\ell}\rho_{m,i,h;\lambda_\ell}(z,\{\hat{F}_\lambda\})\{F^\ell(i,h;\lambda_\ell)-\hat{F}^\ell(i,h;\lambda_\ell)\} \\ &+ \text{higher order terms}\Big], \end{aligned} \tag{3-3}$$

where $\{\hat{F}_\lambda\}$ represents a set of all the related uncertainties at their reference values and a sensitivity function $\rho_{m;\lambda_\xi}(z,\{F_\lambda\})$ is defined such that

$$\rho_{m;\lambda_\xi}(z,\{\hat{F}_\lambda\}) \equiv \frac{1}{g_m(z,\{F_\lambda\})}\ \frac{\partial g_m(z,\{F_\lambda\})}{\partial F^\xi(\lambda_\xi)}\ \Bigg|_{\{F_\lambda\}\ =\ \{\hat{F}_\lambda\}}. \tag{3-4}$$

For sufficiently small deviation of $F^\xi(\lambda_\xi)$, an element $\hat{F}^\xi(\lambda_\xi)$ of $\{\hat{F}_\lambda\}$ may be fixed at its nominal value $\tilde{F}^\xi(\lambda_\xi)$. However, in a case that the value of an uncertainty is not well-localized, the interval of deviation may be divided into a reasonable number of subintervals in each of which a reference value is chosen so that a set of the values of uncertainties $\{F_\lambda\}$ for which a fuel pin gap is evaluated with expression (3-3) are always in the neighbourhood of

$\{\hat{F}_\lambda\}$. Then, the higher order terms in expression (3-3) which correspond to cross correlations of more than two uncertainties with $g_m(z,\{F_\lambda\})$ become of less significance. The effect of neglecting those higher order terms on $g_m(z,\{F_\lambda\})$ is discussed numerically in section 3.4.2. Values of sensitivity functions $\rho_{m;\lambda_\xi}(z,\{\hat{F}_\lambda\})$ for all m and ξ at necessary reference sets $\{\hat{F}_\lambda\}$ can be computed using MULTIBOW-3D code explained in section 2.2.7. Discussion on the results of numerical calculations is to be given in section 3.4. It then follows that expression (3-2) with the conditional integration on Ω may be replaced by

$$P(g_m,z) = \int\cdots\int \prod_{\lambda_s} P^s(\lambda_s)\, dF^s(\lambda_s) \prod_i \prod_{\lambda_f} P^f(i;\lambda_f)\, dF^f(i;\lambda_f)$$

$$\times \prod_h \prod_{\lambda_\ell} P^\ell(i,h;\lambda_\ell)\, dF^\ell(i,h;\lambda_\ell)\, \delta\{g_m(z,\{F_\lambda\});(g_m,g_m+dg_m)\}, \quad (3\text{-}5)$$

where $\delta\{g_m(z,\{F_\lambda\});(g_m,g_m+dg_m)\}$ is defined such that

$$\delta\{g_m(z,\{F_\lambda\});(g_m,g_m+dg_m)\} \equiv 1 \text{ if } g_m(z,\{F_\lambda\}) \in (g_m,g_m+dg_m), \quad (3\text{-}6a)$$

$$\equiv 0 \text{ if } g_m(z,\{F_\lambda\}) \notin (g_m,g_m+dg_m). \quad (3\text{-}6b)$$

Once all the necessary values of sensitivity functions are computed, the probabilistic distributions of arbitrary fuel pin gaps in a subassembly may easily be obtained by integrating the product of probabilitic density functions of all uncertainties numerically according to expression (3-5).

For evaluating the measure of deviation in fuel pin gap due to a particular uncertainty $F^\xi(\lambda_\xi)$, we define a normalized pin gap deviation $G_m\{z,F^\xi(\lambda_\xi)\}$ due to $F^\xi(\lambda_\xi)$ such that

$$G_m\{z,F^\xi(\lambda_\xi)\} \equiv \frac{g_m(z,F^\xi(\lambda_\xi)) - g_m(z,\{\tilde{F}_\lambda\})}{g_m(z,\{\tilde{F}_\lambda\})}, \quad (3\text{-}7)$$

where $g_m(z,F^{\xi}(\lambda_{\xi}))$ is the mth fuel pin gap at z with all the related uncertainties fixed at their nominal values except for $F^{\xi}(\lambda_{\xi})$. The corresponding particular sensitivity $\rho_{m;\lambda_{\xi}}(z,\hat{F}^{\xi}(\lambda_{\xi}))$ of $F^{\xi}(\lambda_{\xi})$ at $\hat{F}^{\xi}(\lambda_{\xi})$ to the fuel pin gap under consideration may be computed setting all the reference values of uncertainties equal to the corresponding nominal values except for $\hat{F}^{\xi}(\lambda_{\xi})$ in expression (3-4).

3.3 Computational scheme

Computer program WIREGAP, which computes the sensitivity of uncertainties to pin gaps between any adjacent pairs of fuel pins at arbitrary positions in a fuel subassembly and the corresponding probabilistic pin gap distributions based on the factory data of tolerances, has been completed utilizing the hitherto developed analytical procedures and MULTIBOW-3D program[8]. The brief computational scheme is explained in Table 3.2.

Table 3.2 Flow diagram of WIREGAP code illustrating brief computational schemes.

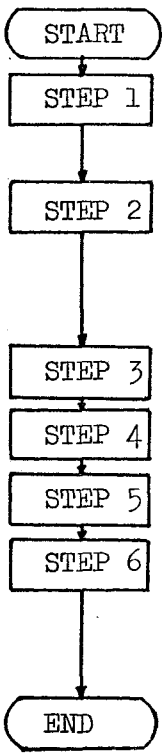

Set nominal parameters, distributions of uncertainties and a reactor operating condition.

Compute pin bundle deflection with thermal and hydraulic characteristics in a reactor operating condition by using MULTIBOW-3D code.

Compute all sensitivity functions $\rho_{m;\lambda_{\xi}}(z,F^{\xi}(\lambda_{\xi}))$.

Select uncertainties of dominant sensitivity.

Check the contributions of higher order terms.

Compute probabilistic distributions of fuel pin gaps, taking all possible combinations based on eqs. (3-3), (3-4) and (3-5).

3.4 Numerical results and discussion

3.4.1 Sensitivity of uncertainties

Sample calculations on the sensitivity of uncertainties to fuel pin gaps in a fuel subassembly have been performed with respect to a typical FBR core based on the currently available factory data of fuel subassemblies for test production[12]. A sector of a fuel pin bundle brought into the present pin gap analyses is schematically shown in Fig. 3.2, where the related nominal geometries, thermal and hydraulic properties and the probabilistic distributions of uncertainties are listed in Tables 3.3 and 3.4, respectively. The design clearance value between any pair of non-deflected fuel pins with an intervening wire spacer is 0.1mm at the initial stage of fuel life. A nominal equilibrium fuel pin configuration in a reactor operating condition is illustrated in Fig. 3.3 with respect to the fuel pins in a corner to corner array of a fuel subassembly under consideration. Fig. 3.4 shows the detailed equilibrium fuel pin configuration in the neighbourhood of the pin gap between a pair of fuel pins 7 and 8 at z* corresponding to the core and upper blanket interface where a cladding hot spot usually appears in a case of an LMFBR core. In the following sections, the effects of the related uncertainties on the pin gap between a pair of fuel pins 7 and 8 at z* and the corresponding normalized pin gap deviations are discussed. Figs. 3.5 ~ 3.9 show particular sensitivities of uncertainties whose effects to the pin gap exceed 0.1 % in normalized pin gap deviation. In these figures, the first and the third quadrants correspond to the increase in the fuel pin gap with respect to its nominal value.

1) Core and subassembly uncertainties

The normalized fuel pin gap deviation due to fuel pin thermal expansion coefficient is of the order of 0.05 % and those due to other uncertainties included in this category are of the order of less than 0.01 %.

Table 3.3 Geometries of fuel subassemblies and thermal-hydraulic parameters employed in the illustrative calculation.

Geometry	
outer diameter of fuel pin (mm)	6.5
diameter of wire spacer (mm)	
inner fuel pin	1.3
peripheral fuel pin	1.0
length of fuel pin (mm)	
lower blanket region	350
core region	930
upper blanket region	300
gas plenum region	1200
number of pins per subassembly	169
number of wire spacers per pin	
inner fuel pin	single
peripheral fuel pin	double
wrapping pitch of spacer wire (mm)	306
wrapping direction of spacer wire	counter-clockwise from the lower end
flat to flat distance of wrapper tube (mm)	104.6
fuel pin gap (mm)	1.4
fuel pin pitch in end supporting matrix (mm)	7.9
initial fuel pin bowing amplitude (mm)	
inner fuel pin	0.25
peripheral fuel pin	0.15

Subassembly Thermal and Hydraulic Data	
peak to ave. power distribution	
radial	flat
axial	1.2
heat generation rate (MW)	4.6
Na-coolant flow rate (kg/sec)	20.2
inlet coolant temperature (°C)	397

Table 3.4 Probabilistic distributions of the normalized uncertainties employed in the illustrative calculation.

Category	Symbol	Distribution of Normalized Uncertainty		
		Type	Mean Value	Deviation Range
core and subassembly uncertainties	$F^s(1)$	chopped normal	1.0	$\pm 1.0 \times 10^{-2}$
	$F^s(2)$	uniform	1.0	± 0.20
	$F^s(3)$	chopped normal	1.0	$\pm 5.0 \times 10^{-3}$
	$F^s(4)$	chopped normal	1.0	$\pm 2.39 \times 10^{-3}$
fuel pin uncertainties	$F^f(i;1)$	chopped normal	1.0	$\pm 4.62 \times 10^{-3}$
	$F^f(i;2)$	chopped normal	1.0	$\pm 7.69 \times 10^{-3}$
	$F^f(i;3)$	nearly uniform	0.993	$+5.06, -8.86 \times 10^{-3}$
	$F^f(i;4)$	nearly uniform*	1.0	$\pm 3.24 \times 10^{-4}$
	$F^f(i;5)$	nearly uniform*	1.0	$\pm 3.24 \times 10^{-4}$
local uncertainties	$F^\ell(i,h;1)$	nearly chopped normal	1.0	$\pm 4.9 \times 10^{-2}$
	$F^\ell(i,h;2)$	nearly chopped normal	0.97	+0.2, -0.6

* Nominal angle is set to be 360°.

2) Fuel pin uncertainties

i) Fuel pin outer diameter and fuel pin pitch at the lower end

The normalized fuel pin gap deviations due to the outer diameter of fuel pins 7 or 8 and the pin pitch at the end supporting matrix are of the order of less than 0.01 % and 0.02 %, respectively. Those due to the uncertainties associated with the fuel pins surrounding the pin pair under consideration are negligible.

ii) Wire spacer diameter

The normalized fuel pin gap deviation due to wire spacer diameter wrapped along a pair of fuel pins 7 and 8 and that of the surrounding fuel pins are about 0.5 % and 0.05 %, respectively and the corresponding particular

sensitivity is shown in Fig. 3.5. In an equilibrium configuration under a reactor operating condition, a pair of fuel pins 7 and 8 make mutual contacts at A and B just above and below z* as illustrated in Fig. 3.4. Since in this particular example, contact point A where the wire spacer of fuel pin 8 is intervening is closer to z* in comparison with contact point B, the wire spacer diameter of fuel pin 8 has more dominant correlation to the fuel pin gap at z* under consideration as in Fig. 3.5. The sensitivity of wire spacer diameter wrapped along fuel pin 9 to the pin gap becomes significant for the normalized deviation exceeding $\pm 5 \times 10^{-3}$. With decrease in wire spacer diameter of fuel pin 9, contact point F indicated in Fig. 3.4 is to be released and fuel pin 8 tends to be displaced to the positive x-direction expanding the pin gap in the equilibrium pin bundle configuration. On the other hand, with increase in wire spacer diameter, fuel pin 9 is to come into contact with fuel pin 8 at I releasing contact point D and consequently fuel pin 8 tends to be locally displaced to the positive x-direction expanding the fuel pin gap. These tendencies correspond to the behaviour of particular sensitivity functions shown in Fig. 3.5.

iii) Fuel pin welding angle at the lower end plug

The normalized fuel pin gap deviation due to fuel pin welding angle at its lower end plug of fuel pin 7 or fuel pin 8 is of the order of 0.1 % and that of the surrounding fuel pins is of 0.01 %. The corresponding particular sensitivity is shown in Fig. 3.6. The effect of the variation in fuel pin welding angle at the lower end plug of fuel pin 8 to the equilibrium pin bundle configuration is as follows: For the normalized deviation within $\pm 0.01/360$, a pin bundle exhibits almost a stationary configuration, however in the vicinity of -0.035/360, fuel pin 8 comes into contact with fuel pin 7 at z=67.7 cm and its deflection mode is such as to expand the fuel pin gap under consideration. Beyond the normalized deviation of -0.08/360, additional

pin contacts between fuel pins 7 and 8 at z=21.8 cm and fuel pins 6 and 7 at z=52.4 cm cause the particular sensitivity being further reduced due to the local displacement of fuel pins 6 and 7 to the positive x-direction. In the vicinity of normalized deviation 0.035/360, fuel pin 8 comes into contact with fuel pin 9 at z=67.7 cm and is locally deflected to the negative x-direction contracting the fuel pin gap. For the normalized deviation exceeding 0.08/360, additional pin contacts between fuel pins 8 and 9 at z=21.8 cm and fuel pins 9 and 10 at z=52.4 cm cause the absolute value of the particular sensitivity being further reduced. The particular sensitivity of the welding angle at the lower end plug of fuel pin 7 shows almost the symmetric characteristics with respect to that of fuel pin 8 as is clear from their geometrical correlation.

iv) Installation angle of a pin end support tube

The particular sensitivity of the installation angle of a pin end support tube shows the similar characteristics to that of the welding angle of a fuel pin end plug as shown in Fig. 3.7. Since the point of deflection is more distant to the fuel pin gap under consideration by the height of a pin end support tube, the effect of the installation angle of a pin end support tube on the equilibrium pin bundle configuration is slightly dominant and the behaviours of particular sensitivity functions are complicated as seen by comparing Fig. 3.7 with Fig. 3.6.

3) Local uncertainties

i) Wrapping pitch of wire spacer

The normalized fuel pin gap deviation due to the local deviation in the wire spacer wrapping pitch of fuel pins 7 and 8 at z=144.2 cm and z=128.9 cm, which are just above and below z^*, is about 0.5 %, while that of the local deviation away from z^* is of the order of less than 0.1 %. Supposing that the wire spacer wrapping pitch of fuel pin 8 locally increases at z=128.9 cm

and then contact point A is shifted upward in Fig. 3.4, fuel pins 7 and 8 are locally deflected due to the constraints at contact points E and F so as to expand the fuel pin gap under consideration. On the other hand, for the downward shift of contact point A due to the local decrease in wire spacer wrapping pitch of fuel pin 8, the pin gap contracts. With the similar reasonings, for the upward shift of contact point E due to the local increase in wire spacer wrapping pitch of fuel pin 7, the pin gap contracts. The corresponding particular sensitivities are shown in Fig. 3.8.

ii) Initial pin bowing

The normalized fuel pin gap deviation due to the initial bowing of fuel pins 7 and 8 is about 1.0 % and that of fuel pin 9 is about 0.3 %. However, the contribution of the other fuel pins is of the order of less than 0.05 %. The corresponding particular sensitivity is shown in Fig. 9. Supposing that the amplitude of the initial bowing of fuel pin 8 is reduced in the vicinity of the pin gap under consideration, contact point B indicated in Fig. 3.4 is to be released expanding the pin gap. On the other hand, the local increase in the bowing amplitude of fuel pin 8 affects the equilibrium pin bundle configuration in the vicinity of the pin gap under consideration, where contact point B is shifted to the negative x-direction with slight contraction in the pin gap. With the local increase in the initial bowing amplitude of fuel pin 7 in the vicinity of the pin gap under consideration, contact point B indicated in Fig. 3.4 is to be released expanding the pin gap and with the local decrease, the pin gap contracts.

3.4.2 Evaluation of higher order terms

In order to evaluate the contribution of higher order terms appeared in expression (3-3) which correspond to cross-correlation of more than two uncertainties to the pin gap under consideration, several sets of uncertainties listed in Table 3.5 whose contributions are comparatively dominant have

been taken into consideration in evaluating the pin gap based on expression (3-3) with and without higher order terms. The results are summarized in Table 3.5, which indicate that the contributions of higher order terms with the normalized deviation ranges of uncertainties listed are within -0.21 % and +0.16 % of the nominal pin gap.

3.4.3 Probabilistic distribution of the pin gap

A probabilistic distribution of the pin gap under consideration was computed based on expression (3-5) with respect to uncertainties whose contributions exceed 0.1 % in normalized fuel pin gap deviation. These uncertainties include $F^{f}(i;2)$, $F^{f}(i;4)$ and $F^{f}(i;5)$ with i=7 and 8, and $F^{\ell}(i,h;1)$ and $F^{\ell}(i,h;2)$ with i=7, 8 and 9 and z_h= 128.9 cm and 144.2 cm. In calculating the probabilistic distribution, higher order terms in expression (3-3) are neglected. The result is shown in Fig. 3.10 where $\tilde{g}_m(z^*)$ and g_m^N are the value of the nominal pin gap under consideration in an equilibrium pin bundle configuration with the initial fuel pin bowing amplitude set at the most probable value and the design pin gap value with non-deflected pin bundle configuration, respectively. Here, attention should be paid that the probabilistic distribution of the fuel pin gap under consideration, which corresponds to the cladding hottest spot in the center fuel subassembly, is shifted to the narrower gap side though the distributions of uncertainties considered are almost symmetric. This tendency is due to the confinement of fuel pins within a wire-spaced fuel pin bundle of an externally bounded system with a wrapper tube and should be considered in thermal design of a FBR core.

3.5 Conclusions

Some of the conclusions obtained through present studies are as follows: (i) Most sensitive uncertainties affecting a fuel pin gap in a reactor operating condition are initial bowing amplitude of a fuel pin, wrapping pitch

of a wire spacer, diameter of a wire spacer, installation angle of a fuel pin end support tube and fuel pin welding angle at the lower end plug.

(ii) A pin gap is affected mostly by fuel pin uncertainties associated with a pair of fuel pins whose pin gap is under consideration and the corresponding local uncertainties in the vicinity of the pin gap.

(iii) The contribution of higher order terms in expression (3-3) to the pin gap is approximately 0.2 % of the nominal value. A sufficiently accurate pin gap may usually be obtained without higher order terms.

(iv) With the reliability level of 99.87 %, the maximum deviation of the pin gap at the cladding hot spot of a fuel subassembly under consideration is 8.05 % from the design nominal value g_m^N.

(v) The probabilistic distribution of a fuel pin gap tends to shift to the narrower side due to the confinement of fuel pins of an externally bounded system though the probabilistic distributions of the related uncertainties are almost symmetric.

Table 3.5 Comparison of calculated fuel pin gaps with and without higher order terms in expression (3-3).

Case	Deviated Uncertainty		$\{g_m(z^*)/g_m^N\}$ with Higher Order Terms	Difference* (%)
	Symbol	Value of Normalized Deviation		
1	$F^f(8;3)$	5.06×10^{-3}	0.9379	-0.0312
	$F^f(8;5)$	3.24×10^{-4}		
2	$F^f(8;3)$	5.06×10^{-3}	0.9376	0.0
	$F^f(7;5)$	-3.24×10^{-4}		
3	$F^f(8;5)$	3.24×10^{-4}	0.9413	-0.0636
	$F^\ell(8,h;2)$	0.2		
4	$F^f(8;4)$	-3.24×10^{-4}	0.9264	-0.195
	$F^f(8;5)$	-3.24×10^{-4}		
	$F^\ell(8,h;2)$	-0.6		
5	$F^f(8;2)$	7.69×10^{-3}	0.9251	-0.214
	$F^f(8;5)$	3.24×10^{-4}		
	$F^\ell(8,h;1)$	3.27×10^{-2}		
	$F^\ell(8,h;2)$	0.2		
6	$F^f(6;4)$	1.39×10^{-4}	0.9241	+0.0171
	$F^\ell(7;5)$	-3.24×10^{-4}		
	$F^\ell(8,h;1)$	3.27×10^{-2}		
	$F^\ell(8,h;2)$	-0.6		
7	$F^s(4)$	2.39×10^{-3}	0.9406	+0.158
	$F^f(7;1)$	4.62×10^{-3}		
	$F^f(8;1)$	4.62×10^{-3}		
	$F^f(6;4)$	3.24×10^{-4}		
	$F^f(9;5)$	-3.24×10^{-4}		
	$F^\ell(8,h;1)$	-4.9×10^{-2}		
	$F^\ell(8,h;2)$	0.2		

* difference in normalized pin gap with and without higher order terms.

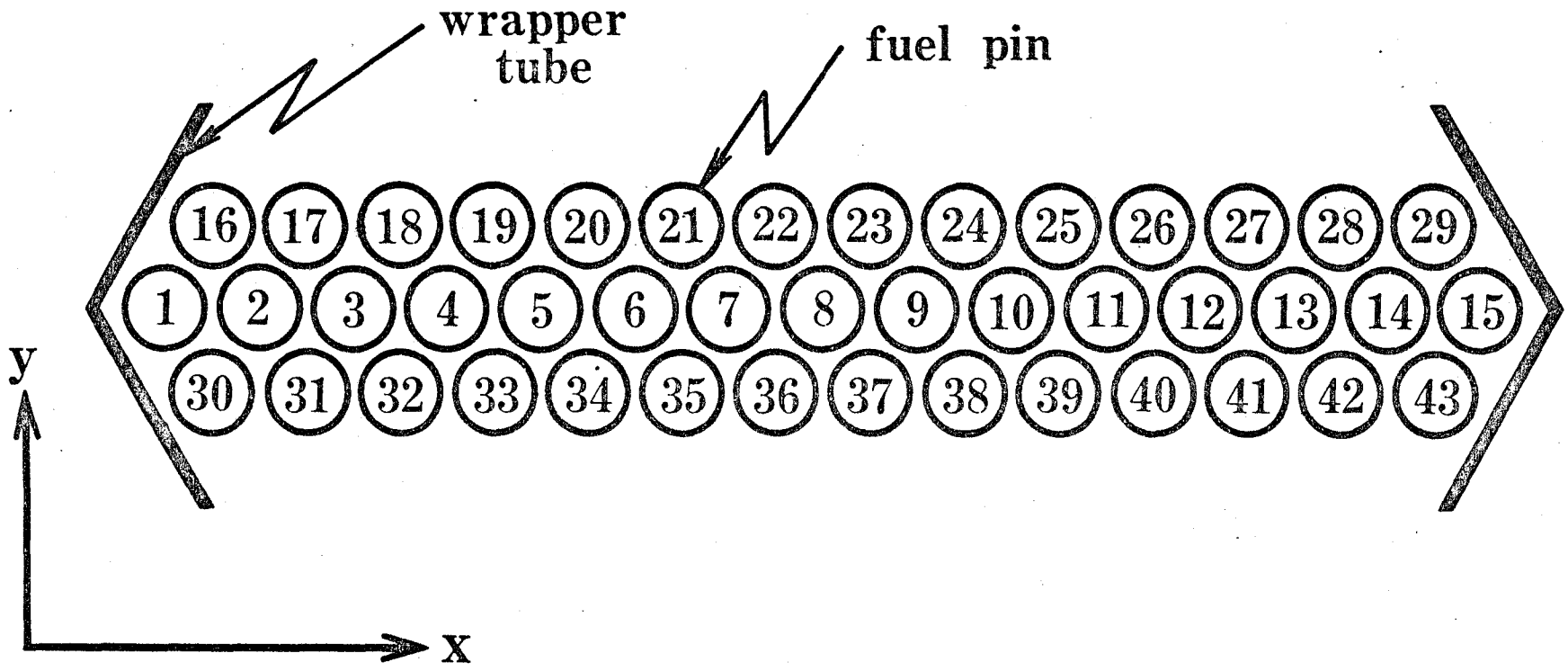

Fig. 3.2 Schematic representation of a sector of fuel subassembly with pin numbers brought into analyses.

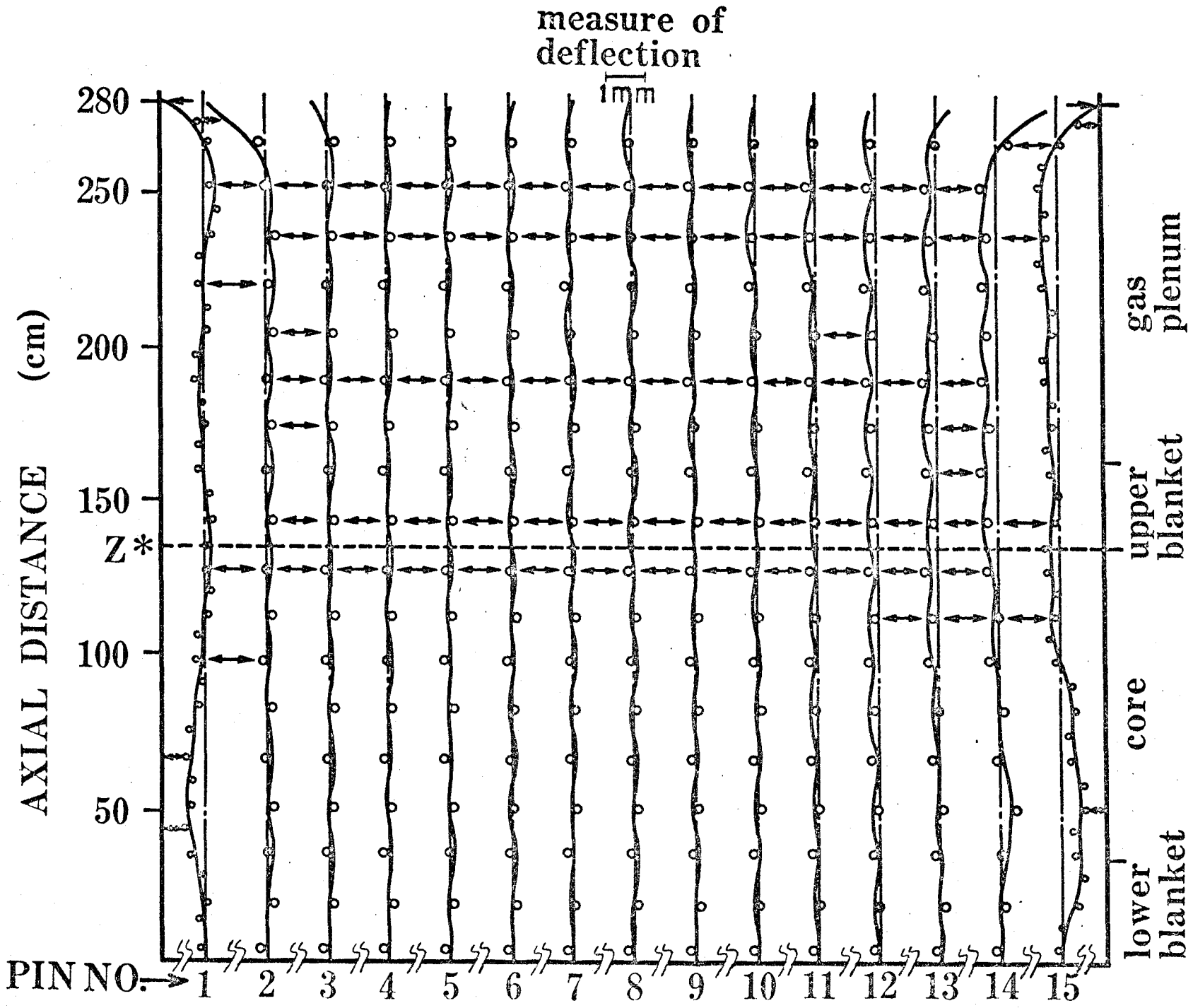

Fig. 3.3 Equilibrium fuel pin configuration in a nominal reactor operating condition.

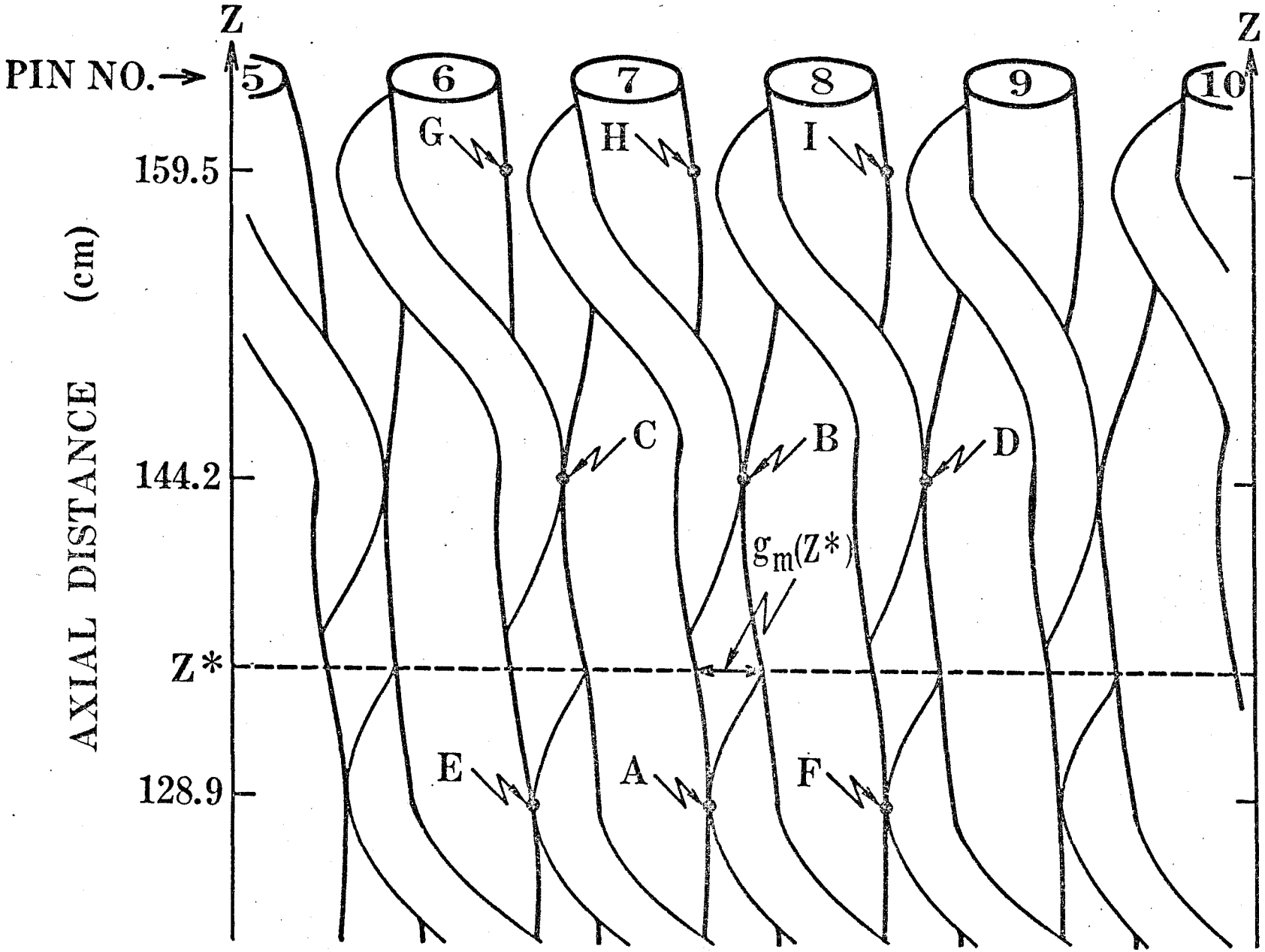

Fig. 3.4 Detailed equilibrium pin bundle configuration in the vicinity of the fuel pin gap under consideration.

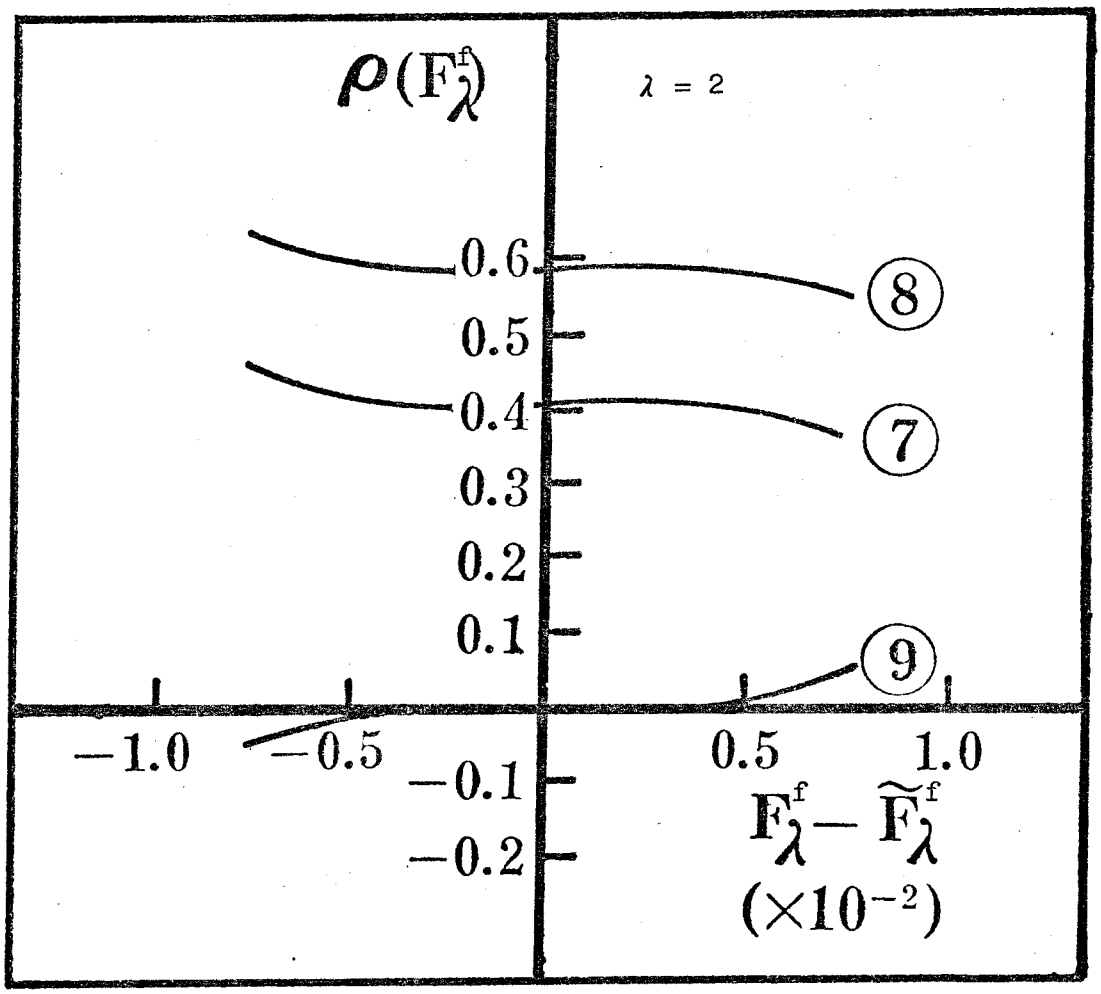

Fig. 3.5 Particular sensitivity of normalized wire spacer diameter to the pin gap under consideration. 7, 8 and 9 indicate fuel pin numbers.

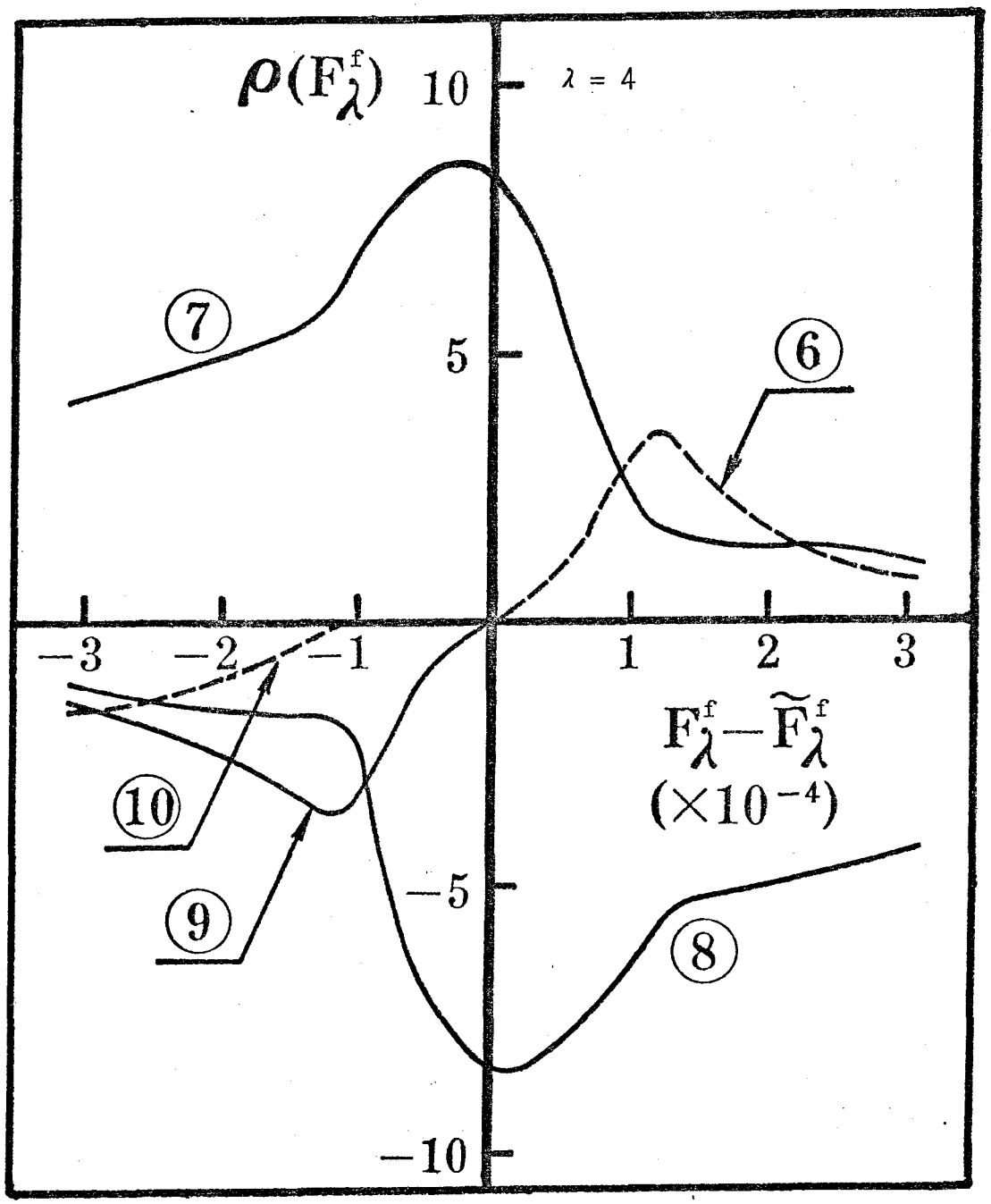

Fig. 3.6 Particular sensitivity of normalized fuel pin welding angle at a lower end plug. 6, 7, 8, 9 and 10 indicate fuel pin numbers.

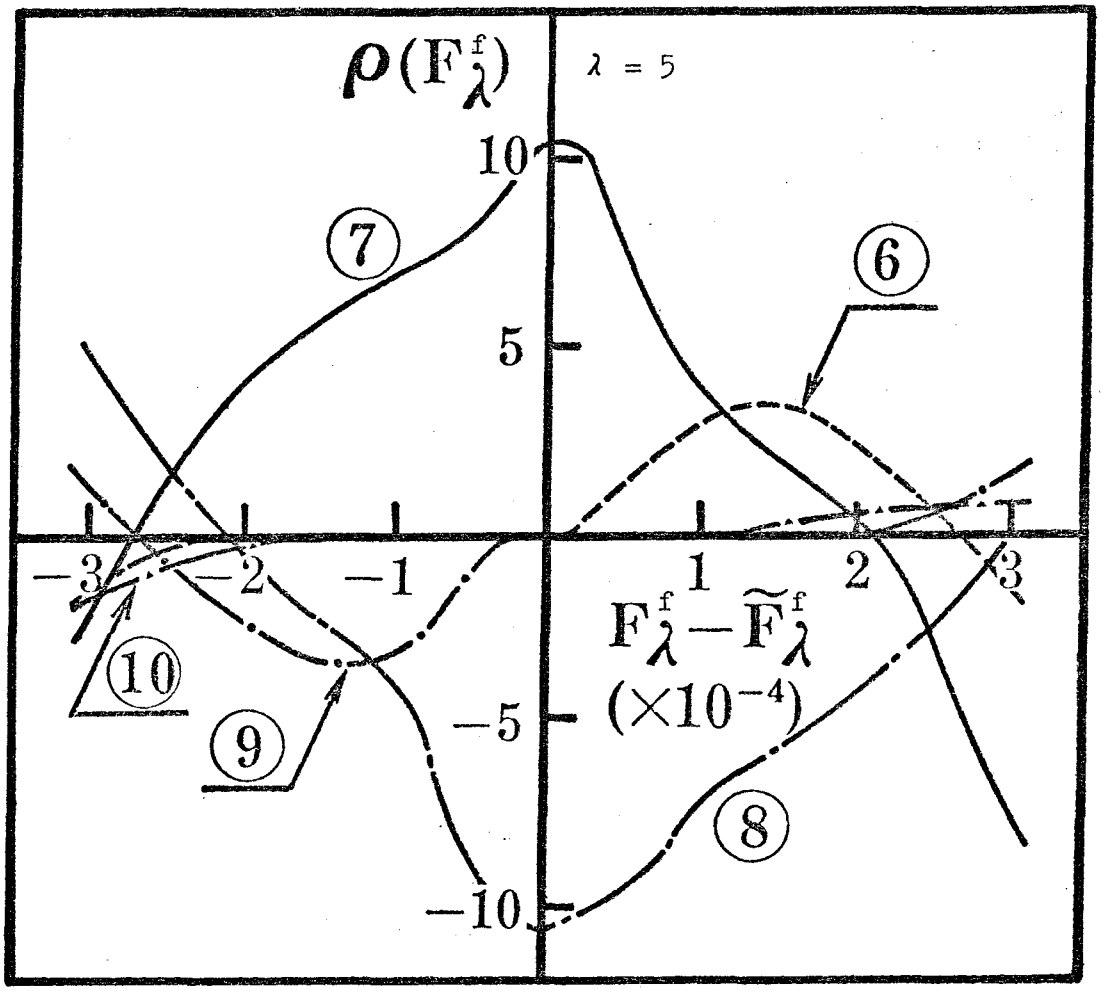

Fig. 3.7 Particular sensitivity of normalized installation angle of a pin end support tube. 6, 7, 8, 9 and 10 indicate fuel pin numbers.

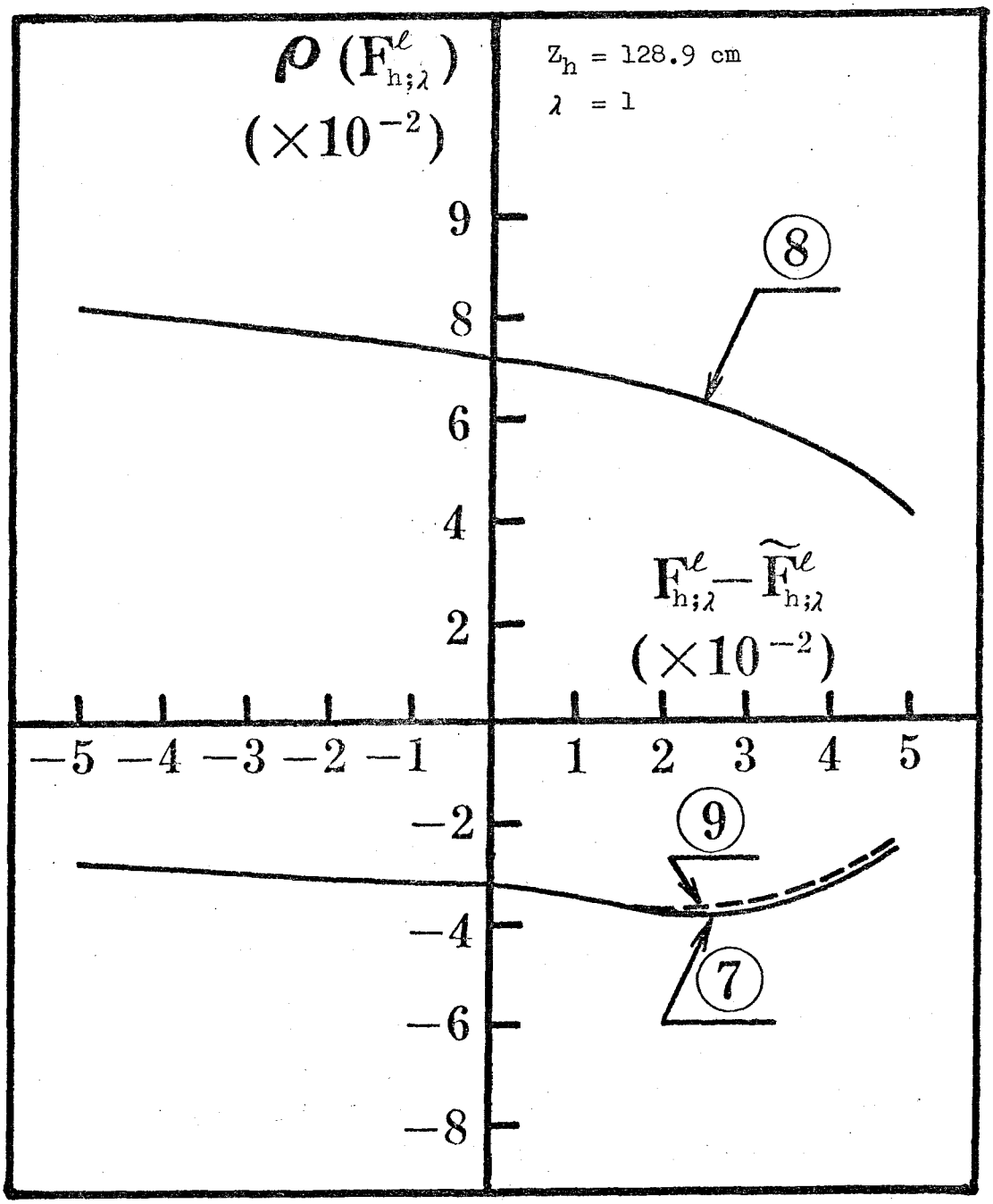

Fig. 3.8 Particular sensitivity of normalized local wrapping pitch of wire spacer. 7, 8 and 9 indicate fuel pin numbers.

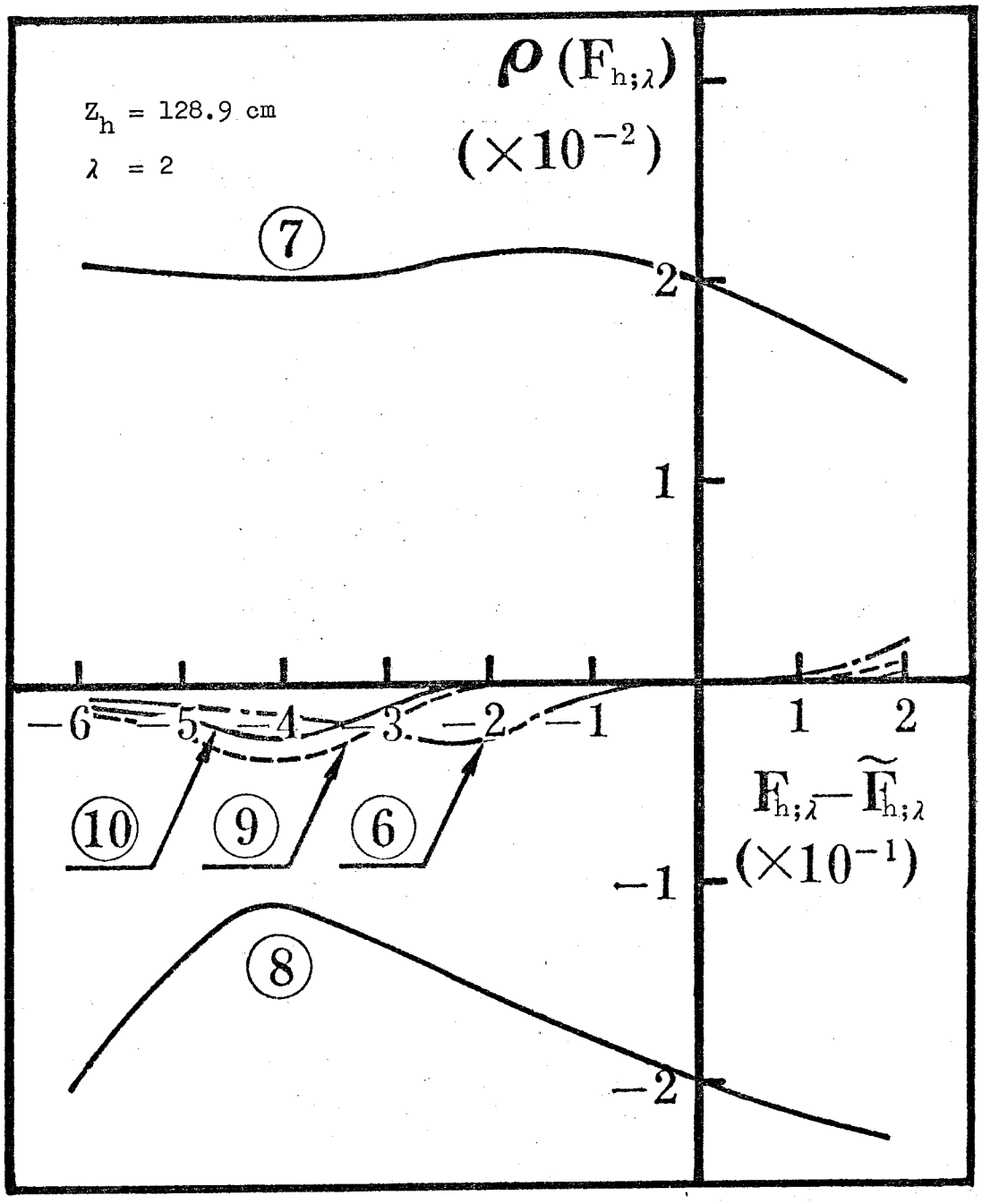

Fig. 3.9 Particular sensitivity of normalized local initial pin bowing. 6, 7, 8, 9 and 10 indicate fuel pin numbers.

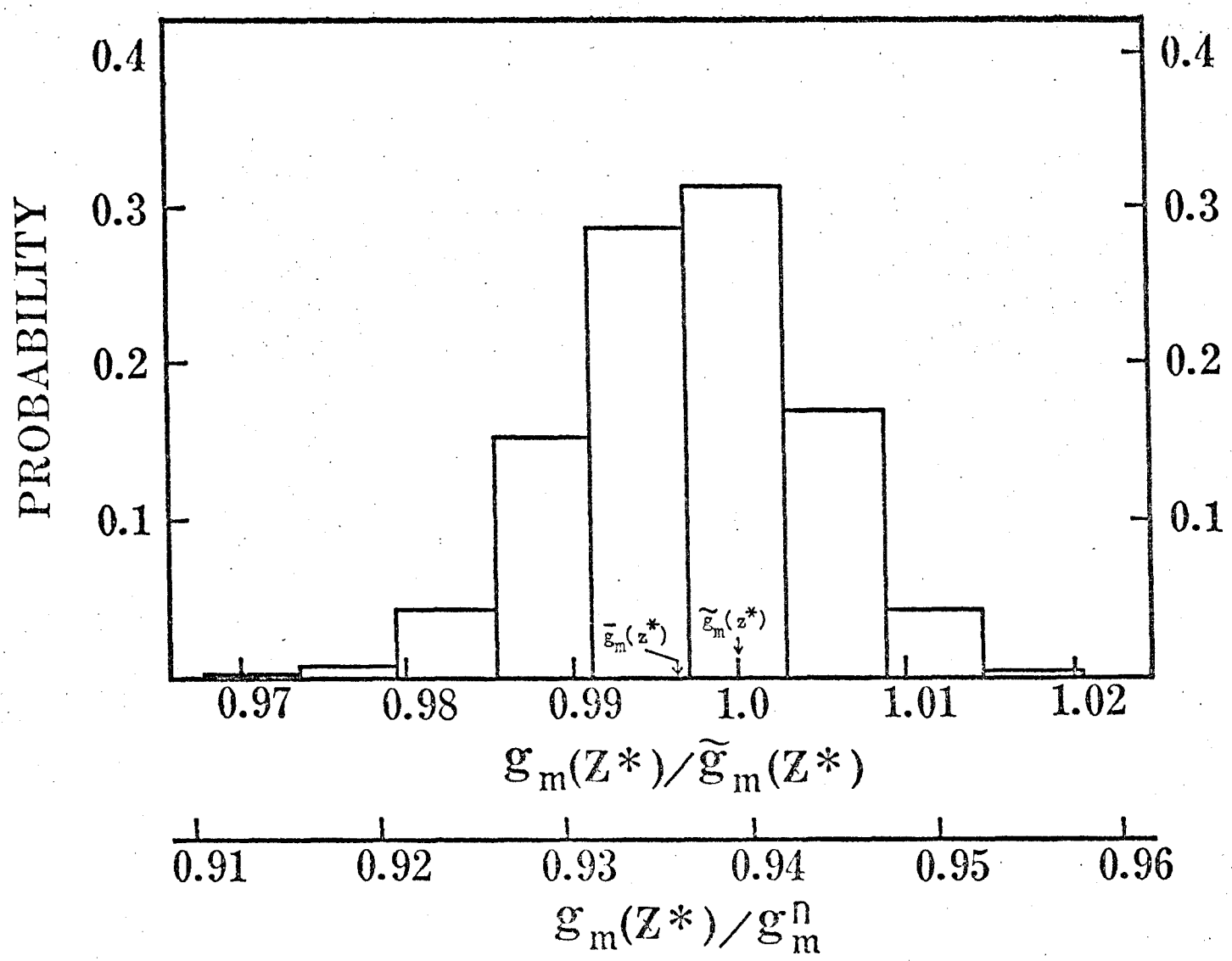

Fig. 3.10 Probabilistic distribution of the pin gap under consideration.

g_m^n: design nominal pin gap under non-deflected pin bundle configuration.

$\tilde{g}_m(z^*)$: nominal pin gap calculated with design nominal values of all core design parameters.

$\bar{g}_m(z^*)$: expectation value of $g_m(z^*)$.

References for Chapter 3

(1) K. Sakai, Y. Okubo and H. Hishida, Development of a Computational Method for Evaluating Fuel Pin Gaps in a FBR Fuel Subassembly, PNC Report SJ206 77-10, Mar. (1977).

(2) K. Sakai, Y. Okubo and H. Hishida, Preliminary Studies on a Probabilistic Distribution of Fuel Pin Gaps within a Wire-Spaced Fuel Subassembly, Trans. of At. Energy Soc. Japan, Oct. (1977) C53.

(3) K. Sakai, Y. Nakai and H. Hishida, Probabilistic Distributions of Fuel Pin Gaps within a Wire-spaced Fuel Subassembly and Sensitivities of the Related Uncertainties to Pin Gaps, Nucl. Eng. Design, 48 (1978) 505.

(4) D. B. Atcheson and M. I. Temme, Core-Wide Statistical Evaluation of the Effect of Uncertainties in Clad Temperature, Material Property Data, and Burnup on the Probability of LMFBR Fuel Rod Failure due to Creep Rupture, Nucl. Eng. Design, 31 (1974) 391.

(5) H. Hishida and M. Higashi, Statistical Evaluation of Pin Gaps in Fuel Clusters for FUGEN, Nucl. Eng. Design, 35 (1975) 191.

(6) K. Sakai, Y. Okubo, H. Hishida, et al., Development of Statistical Evaluating Method on Fuel Pin Gaps within a FUGEN Fuel Subassembly, Trans. of At. Energy Soc. Japan, Oct. (1976) B47.

(7) K. Sakai, Y. Okubo and H. Hishida, Deflection of Wire-Spaced Fuel Pin Bundles, Trans. of A.N.S., 26 (1) (1977) 460.

(8) K. Sakai, Y. Okubo and H. Hishida, Three Dimensional Deflection Analyses of Wire-Spaced Fuel Pin Bundles under Temperature and Hydrodynamical Force Fields with Irradiation Effects, Nucl. Eng. Design, to be published (1978).

(9) J. P. Wei and J. D. Stephen, PACT: A Probabilistic Method for Analysis of LMFBR Coolant and Cladding Temperature Distributions, Trans. of A.N.S. 24 (1976) 346.

(10) A. Amendola, Advanced Statistical Hot Spot Analysis, KFK 1134-EUR 3687 (1970).

(11) K. Sakai and H. Hishida, Probabilistic Evaluation of Core-Internal Coolant Flow Distribution with Correlation Among Fuel Subassemblies, Nucl. Eng. Design, 44 (1977) 235.

(12) Test Production Data for MONJU Fuel Subassemblies, PNC Internal Memo, Feb. (1976).

Chapter 4

Probabilistic evaluation of subassembly coolant flow rates due to the variation of core design parameters

4.1 Introduction

In this chapter, discussion on the inter-subassembly thermal and hydraulic characteristics described in section 1.3.3 will be given. A liquid metal fast breeding reactor is usually provided with orificing devices within coolant flow channels in order to optimize coolant flow rate based on the channel heat generation rates. However, coolant flow rate deviates from the nominal value probabilistically due to manufacturing and assembling tolerances associated with core internals and flow regulating devices and the evaluation on the probabilistic deviation in flow rate of each coolant channel plays an important role in connection to thermal and hydraulic design of the core[1]~[4].

Conventionally, the variation in the coolant flow rate of the hottest channel is evaluated on the tolerances and the corresponding engineering hot spot subfactors are combined with the related subfactors statistically or cumulatively according to their natures to verify the limiting characteristics of the core, where the coolant flow correlations among the hottest and the rest of the channels are not taken into consideration in calculating the pressure drop performance of the hottest channel[5] ~ [8].

In this chapter, the effect of local and global uncertainties on the probabilistic variation in coolant flow rate of the hottest channel or any arbitrary channel is discussed in terms of the coolant flow correlation among all the core-internal coolant channels under the condition of constant coolant flow rate at the core inlet. Uncertainties may include those due to manufacturing and assembling tolerances inherent in core components as well as due

to ambiguity included in material properties and are classified into four categories according to their contribution, similar to Amendola's global hot spot analysis[4], [8], namely (i) core uncertainties, (ii) pressure plenum uncertainties, (iii) flow zone uncertainties, and (iv) subassembly uncertainties. Giving measured or assumed probabilistic distributions of the uncertainties and taking their possible combinations with coolant flow correlations within and among the flow categories, an analytical method of evaluating the probabilistic variation in local coolant flow rate is presented by utilizing the central limit theorem. Here, attention should be paid that some uncertainties of statistical nature might sometimes be treated cumulatively based on engineering judgement in connection to safety consideration. Those uncertainties should be included in evaluating core-internal coolant flow deviation from systematic origins.

For numerical evaluation, a computer programme ORIFS-PFD has been developted [1]~[4]. ORIFS computes the thermal and hydraulic characteristics of a core under the nominal conditions and PFD evaluates the probabilistic variation of subassembly coolant flow rate due to uncertainties. Several cases of sample calculations have been performed in order to compare the deviation in subassembly coolant flow rate based on the conventional one-spot model and the proposed method which takes into consideration the coolant flow correlation among all subassemblies. The results are shown with the corresponding probability of occurrences in terms of the probabilistic distributions of uncertainties.

4.2 Analytical formulation

The procedures of calculating probabilistic coolant flow distribution to be discussed consist of two parts. The first part is concerned with the evaluation of coolant flow rates in various coolant channels and the corresponding temperature distribution under the nominal core condition. The

second part takes into consideration the probabilistic deviation in flow rate and temperature distribution due to manufacturing and assembling tolerances associated with core components. The coolant channels under consideration are schematically shown in Fig. 1.1 and Diagram 4.1. Ambiguity inherent in material properties and experimental data may as well be taken into consideration.

4.2.1 Nominal calculation

Equations of continuity and the conservation of energy and momentum are solved simultaneously for coolant temperature and flow rate distributions through iterative procedures by balancing the pressure difference across each flow channel under the nominal core conditions. The pressure drop is evaluated in terms of experimental data and available formulas.

In calculating the pressure drop across the fuel pin bundle section of a fuel subassembly, edge flow effect is taken into consideration in relation to the momentum balance within a fuel subassembly, where edge flow coefficient f_w is defined such that

$$f_w \equiv \frac{\bar{w}}{\bar{w}_{in}} . \qquad (4\text{-}1)$$

$\bar{w}$ is an averaged coolant flow rate per fuel pin while $\bar{w}_{in}$ is an averaged coolant flow rate per fuel pin belonging to the interior subchannels. f_w is weakly dependent upon subassembly flow rate unless the flat to flat distance of a wrapper tube deviates. Computer programme ORIFS determines pressure drop across each coolant channel as well as the nominal hydraulic resistance coefficients at the normal operating conditions under the condition of constant total coolant flow rate w^T at the core inlet.

4.2.2 Evaluation of pressure loss performance

We consider, in the preceding sections, probabilistic variation in coolant flow rate due to manufacturing and assembling tolerances. Uncertainties to

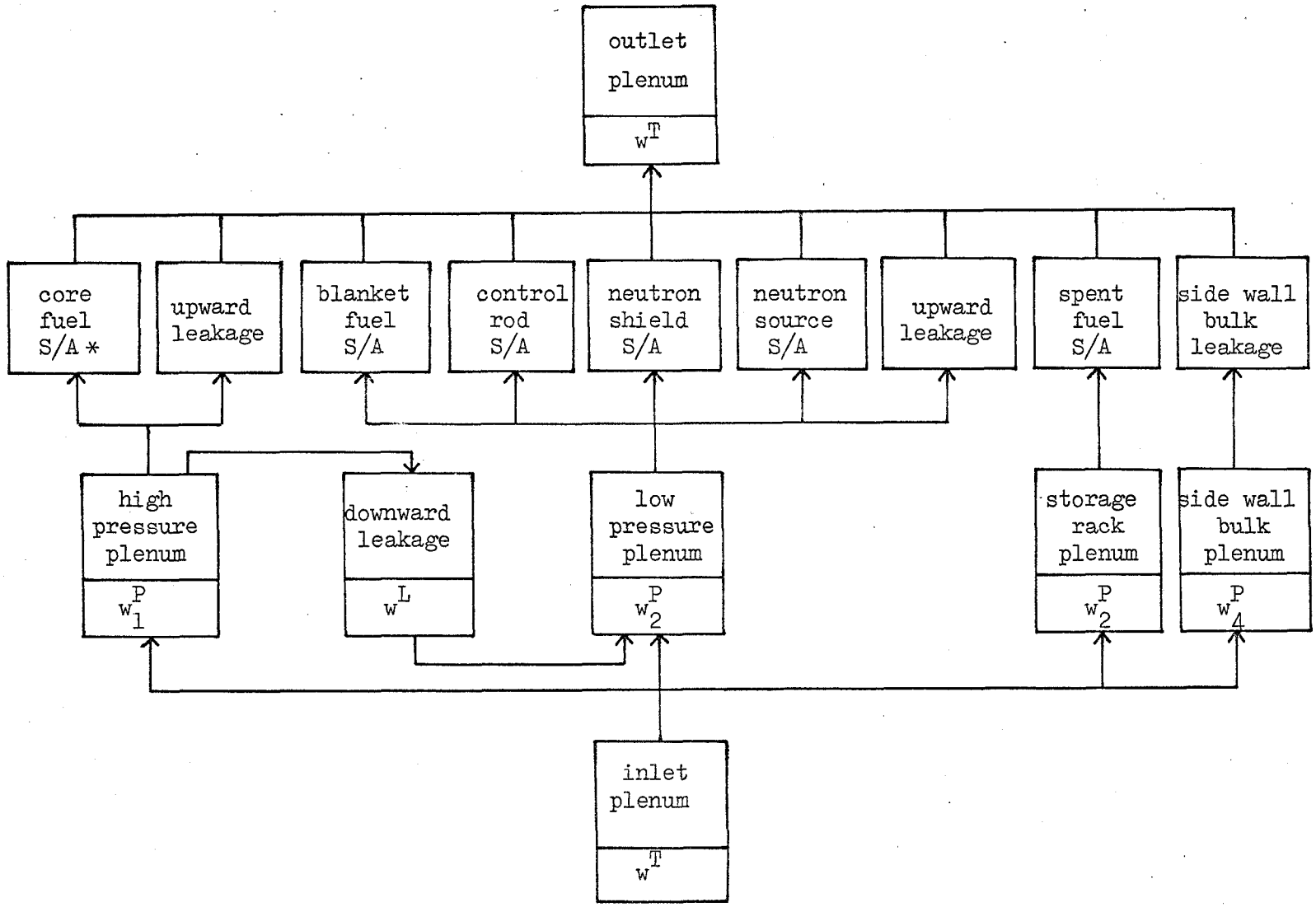

Diagram 4.1 Schematic representation of the core-internal coolant flow channels.

* S/A indicates a subassembly such as a fuel subassembly, a control rod subassembly, etc.

be considered are classified into four categories according to their scope of influence, namely, (i) core uncertainties, (ii) pressure plenum uncertainties, (iii) flow zone uncertainties and (iv) subassembly uncertainties. We define a normalized uncertainty $F(\varepsilon;\lambda)$ such that

$$F(\varepsilon;\lambda) \equiv \frac{\xi(\varepsilon,\lambda)}{\tilde{\xi}(\varepsilon,\lambda)} \quad , \tag{4-2}$$

where $\tilde{\xi}(\varepsilon;\lambda)$ is the nominal value of the λth uncertainty in the εth category and $\xi(\varepsilon;\lambda)$ is a deviated value of the uncertainty in the vicinity of the nominal value $\tilde{\xi}(\varepsilon;\lambda)$. Uncertainties under consideration are listed in Table 4.1.

The pressure drop across flow channels, such as a core fuel subassembly and a blanket fuel subassembly, may in general be expressed in terms of $F(\varepsilon,\lambda)$'s as follows:

across a core fuel subassembly:

$$\begin{aligned}\Delta p_1(1,\nu,\omega) = {} & \alpha^{OR}(1,\nu,\omega)F^s(1,\nu,\omega;2)F^s(1,\nu,\omega;3)F^z(1,\nu;2)\{F^c(1)\}^{-1}w^2(1,\nu,\omega) \\ & + \alpha^{NS}(1,\nu,\omega)\{F^c(1)\}^{-1}F^p(1;1)w^2(1,\nu,\omega) \\ & + \alpha^{FB}(1,\nu,\omega)\{F^c(1)\}^{0.2}\{F^c(2)\}^{-0.8}F^p(1;2)\{F^s(1,\nu,\omega;1)\}^{-1.8}w^{1.8}(1,\nu,\omega) \\ & + \alpha^{Pl}\{w_1^P\}^2 + F^c(1)\,\bar{\rho}(1,\nu,\omega)h_s, \end{aligned} \tag{4-3}$$

across a blanket fuel subassembly:

$$\begin{aligned}\Delta p_2(2,\nu,\omega) = {} & \alpha^{OR}(2,\nu,\omega)F^s(2,\nu,\omega;2)F^s(2,\nu,\omega;3)F^z(2,\nu;2)\{F^c(1)\}^{-1}w^2(2,\nu,\omega) \\ & + \alpha^{NS}(2,\nu,\omega)\{F^c(1)\}^{-1}F^p(2;1)w^2(2,\nu,\omega) \\ & + \alpha^{FB}(2,\nu,\omega)\{F^c(1)\}^{0.2}\{F^c(2)\}^{-0.8}F^z(2,\nu;1)\cdot \\ & \cdot\{F^s(2,\nu,\omega;1)\}^{-1.8}w^{1.8}(2,\nu,\omega)+F^c(2)\,\bar{\rho}(2,\nu,\omega)h_s. \end{aligned} \tag{4-4}$$

Table 4.1 Classification of uncertainties. Keys: p.ℓ.c. = pressure loss coefficient, ν_0 = number of flow zones of blanket fuel region, $\nu_1 = \nu_0$ + number of flow zones consisting of control rod S/A, $\nu_2 = \nu_1$ + number of flow zones of neutron shield region, $\nu_3 = \nu_2$ + number of flow zones consisting of neutron sources.

category	symbol	specification of uncertainties
core	$F^c(1)$	coolant density
	$F^c(2)$	coolant kinematic viscosity
pressure plenum	$F^p(1;1)$	p.ℓ.c. of core fuel S/A* axial neutron shield
	$F^p(1;2)$	p.ℓ.c. of core fuel S/A pin bundle
	$F^p(1;3)$	p.ℓ.c. of downward leakage from high pressure plenum
	$F^p(1;4)$	p.ℓ.c. of upward leakage from high pressure plenum
	$F^p(2;1)$	p.ℓ.c. of blanket fuel S/A axial neutron shield
	$F^p(2;2)$	p.ℓ.c. of depressurizing mechanism for low pressure plenum
	$F^p(2;3)$	p.ℓ.c. of upward leakage from low pressure plenum
	$F^p(3;1)$	p.ℓ.c. of depressurizing mechanism for storage rack plenum
	$F^p(4;1)$	p.ℓ.c. of side wall bulk plenum leakage
flow zone	$F^z(2,\nu;1)$	p.ℓ.c. of blanket fuel S/A pin bundle ($\nu \leq \nu_0$)
	$F^z(2,\nu;1)$	p.ℓ.c. of control rod S/A ($\nu_0 < \nu \leq \nu_1$)
	$F^z(2,\nu;1)$	p.ℓ.c. of neutron shield S/A ($\nu_1 < \nu \leq \nu_2$)
	$F^z(2,\nu;1)$	p.ℓ.c. of neutron source S/A ($\nu_2 < \nu \leq \nu_3$)
	$F^z(\mu,\nu;2)$	p.ℓ.c. of orificing mechanism in S/A entrance nozzle
S/A	$F^s(\mu,\nu,\omega;1)$	p.ℓ.c. of pin bundle section in S/A (due to fabrication tolerances)
	$F^s(\mu,\nu,\omega;2)$	p.ℓ.c. of orificing section in S/A (due to installation tolerances)
	$F^s(\mu,\nu,\omega;3)$	p.ℓ.c. of orificing section in S/A (due to fabrication tolerances)

* S/A indicates a subassembly such as a fuel subassembly, a control rod subassembly, etc.

Pressure drop across other channels, such as a control rod subassembly, a reflector subassembly, a neutron source subassembly and an expended fuel storage rack may also be expressed in similar formulae as expressions (4-3) and (4-4).

$F^{S}(\mu,\nu,\omega;\lambda_{s})$ represents a normalized subassembly uncertainty of the λ_{s}th kind which belongs to the ωth subassembly in the νth flow zone connected to the μth pressure plenum. $F^{Z}(\mu,\nu;\lambda_{z})$, $F^{P}(\mu;\lambda_{p})$ and $F^{C}(\lambda_{c})$ represent a normalized flow zone uncertainty of the λ_{z}th kind belonging to the νth flow zone connected to the μth pressure plenum, a normalized plenum uncertainty of the λ_{p}th kind belonging to the μth pressure plenum and a normalized core uncertainty of the λ_{c}th kind, respectively. α^{OR}, α^{NS} and α^{FB} are the nominal hydraulic resistance coefficients across an orificing section, a neutron shield section and a fuel bundle section of a fuel subassembly, respectively. These values are computed in advance with ORIFS code taking into consideration the temperature dependency of coolant properties along the flow channel under consideration. α^{Pl} is the hydraulic resistance coefficient across connecting pipes in the high pressure plenum and is treated constant in the present analysis since the corresponding pressure drop is considerably small. $\overline{\rho}(\mu,\nu,\omega)$ is the averaged coolant density over the axial length of the ωth fuel subassembly in the νth flow zone connected to the μth pressure plenum and is also computed in advance with ORIFS code. h_{s} is the axial length of a subassembly.

4.2.3 Probabilistic variation in coolant flow rate

In order to discuss the probabilistic variation in the coolant flow rate along the τth coolant flow channel, where τ is a sequence number corresponding to (μ,ν,ω) under consideration, let $P(w_{\tau}\,|\,w^{T})$ be the probabilistic density such that the coolant flow rate w_{τ} along the τth channel, such as the τth core subassembly, is included in the interval $(w_{\tau}, w_{\tau}+dw_{\tau})$ under the

condition of constant total coolant flow rate w^T at a reactor core inlet. Then, since w_τ is determined through the flow correlation among all the coolant flow channels, $P(w_\tau|w^T)$ may generally be expressed in terms of the product of probabilistic density functions of all uncertainties listed in Table 4.1 as follows:

$$P(w_\tau|w^T)=\int\cdots\int_{\text{on}\Omega_1}\prod_{\lambda_c}P^c(\lambda_c)dF^c(\lambda_c)\prod_{\mu}\prod_{\lambda_p}P^p(\mu;\lambda_p)dF^p(\mu;\lambda_p)\cdot$$

$$\cdot\prod_{\nu}\prod_{\lambda_z}P^z(\mu,\nu;\lambda_z)dF^z(\mu,\nu;\lambda_z)\prod_{\omega}\prod_{\lambda_s}P^s(\mu,\nu,\omega;\lambda_s)dF^s(\mu,\nu,\omega;\lambda_s). \tag{4-5}$$

In expression (4-5), $P^c(\lambda_c)$, $P^p(\mu;\lambda_p)$, $P^z(\mu,\nu;\lambda_z)$ and $P^s(\mu,\nu,\omega;\lambda_s)$ are probabilistic density functions of the uncertainties $F^c(\lambda_c)$, $F^p(\mu;\lambda_p)$, $F^z(\mu,\nu;\lambda_z)$ and $F^s(\mu,\nu,\omega;\lambda_s)$, respectively. Indicies $\mu,\nu,\omega,\lambda_c,\lambda_p$ and λ_s vary so as to cover all the uncertainties. Ω_1 indicates the integration should conditionally be carried out on F^c, F^p, F^z, and F^s such that the coolant flow rate in the τth subassembly is w_τ and the total coolant flow rate at a reactor core inlet is w^T. However, computational difficulties are involved in carrying through the integration conditionally on Ω_1 appeared in expression (4-5), that is, equations of continuity and conservation of momentum and energy should be solved once for every possible combination of F^c, F^p, F^z and F^s in order to assure whether the integrating condition is satisfied. In order to avoid such computational difficulties, we replace the kernel of expression (4-5) by a probabilistic density function depending conditionally on the coolant pressure drop Δp between the inlet and the outlet plenums.

Suppose $P(\xi|\alpha,\beta,\gamma,\cdots)$ be a conditional probabilistic density that ξ is included in the interval $(\xi,\xi+d\xi)$ under the fixed parametric values of $\alpha,\beta,\gamma,\cdots$, then the expression (4-5) may be rewritten as follows:

$$P(w_\tau|w^T)=\int_{\text{min. values}}^{\text{max. values}}\cdots\cdots\int\prod_{\lambda_c}P^c(\lambda_c)\prod_{\mu}\prod_{\lambda_p}P^p(\mu,\lambda_p)\prod_{\nu}\prod_{\lambda_z}P^z(\mu,\nu;\lambda_z)\cdot$$

$$\cdot P(w_\tau|w^T,\Delta p,F^c,F^p,F^z)d(\Delta p)dF^c(\lambda_c)dF^p(\mu;\lambda_p)dF^z(\mu,\nu;\lambda_z), \quad (4\text{-}6)$$

where F^c, F^p, F^z indicate $F^c(\lambda_c)$'s, $F^p(\mu;\lambda_p)$'s and $F^z(\mu,\nu;\lambda\ )$'s with μ, ν, λ_c, λ_p and λ_z being running indices covering all the uncertainties belonging to the first three categories. Variation in the subassembly uncertainties is implicitly taken into consideration through integrating $P(w_\tau|w^T,\Delta p,F^c,F^p,F^z)$ with respect to Δp. It should be clear that

$$P(w_\tau|w^T,\Delta p,F^c,F^p,F^z)$$

$$=\int_{\text{on }\Omega_2}\cdots\cdots\int\prod_{\mu}\prod_{\nu}\prod_{\omega}\prod_{\lambda_s}P^s(\mu,\nu,\omega;\lambda_s)dF^s(\mu,\nu,\omega;\lambda_s), \quad (4\text{-}7)$$

where Ω_2 indicates that the integration should conditionally be carried out on F^s such that the coolant in the τth subassembly is w_τ and $w^T,\Delta p,F^c$, F^p and F^z are parametrically fixed.

For computational convenience, the kernel in expression (4-6) is further decomposed into the following form according to the multiplication formula:

$$P(w_\tau|w^T)=\int_{\text{min. values}}^{\text{max. values}}\cdots\cdots\int\prod_{\lambda_c}P^c(\lambda_c)\prod_{\mu}\prod_{\lambda_p}P^p(\mu;\lambda_p)\prod_{\nu}\prod_{\lambda_z}P^z(\mu,\nu;\lambda_z)\cdot$$

$$\cdot P(w_\tau|w^z,\Delta p,F^c,F^p,F^z)\cdot P(w^z|w^p,\Delta p,F^c,F^p,F^z)\cdot$$

$$\cdot P(w^p|w^T,\Delta p,F^c,F^p,F^z)dw^z dw^p d(\Delta p)dF^c(\lambda_c)dF^p(\mu;\lambda_p)dF^z(\mu,\nu;\lambda_z).$$

(4-8)

Here, w^z and w^p are the coolant flow rates of the flow zone and the pressure plenum to which the τth subassembly under consideration belongs, respectively.

So far, uncertainties have been expressed in terms of probabilistic density functions. However in representing the results of measurement on

uncertainties, histograms are of direct means. We divide the interval between the maximum and the minimum values of variable ξ into r_0 subintervals and let the midpoint of the rth subinterval be $\xi(r)$, then the probabilistic distribution $\overline{P}(\xi(r)|\alpha,\beta,\gamma,\cdots)$ is defined such that

$$\overline{P}(\xi(r)|\alpha,\beta,\gamma,\cdots) \equiv \int_{\xi(r)-\Delta\xi/2}^{\xi(r)+\Delta\xi/2} P(\xi|\alpha,\beta,\gamma,\cdots)d\xi, \qquad (4\text{-}9)$$

where $\Delta\xi$ corresponds to the width of the subinterval.

1) Computation of $\overline{P}(w_\tau(r)|w^z,\Delta p,F^c,F^p,F^z)$

Based on Bayes' theorem[9], a conditional probabilistic distribution function $\overline{P}(w_\tau(r)|w^z,\Delta p,F^c,F^p,F^z)$ may be expressed as follows:

$$\overline{P}(w_\tau(r)|w^z,\Delta p,F^c,F^p,F^z) = \frac{\overline{P}(w_\tau(r)|\Delta p,F^c,F^p,F^z)\ \overline{P}(w^z|w_\tau(r),\Delta p,F^c,F^p,F^z)}{\overline{P}\ (w^z|\Delta p,F^c,F^p,F^z)}. \qquad (4\text{-}10)$$

$\overline{P}(w_\tau(r)|\Delta p,F^c,F^p,F^z)$ on the right side of eq. (4-10) may easily be calculated according to expressions (4-3) or (4-4) which give the relations between subassembly coolant flow rate and the corresponding pressure loss coefficients under given pressure drop Δp. Here, pressure drop across plenums should be known in order to relate Δp to Δp_1 or Δp_2, in connection to which discussion is to be given later at engineering points of view. Suppose the flow zone under consideration, which includes the τth subassembly, consists of N_z statistically identical subassemblies, then $\overline{P}(w^z|\Delta p,F^c,F^p,F^z)$ may be obtained through taking all the possible combinations of $\overline{P}(w_\tau(r)|\Delta p,F^c,F^p,F^z)$ over N_z subassemblies, namely,

$$\bar{P}(w^Z|\Delta p,F^C,F^P,F^Z)=\sum_{\alpha=0}^{N_Z}\sum_{\beta=0}^{N_Z-\alpha}\cdots\sum_{\eta=0}^{N_Z-\alpha-\beta-\cdots} {}_{N_Z}C_{\alpha}\cdot{}_{N_Z-\alpha}C_{\beta}\cdots{}_{N_Z-\alpha-\beta-\cdots}C_{\eta}$$

$$\cdot[\bar{P}(w_\tau(1)|\Delta p,F^C,F^P,F^Z)]^{\alpha}\cdot[\bar{P}(w_\tau(2)|\Delta p,F^C,F^P,F^Z)]^{\beta}\cdots$$

$$\cdot[\bar{P}(w_\tau(r_o)|\Delta p,F^C,F^P,F^Z)]^{N_Z-\alpha-\beta-\cdots-\eta}\delta\{\overleftarrow{w}^Z,(w^Z,w^Z+\Delta w^Z)\}, \quad (4\text{-}11)$$

where $\overleftarrow{w}^Z$ and ${}_{N_Z}C_{\alpha}$ are defined such that

$$\overleftarrow{w}^Z \equiv \alpha\cdot w(1)+\beta\cdot w(2)+\cdots\cdots+(N_Z-\alpha-\beta-\cdots\cdots-\eta)\cdot w(r_o), \quad (4\text{-}12)$$

$${}_{N_Z}C_{\alpha}\equiv\frac{N_Z!}{(N_Z-\alpha)!\,\alpha!}, \quad (4\text{-}13)$$

and

$$\delta\{\overleftarrow{w}^Z,\ (w^Z,w^Z+\Delta w^Z)\}\equiv 1 \text{ if } \overleftarrow{w}^Z\in(w^Z,w^Z+\Delta w^Z), \quad (4\text{-}14a)$$

$$\equiv 0 \text{ if } \overleftarrow{w}^Z\notin(w^Z,w^Z+\Delta w^Z). \quad (4\text{-}14b)$$

$\bar{P}(w^Z|w_\tau(r),\Delta p,F^C,F^P,F^Z)$ may be calculated without difficulties similar to expression (4-11) by means of keeping the flow rate in the τth subassembly at $w_\tau(r)$ and taking all the possible combinations of probabilistic distributions of the rest of (N_Z-1) subassemblies which belong to the flow zone under consideration.

2) Computation of $\bar{P}(w^Z|w^P,\Delta p,F^C,F^P,F^Z)$

$\bar{P}(w^Z|w^P,\Delta p,F^C,F^P,F^Z)$ may also be expressed based on Bayes' theorem such that

$$\bar{P}(w^Z|w^P,\Delta p,F^C,F^P,F^Z)=\frac{\bar{P}(w^Z|\Delta p,F^C,F^P,F^Z)\cdot\bar{P}(w^P|w^Z,\Delta p,F^C,F^P,F^Z)}{\bar{P}(w^P|\Delta p,F^C,F^P,F^Z)}, \quad (4\text{-}15)$$

where $\bar{P}(w^Z|\Delta p,F^C,F^P,F^Z)$ is already given by expression (4-11). $\bar{P}(w^P|\Delta p,F^C,F^P,F^Z)$ is derived in terms of $\bar{P}(w^Z|\Delta p,F^C,F^P,F^Z)$. Since flow zones are in

general not identical to one another, $P(w_\nu^z(a)|\Delta p,F^c,F^p,F^z)$ should be evaluated for every zone and taking all the possible combinations we have

$$\overline{P}(w^p|\Delta p,F^c,F^p,F^z)$$
$$= \sum_{a_1=1}^{A_1}\sum_{a_2=1}^{A_2}\cdots\sum_{a_{M_z}=1}^{A_{M_z}} \overline{P}(w_1^z(a_1)|\Delta p,F^c,F^p,F^z)\overline{P}(w_2^z(a_2)|\Delta p,F^c,F^p,F^z)\cdots$$
$$\cdots \overline{P}(w_{M_z}^z(a_{M_z})|\Delta p,F^c,F^p,F^z)\,\delta\{\overleftarrow{w}^p,\ (w^p,w^p+\Delta w^p)\}, \qquad (4\text{-}16)$$

where

$$\overleftarrow{w}^p \equiv w_1^z(a_1) + w_2^z(a_2) + \cdots + w_{M_z}^z(a_{M_z}). \qquad (4\text{-}17)$$

Again, $\overline{P}(w^p|w^z(a),\Delta p,F^c,F^p,F^z)$ may be obtained in similar means to expression (4-16) by keeping the flow rate in the flow zone under consideration at $w^z(a)$ and taking all the possible combinations of probabilistic distributions for the rest of (M_z-1) zones which belong to the pressure plenum.

3) Computation of $\overline{P}(w^p|w^T,\Delta p,F^c,F^p,F^z)$

For the fixed total coolant flow rate w^T, the upper and the lower bounds of the pressure drop Δp may be found with the sets of the maximum and the minimum pressure loss coefficients. Then, it follows that $\overline{P}(w^p|w^T,\Delta p,F^c,F^p,F^z)$ may be calculated within the pressure drop interval in terms of $\overline{P}(w^p|\Delta p,F^c,F^p,F^z)$ given by expression (4-16) simply as follows:

$$\overline{P}(w^p|w^T,\Delta p,F^c,F^p,F^z)$$
$$= \sum_{b_1=1}^{T_1}\cdots\sum_{b_{L_p}=1}^{T_{M_p}} \overline{P}(w_1^p(b_1)|\Delta p,F^c,F^p,F^z)\cdots\overline{P}(w_{M_p}^p(b_{M_p})|\Delta p,F^c,F^p,F^z)\cdot$$
$$\cdot\,\delta\{\overleftarrow{w}^T,(w^T,w^T+w^T)\}, \qquad (4\text{-}18)$$

where

$$\overleftarrow{w}^T \equiv w_1^p(b_1) + w_2^p(b_2) + \cdots\cdots + w_{M_p}^p(b_{M_p}), \qquad (4\text{-}19)$$

and b_μ corresponding to W^p under consideration is fixed.

So far, the mathematical derivations are in general, however, in actually calculating the effect of uncertainties on the coolant flow rate distribution, the following assumptions are employed, which are sufficiently reasonable at engineering points of view.

(i) The pressure loss coefficients for leakage flow paths are kept at the minimum values since leakage flow rates are negligible in comparison with the corresponding main flow rates.

(ii) In estimating the flow deviation in high pressure coolant channels, pressure loss coefficients of the low pressure coolant channels are kept constant at their minimum or nominal values since flow rates w_2^p, w_3^p and w_4^p defined in Diagram 4.1 are considerably small in comparison to w_1^p.

Then, a relation of Δp to Δp_1 and Δp_2 previously pointed out is easily given by solving the momentum and mass balance equations within a reactor core under the given Δp and w^T, and w_1^p, w_2^p, w_3^p and w_4^p are simultaneously determined.

(iii) On the other hand, in estimating the flow deviation in low pressure coolant channels, probabilistic variation in pressure loss coefficients of the high pressure coolant channels are taken into consideration through flow correlation.

4.3 Numerical results and conclusions

Computer programme ORIFS-PFD computes the nominal coolant flow rate distribution inside a reactor core and probabilistic deviation in subassembly coolant flow rate due to manufacturing and assembling tolerances, etc. of the core component in connection to the evaluation of hot spot temperature. The programme is based on the computational schemes shown in Diagram 4.2.

Several cases of sample calculation have been performed using ORIFS-PFD code for a prototype LMFBR core in order to compare the deviation in coolant flow rate of a fuel subassembly based on the conventional one-spot model and

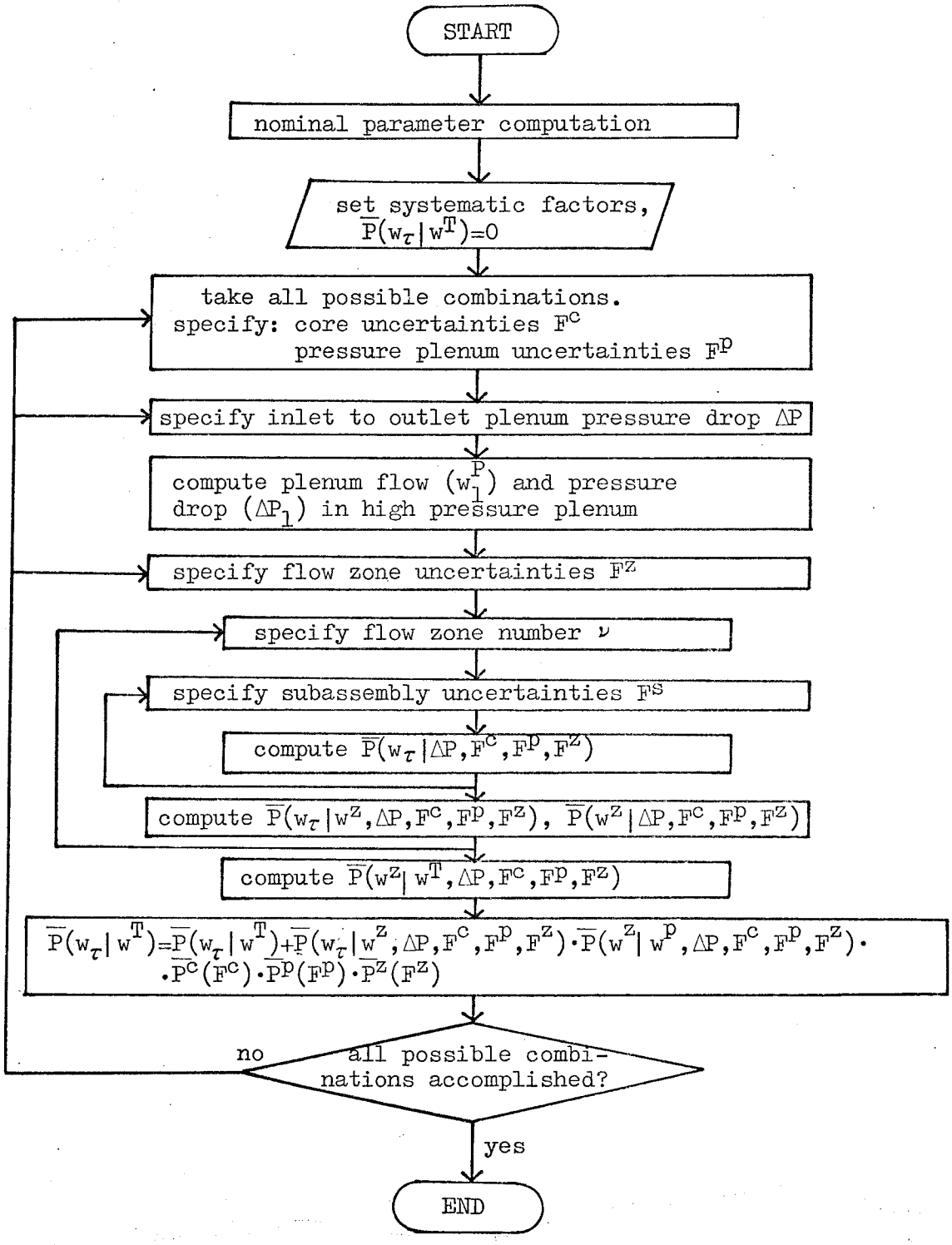

Diagram 4.2 Computational flow diagram for estimating the flow deviation in subassemblies connected to the high pressure plenum.

the proposed method which takes into consideration the coolant flow correlation among all subassemblies. A prototype LMFBR core brought into the current sample calculations consists of 198 core fuel subassemblies, 172 blanket fuel subassemblies and subassemblies associated with control rods, neutron shields and neutron sources. The core fuel subassemblies and the blanket fuel subassemblies are divided into 8 and 3 different flow zones, respectively. Control rod and neutron shield subassemblies belong to another flow zones.

The probabilistic distribution functions for the uncertainties employed in the sample calculations based on the test production and experimental data[10]~[12] are listed in Table 4.2.

4.3.1 Sample calculation 1

The first sample calculation is concerned with the evaluation of the effect of flow correlation among subassemblies. Let a flow zone under consideration consist of N_z subassemblies with statistically identical uncertainties. We estimated the deviation in coolant flow rate of one subassembly which belongs to a subgroup of N_z' subassemblies in the flow zone among which the flow correlation is taken into consideration, while the rest of (N_z-N_z') subassemblies in the flow zone are assumed to have the mean characteristics. In the sample calculation, N_z' is selected to be N_z'=5, 7, 9 and 11. The satisfactory convergence in the coolant flow rate deviation had been found for N_z' being beyond 9, as shown in Fig. 4.1. Consequently, a conclusion may be derived that it is sufficient to apply the central limit theorem in taking into consideration the coolant flow correlation among fuel subassemblies in a flow zone consisting of more than 10 subassemblies of statistically identical characteristics in the case of a prototype FBR core under consideration in connection to evaluating expression (4-11).

4.3.2 Sample calculation 2

Sample calculations on the probabilistic distributions of the core fuel subassembly coolant flow rates $\overline{P}(w_\tau | w^T)$ in every flow zone have been performed. The results are shown in Figs. 4.2 ~ 4.9. Comparison was made on the deviation in coolant flow rate due to uncertainties evaluated based on the conventional method and on the proposed method where the flow correlation over all subassemblies is taken into consideration. Under the conventional method, the coolant flow in the subassembly in which the hottest spot may occur is set to be at the minimum rate with respect to the deviation ranges of all ambiguities.

Flow rate deviation in every flow zone of the core fuel assembly and the corresponding probability of occurrence are shown in Table 4.3, where the minimum appreciable level for the probabilistic flow rate deviation is set to be of the order of 10^{-15} in the present sample calculation. However, the minimum appreciable level should be decided based on safety consideration in the actual design calculations. The computational mesh widths of probability histograms are indicated in Table 4.3 for the results obtained on the proposed method.

4.3.3 Conclusions

Some of the conclusions obtained through present studies with respect to a previously mentioned prototype LMFBR core are as follows:

(i) Setting the minimum appreciable level of probabilistic occurrence to be 10^{-15}, the deviation of the coolant flow rate from the nominal value in a core fuel subassembly is about 30 % smaller than that calculated with the conventional method as shown in Table 4.3.

(ii) It is sufficient to take into consideration the flow correlation among at most 10 fuel subassemblies within one flow zone in evaluating the effect of subassembly uncertainties.

(iii) The hydraulic resistance of an orificing device always deviates to the larger resistance side from its nominal value due to the variation of the installation angle of orificing holes. This deviation shifts the subassembly coolant flow rate under consideration to the lower flow rate side. This tendency is more remarkable in the lower flow rate regions as shown in Figs. 4.2~4.9, since the installation angle of orificing holes affects the hydraulic resistance of an orificing device, where the pressure drop is larger in lower flow rate regions. In a case of the prototype LMFBR core employed in sample calculations, the mean value of the probabilistic distribution of subassembly coolant flow rate deviates from its nominal value by 0.20 % in higher flow rate regions and by 0.57 % in lower flow rate regions as are clear from those figures. The normal distribution of subassembly coolant flow rate assumed in the conventional hot spot analyses should be improved taking into consideration the mutual dependency of core structual parameters through coolant flow correlation within a reactor core based on their actual probabilistic distributions.

(iv) The proposed method may be used to verify the conventional method of hot spot temperature calculation.

Table 4.2 Probabilistic distribution functions for the uncertainties employed in the sample calculations.

Category	Symbol	Distribution		
		Type	Mean Value	Maximum Deviation(%)
core	$F^c(1)$	chopped normal	1.0	± 3
	$F^c(2)$	chopped normal	1.0	± 15
pressure plenum	$F^p(1;1)$	uniform	1.0	± 10
	$F^p(1;2)$	chopped normal	1.0	± 5
	$F^p(1;3)$	δ function	1.0	0
	$F^p(1;4)$	δ function	1.0	0
	$F^p(2;1)$	δ function	0.9	0
	$F^p(2;2)$	δ function	0.95	0
	$F^p(2;3)$	δ function	1.0	0
	$F^p(3;1)$	δ function	0.95	0
	$F^p(4;1)$	δ function	0.95	0
flow zone	$F^z(2,\nu;1)(\nu \leq \nu_0)$	δ function	0.95	0
	$F^z(2,\nu;1)(\nu_0 < \nu \leq \nu_1)$	δ function	0.95	0
	$F^z(2,\nu;1)(\nu_1 < \nu \leq \nu_2)$	δ function	0.95	0
	$F^z(2,\nu;1)(\nu_2 < \nu \leq \nu_3)$	δ function	0.95	0
	$F^z(1,\nu;2)$	chopped normal	1.0	± 6
	$F^z(2,\nu;2)$	δ function	0.95	0
S/A	$F^s(1,\nu,\omega;1)$	chopped normal	1.0	± 0.5
	$F^s(\mu,\nu,\omega;1)(2 \leq \mu \leq 4)$	δ function	1.0	0
	$F^s(1,\nu,\omega;2)$	linearly decending	1.01	+3
	$F^s(\mu,\nu,\omega;2)(2 \leq \mu \leq 4)$	δ function	1.0	0
	$F^s(1,\nu,\omega;3)$	chopped normal	1.005	+1
	$F^s(\mu,\nu,\omega;3)(2 \leq \mu \leq 4)$	δ function	1.0	0

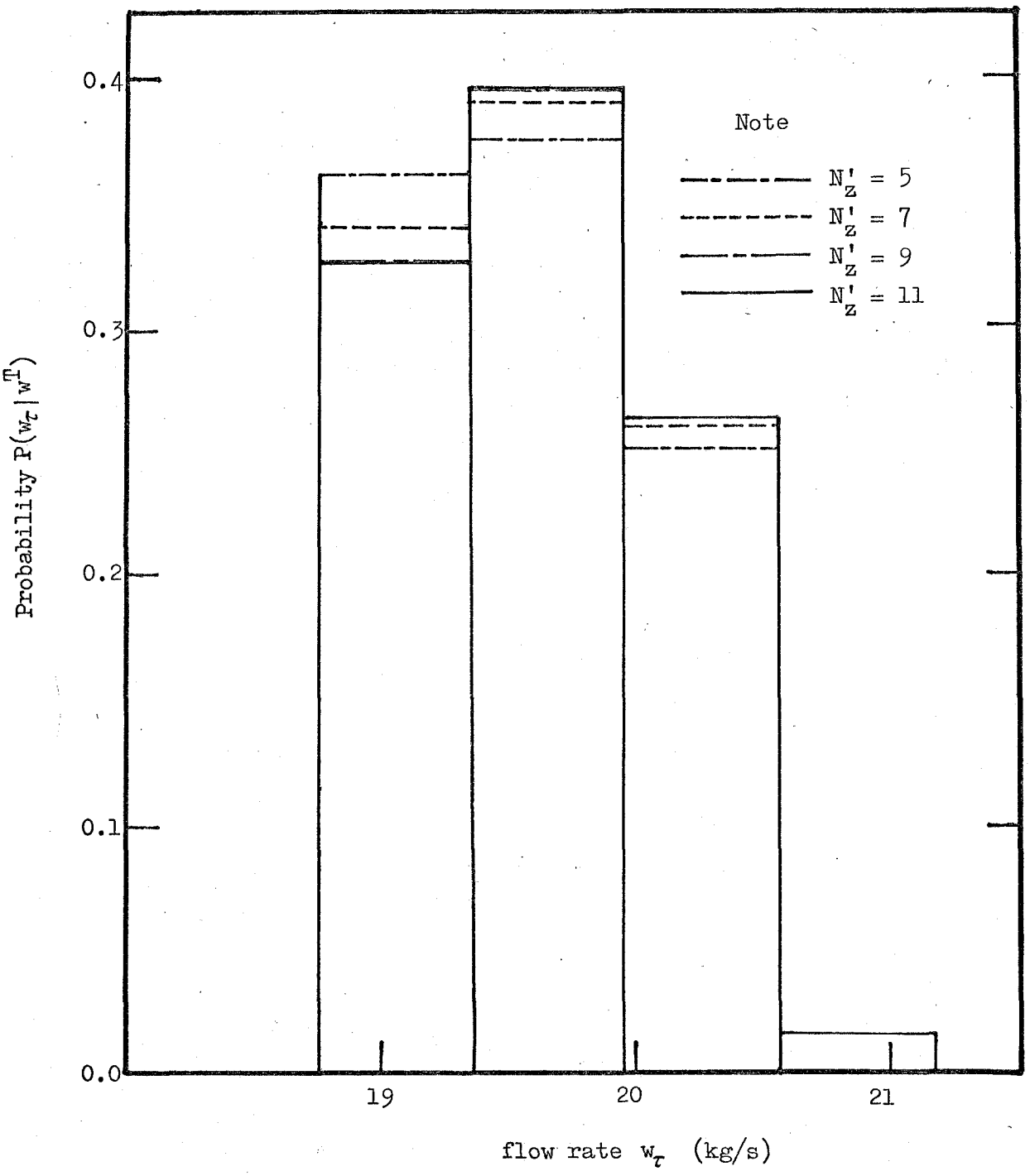

Fig. 4.1 The scale effect of flow correlation among a group of subassemblies.
N'_z is the number of subassemblies in one flow zone among which the flow correlation is taken into consideration.

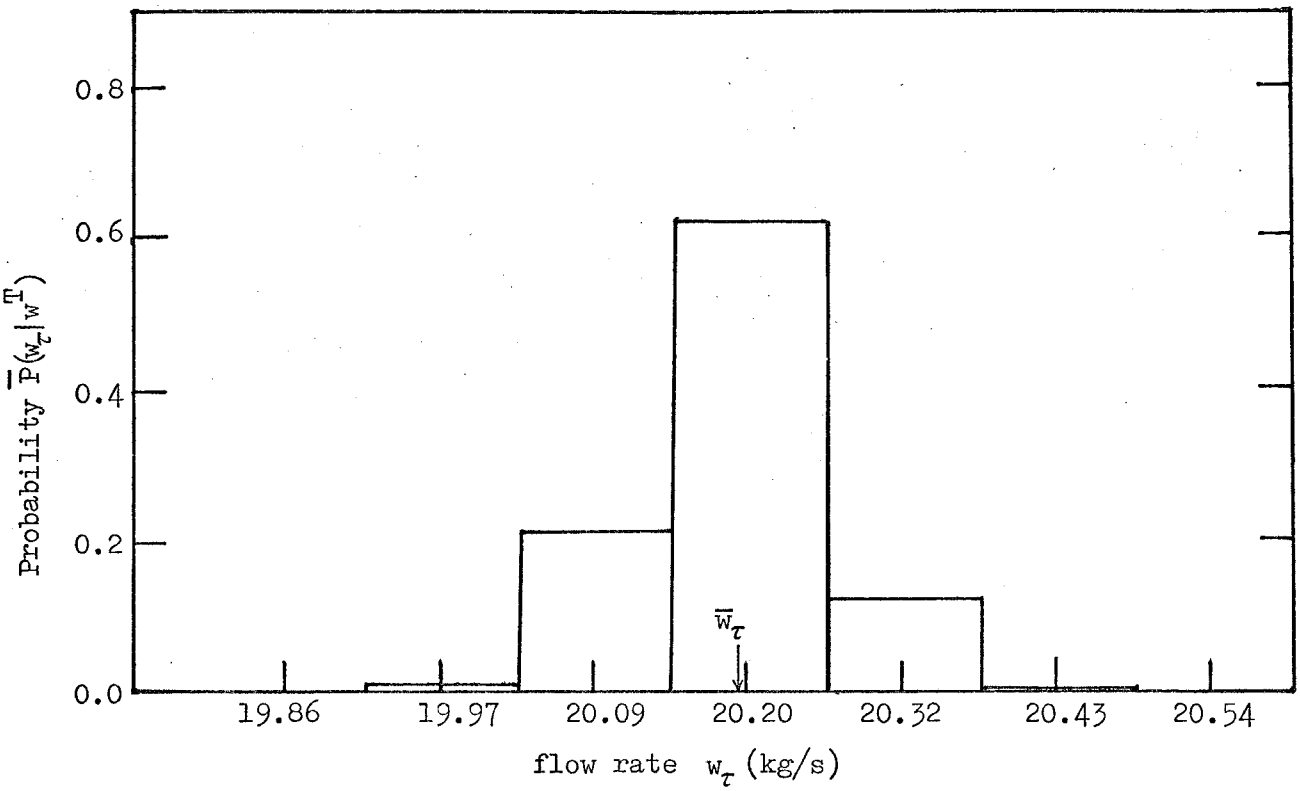

Fig. 4.2 Probabilistic distribution of fuel subassembly coolant flow rate (flow zone 1). $\overline{w}_\tau$ is expectation value of w_τ.

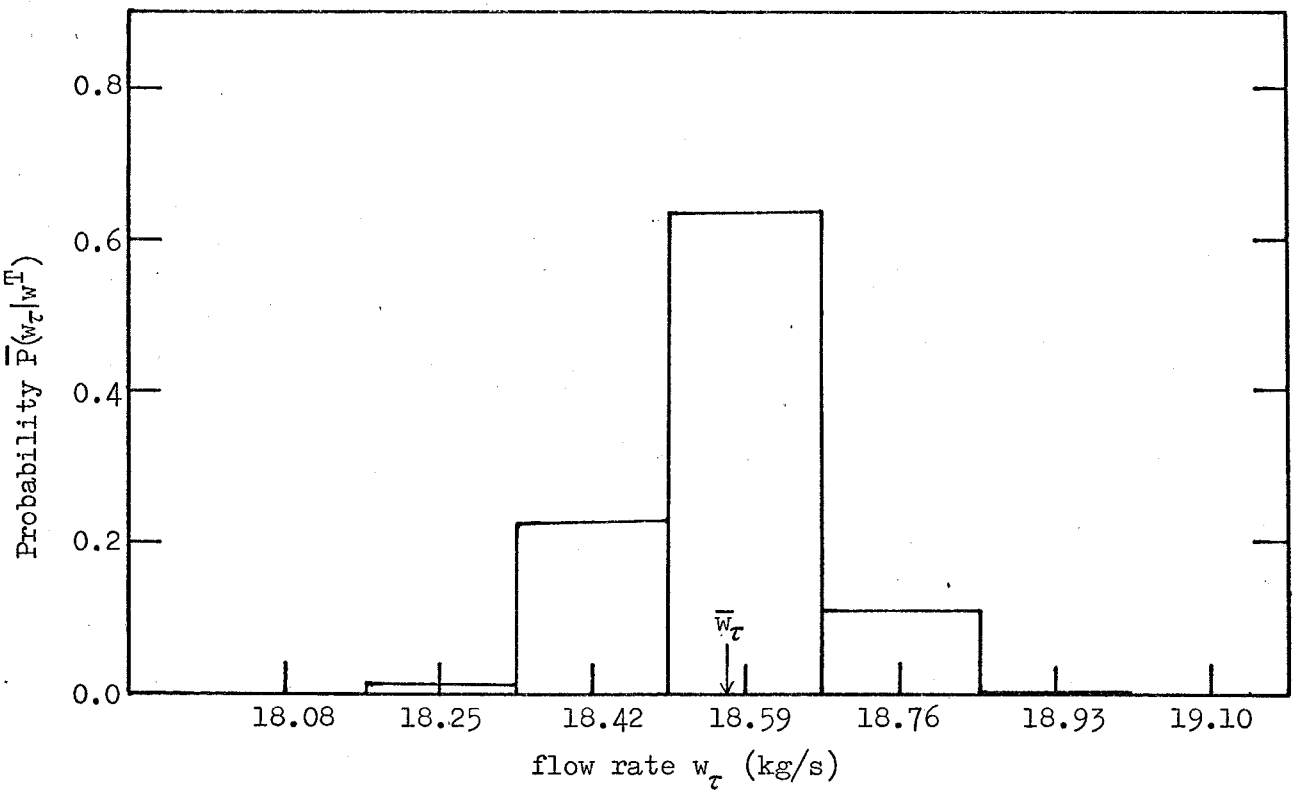

Fig. 4.3 Probabilistic distribution of fuel subassembly coolant flow rate (flow zone 2). $\overline{w}_\tau$ is expectation value of w_τ.

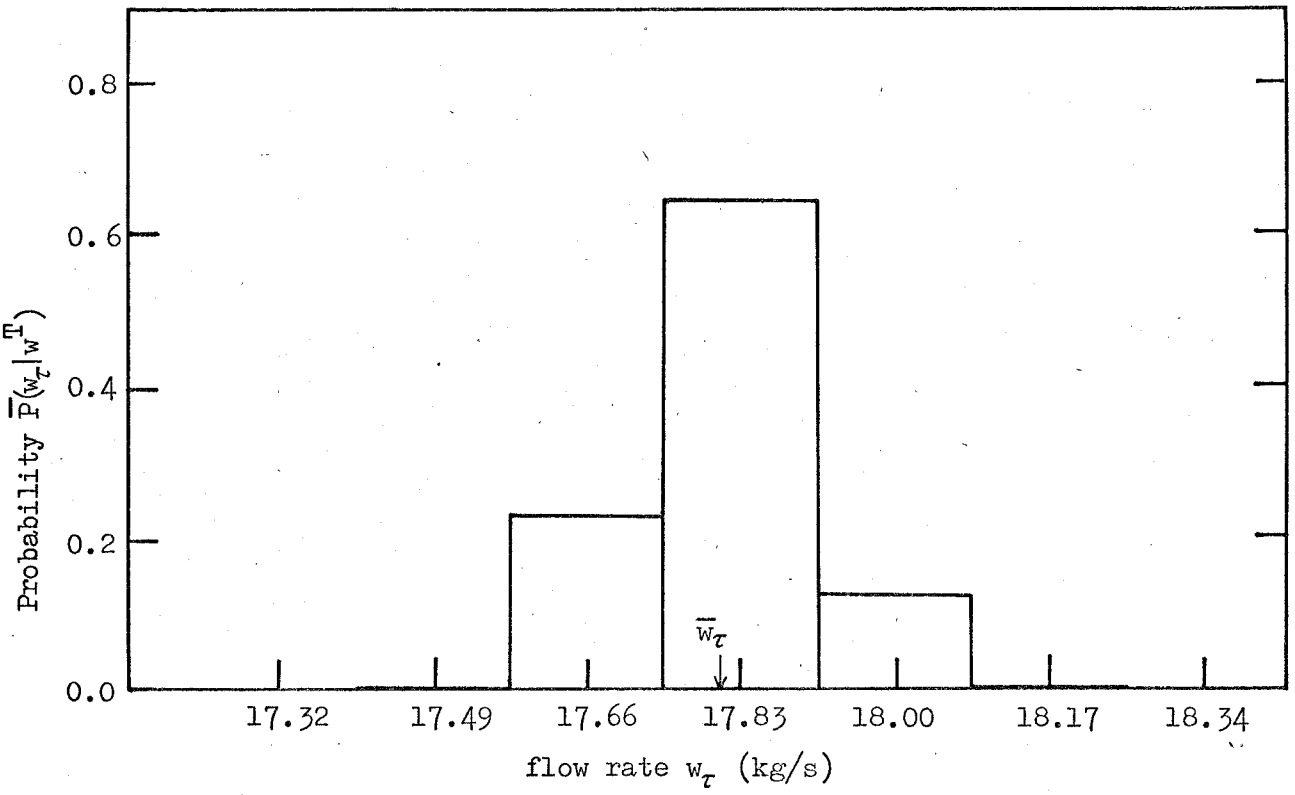

Fig. 4.4 Probabilistic distribution of fuel subassembly coolant flow rate (flow zone 3). $\overline{w}_\tau$ is expectation value of w_τ.

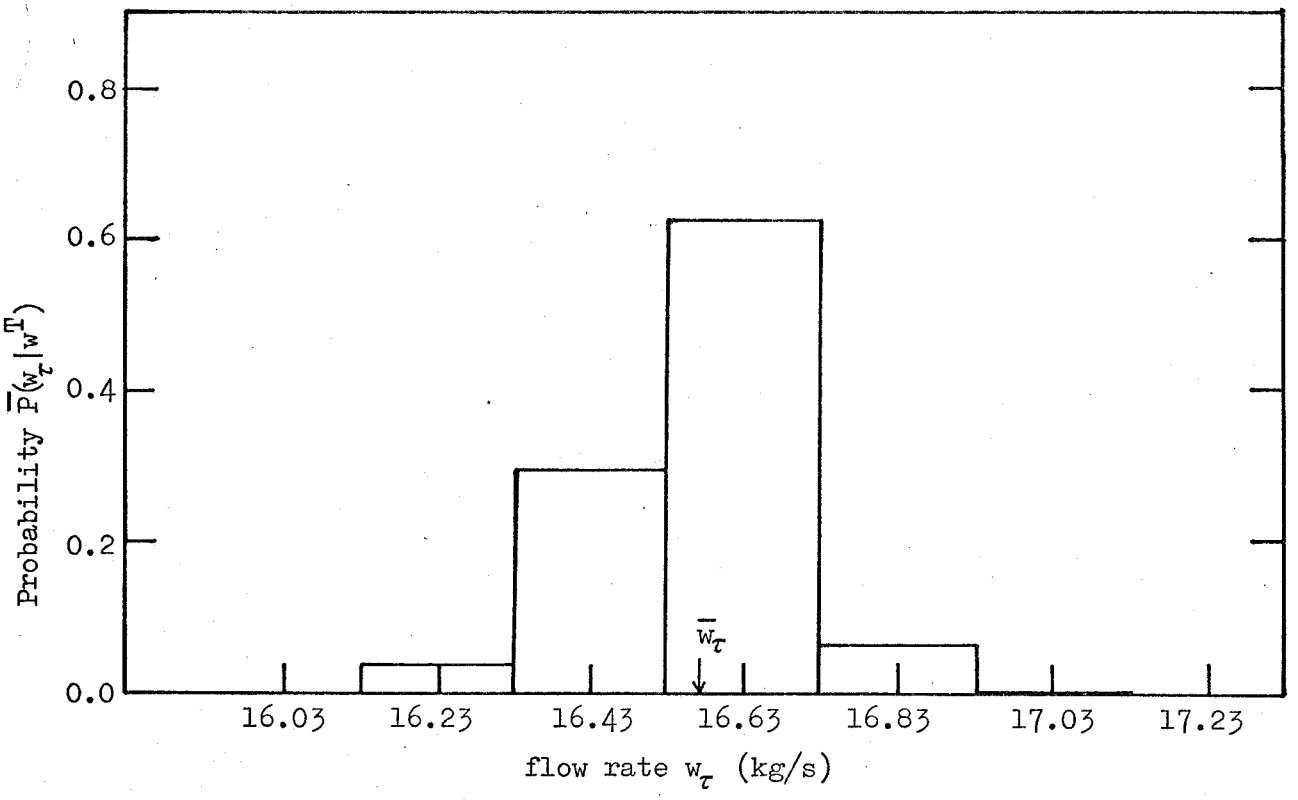

Fig. 4.5 Probabilistic distribution of fuel subassembly coolant flow rate (flow zone 4). $\overline{w}_\tau$ is expectation value of w_τ.

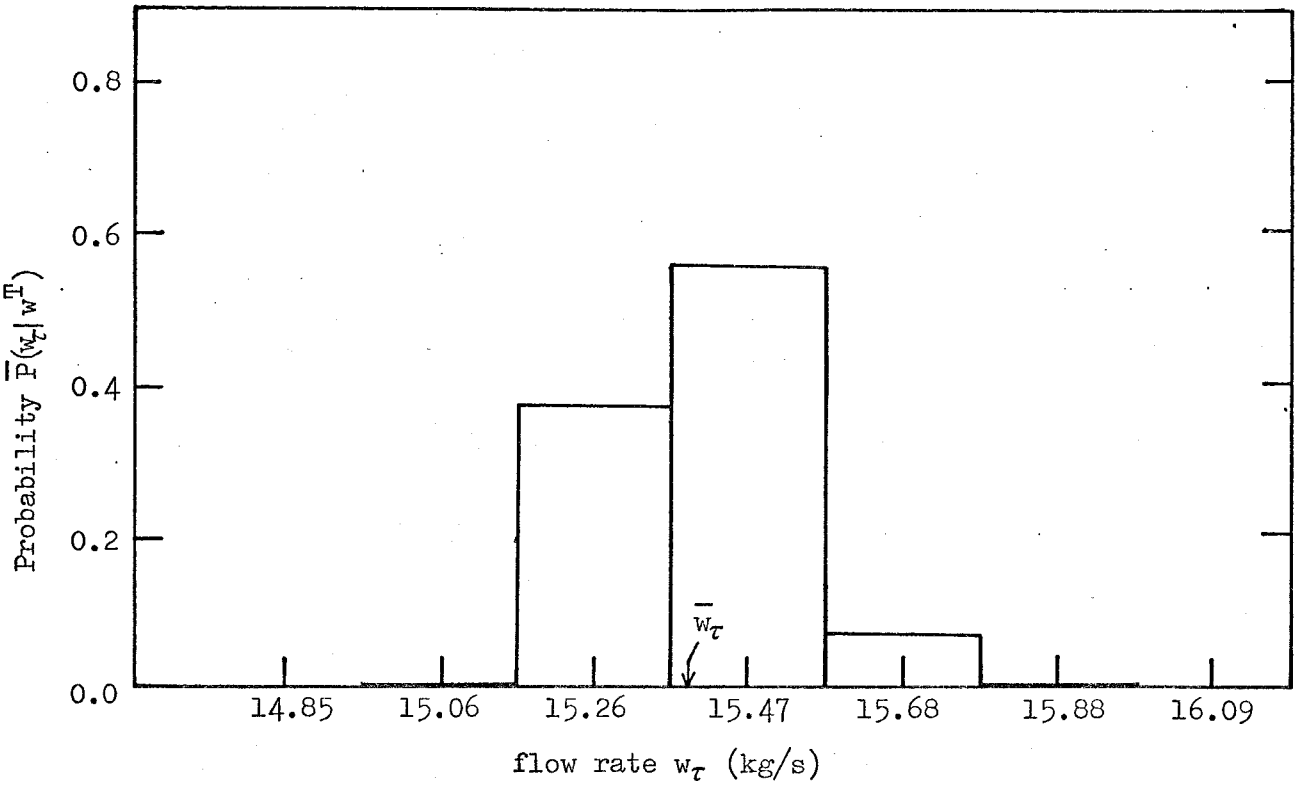

Fig. 4.6 Probabilistic distribution of fuel subassembly coolant flow rate (flow zone 5). $\overline{w}_\tau$ is expectation value of w_τ.

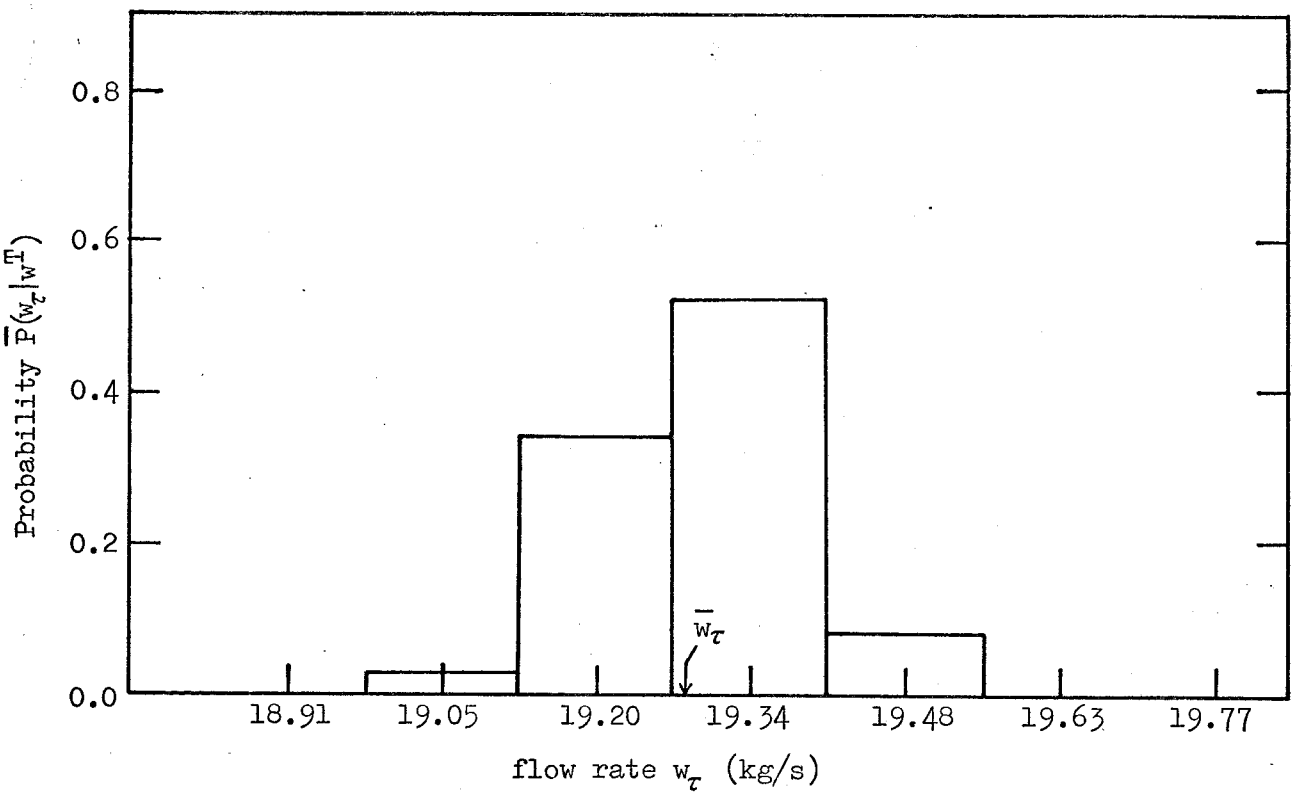

Fig. 4.7 Probabilistic distribution of fuel subassembly coolant flow rate (flow zone 6). $\overline{w}_\tau$ is expectation value of w_τ.

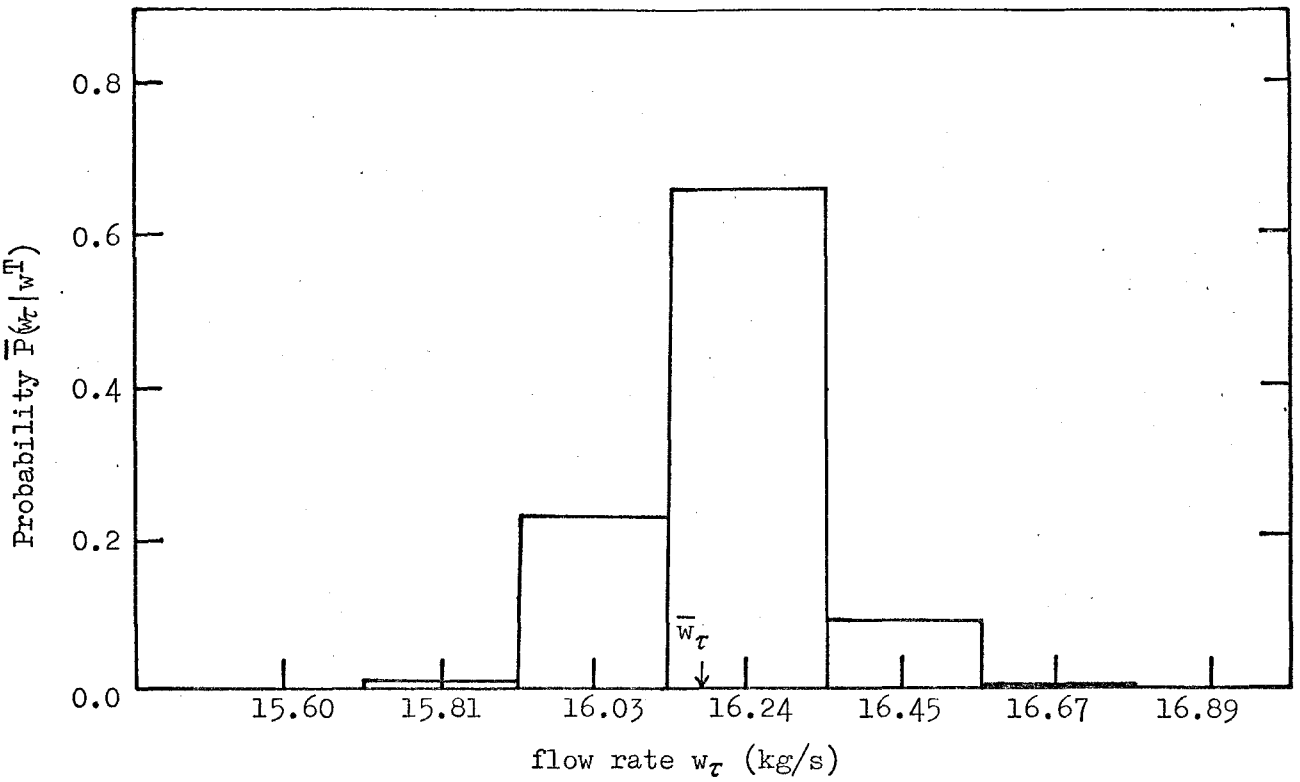

Fig. 4.8 Probabilistic distribution of fuel subassembly coolant flow rate (flow zone 7). $\bar{w}_\tau$ is expectation value of w_τ.

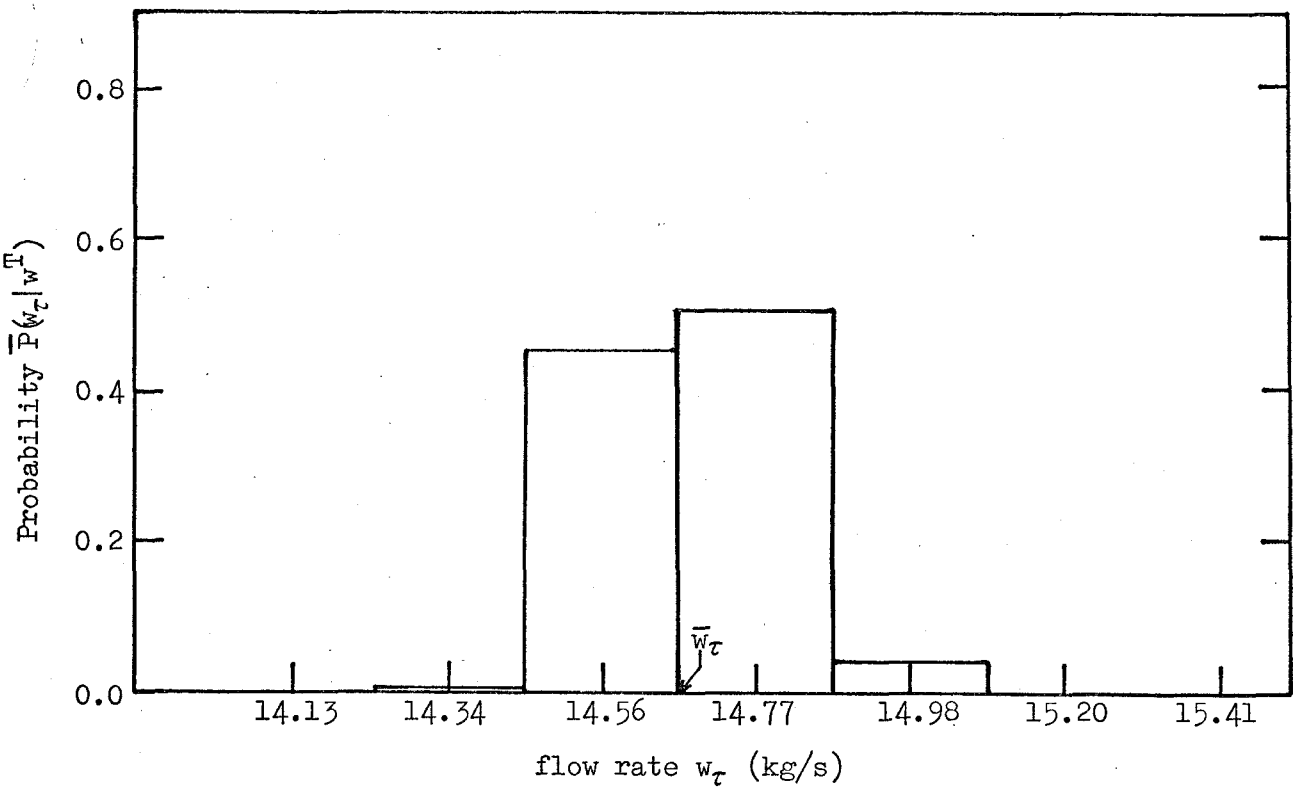

Fig. 4.9 Probabilistic distribution of fuel subassembly coolant flow rate (flow zone 8). $\bar{w}_\tau$ is expectation value of w_τ.

Table 4.3 Probabilistic deviation of coolant flow rate in a prototype LMFBR core.

Flow Zone	Nominal Coolant Flow Rate (kg/s)	Flow Deviation		
		Conventional Method (%)	Proposed Method*	
			(%)	Probability
1	20.20	2.06	$1.50\ ^{-0.57}_{+0}$	8.421×10^{-11}
2	18.59	3.85	$2.49\ ^{-0.91}_{+0}$	1.569×10^{-7}
3	17.83	3.30	$2.34\ ^{-0.96}_{+0}$	3.17×10^{-7}
4	16.63	4.48	$3.25\ ^{-1.23}_{+0}$	1.304×10^{-6}
5	15.47	4.59	$3.25\ ^{-1.34}_{+0}$	2.010×10^{-6}
6	19.34	2.68	$1.94\ ^{-0.74}_{+0}$	4.498×10^{-8}
7	16.24	4.90	$3.59\ ^{-1.32}_{+0}$	3.674×10^{-6}
8	14.77	5.00	$3.56\ ^{-1.45}_{+0}$	2.081×10^{-6}

* The minimum appreciable probability level is of the order of 10^{-15}.

References for Chapter 4

(1) K. Sakai, et al., Development of a Computer Programme for Core-Internal Coolant Flow Distribution Analysis and Evaluation of Probabilistic Coolant Flow Distribution, PNC Report SJ206 75-08, May (1975).

(2) K. Sakai, et al., An Evaluating Method of Core-Internal Coolant Flow Deviation with Correlation Among Fuel Subassemblies, Trans. of At. Energy Soc. Japan, Nov. (1975) E7.

(3) K. Sakai and H. Hishida, Probabilistic Evaluation of Core-Internal Coolant Flow Distribution, Trans. of A.N.S., 24 (1976) 337.

(4) K. Sakai and H. Hishida, Probabilistic Evaluation of Core-Internal Coolant Flow Distribution with Correlation Among Fuel Subassemblies, Nucl. Eng. Design, 44 (1977) 235.

(5) H. Chelemer and L. S. Tong, Engineering Hot-Channel Factors for Open-Lattice Cores, Nucleonics, 20, No. 9 (1962) 68.

(6) A. Amendola, Advanced Statistical Hot Spot Analysis, KFK 1134-EUR 3687 (1970).

(7) T. Inoue, F. Yoshino and A. Izumi, Consideration on Safety Margin in JOYO Thermal Design, N241 73-54, IAEA PANEL Nov. (1973).

(8) Kosoku Zoshyokuro MONJU Chyosei Sekkei (II) PNC Report ZJ222-75-01(5), Sep. (1975) 4.11-1.

(9) M. G. Kendall and A. Stuart, "The Advanced Theory of Statistics Vol. (1)", Charles Griffin Co. (1958) 198.

(10) Test Production Data for MONJU Fuel Subassemblies, PNC Internal Memo, Feb. (1976).

(11) T. Kido, Y. Fukumitsu and M. Kamiya, Fast Breeder Prototype Reactor Fuel Assembly Water Flow Test, PNC Report SJ242 73-02,Mar. (1973).

(12) T. Naganuma, M. Hayano, et al., Hydraulic Testing of a Single Nozzle Flow-Control Mechanism for Monju, PNC Report SJ201 74-05, Dec. (1973).

Chapter 5

General discussion and conclusions

The objective of this study is to accomplish an advanced method for hot spot analyses of the core temperature in core thermal and hydraulic design taking into consideration the mutual dependency of core design parameters through the following correlations, which have been left out in the conventional hot spot analyses, namely,

(i) thermomechanical correlation among fuel pins within a fuel subassembly,

(ii) coolant flow correlation among coolant flow channels within a reactor core, and

(iii) the effect of temperature dependency of material properties on the core hot spot temperature.

In this chapter, conclusions obtained in each section will be reviewed and discussion with respect to their applications to reactor core thermal and hydraulic design will be presented.

1) Lateral drag coefficients of fuel pins corresponding to hydrodynamical force under the coolant flow have experimentally been investigated for several different types of wire-spaced fuel pins as shown in Fig. 2.15.

2) A method of evaluating the fuel pin deflection, the related effects of the core temperature and the mutual contact forces among adjacent fuel pins as well as between a fuel pin and a wrapper tube flat has been accomplished and the following results with respect to a prototype LMFBR core have been obtained.

(i) Due to the temperature gradient across a fuel pin bundle, fuel pin deflection causes to decrease the inner subchannel flow area almost in the core region as shown in Figures 2.17 $\sim$ 2.21 and consequently the hot spot temperature increases. Further, owing to the irradiation swelling and creep,

the fuel pin contact points move to the core center region, where deflection of fuel pins is quite appreciable and thus the hot spot temperature as well as the maximum mutual force acting at the fuel pin contact point generally increases with respect to irradiation time.

(ii) In a case of the prototype LMFBR core employed in sample calculations, the equilibrium fuel pin deflection modes are displayed in Figures 2.17 ~ 2.21. Deviation of subchannel area from the design nominal value is of the order of $^{-10}_{+2}$ % for the inner subchannels and is of the order of +14~+50 % for the peripheral subchannels at the interface between the core and the upper blanket regions. The hot spot subfactor accounting for the fuel pin bundle deflection is 1.023 ~ 1.035 at zero irradiation depending upon the power gradient within a fuel subassembly and it further increases up to 1.045 at 500 day irradiation.

(iii) For the same prototype LMFBR core, the maximum load due to fuel pin contact is 0.52 kg at the upper end of a peripheral fuel pin being in contact with a wrapper tube flat at zero irradiation, however it increases by a factor of about 2.5 in the vicinity of the core center after 500 day irradiation.

3) In the design of a wire-spaced fuel subassembly, the diameter of a spacer wire and the clearance between a fuel pin and a spacer wire being wrapped to the adjacent fuel pin play an important role in connection to thermal and hydraulic characteristics of a core as well as its nuclear characteristics. Through evaluation of the effects of design parameters on the core thermal and hydraulic characteristics by using the proposed method, these parameters may be optimized in connection to the pin bundle pressure drop performance, the core temperature distribution and the pin bundle deflection mode under thermal gradient and irradiation swelling.

4) For the prototype LMFBR fuel subassembly employed in the sample calculations, the effects of the variation in core design parameters such as the

dimensions and the geometries of fuel pins and structual components within a subassembly, material properties and hydraulic parameters on fuel pin gaps have been evaluated based on the currently available test production data of fuel subassemblies. Most sensitive parameters affecting a fuel pin gap which is directly related to the core temperature in a reactor operating condition are as follows:

(i) initial bowing amplitude of a fuel pin ($G_m\{z^*, F^{\xi}(\lambda_{\xi})\}$ defined by (3-7) = -1.38 %~ +1.21 %),

(ii) diameter of a spacer wire (-0.492 %, +0.417 %),

(iii) wrapping pitch of a spacer wire (-0.398 %, +0.198 %),

(iv) installation angle of a fuel pin end support tube (-0.298 %, +0.0479 %),

(v) fuel pin welding angle at the lower end plug (-0.137 %, +0.0465 %).

The values in the above parentheses indicate the maximum deviation of a fuel pin gap due to the variation of each parameter under consideration from its nominal value $\tilde{g}_m(z^*)$ calculated based on the proposed method with all the nominal core design parameters.

Based on these sensitivity studies, assembling and fabrication tolerances of subassembly structual parameters can be optimized in connection to the fabrication cost. The tolerances associated with those structual parameters selected above should be of smaller level than those of the other parameters. Especially, the tolerance of spacer wire wrapping pitch should be of the smallest level at the core and the upper blanket interface as well as at the core center, where the mutual fuel pin contact points appear in the reactor operating condition.

5) Based on the above sensitivity studies, probabilistic distribution of a fuel pin gap within the prototype LMFBR fuel subassembly in its operating condition has been evaluated as shown in Fig. 3.10. The nominal pin gap $\tilde{g}_m(z^*)$ calculated with design nominal values of all the core design parameters

differs by 6.09 % from the design nominal value g_m^N of the pin gap employed in the conventional thermal and hydraulic design. With the confidence level Λ of 99.87 %, the maximum deviation of the pin gap at the cladding hot spot of a fuel subassembly is 8.05 % from the conventional design nominal value g_m^N and is 1.96 % from the currently calculated design nominal pin gap $\tilde{g}_m(z^*)$. The probabilistic distribution of fuel pin gaps tends to shift to the narrower side in the reactor operating condition. The mean value of the pin gap deviates by 0.31 % from the calculated nominal value as shown in Fig. 3.10. This tendency is due to the mutual dependency of core design parameters through mechanical and geometrical correlations in the confinement system of fuel pins externally bounded with a wrapper tube. The normal distribution of fuel pin gap employed in the conventional hot spot analysis is in conflict with this tendency and should be improved.

6) The effects of variation in core design parameters such as the dimensions and the geometries of core structual components, material properties and hydraulic parameters on the fuel subassembly coolant flow rate have been studied and the following conclusions were obtained:

(i) It is sufficient to take into consideration the flow correlation among at most 10 fuel subassemblies within one flow zone in evaluating the effect of subassembly uncertainties.

(ii) The effect of the local variation in core design parameters on the fuel subassembly coolant flow rate is more significant as compared to the global variation in the corresponding parameters. In a case of the prototype LMFBR core employed in the sample calculations, the effect of subassembly-wise variation by 10 % in the hydraulic resistance of a fuel pin bundle on fuel subassembly coolant flow rate is about 1.9 %～ 2.4 % larger than that of the high pressure plenum-wise variation by the same amount. Consequently, the manufacturing tolerances and the experimental inaccuracy of design parameters

corresponding to the local deviation in the hydraulic resistance should be kept at the smallest level. Among these uncertainties, the orificing hole and the installation angle of a subassembly have a larger effect on the subassembly coolant flow rate in the lower flow rate region where the pressure drop at the orificing device is larger. On the other hand, the pressure loss coefficient of a fuel pin bundle, the flat to flat distance of a wrapper tube and the structual parameters of a fuel pin bundle have a larger effect on the subassembly coolant flow rate in the higher flow rate region where the pressure drop in a fuel pin bundle section is dominant.

7) The hydraulic resistance of an orificing device always deviates to the larger resistance side from its nominal value due to the variation of the installation angle of orificing holes. This deviation shifts the subassembly coolant flow rate under consideration to the lower flow rate side. This tendency is more remarkable in the lower flow rate regions as shown in Figs. 4.2 ~ 4.9, since the installation angle of orificing holes affects the hydraulic resistance of an orificing device as mentioned previously. In a case of the prototype LMFBR core employed in sample calculations, the mean value of the probabilistic distribution of subassembly coolant flow rate deviates from its nominal value by 0.20 % in higher flow rate regions and by 0.57 % in lower flow rate regions as are clear from those figures. The normal distribution of subassembly coolant flow rate assumed in the conventional hot spot analyses should be improved taking into consideration the mutual dependency of core structual parameters through coolant flow correlations within a reactor core based on their actual probabilistic distributions. Therefore, it is necessary to set the design nominal values of core design parameters affecting the hydraulic resistance of coolant channels to be at their mean values in designing coolant flow rate control devices within a reactor core so that the design nominal values of channel coolant flow rates

may correspond to their mean values. Based on the evaluation of the effects of core design parameters on channel coolant flow rates and their probabilistic distributions using the method developed in this study, the core-internal coolant flow control devices can be optimized in connection to the manufacturing and assembling cost of core internals and the coolant circulation pump pressure head.

8) For the prototype LMFBR core employed in the sample calculations, the probabilistic distributions of coolant flow rate in core fuel subassemblies have been evaluated based on the currently available factory data as shown in Figs. 4.2 ~ 4.9. Setting the minimum appreciable level of probabilistic occurrence to be 10^{-15}, the deviation of the coolant flow rate from the design nominal value is about 30 % smaller than the maximum deviation calculated with the conventional one-point hot spot temperature evaluation method as shown in Table 4.3. Further, with the confidence level Λ of 99.87 %, the deviation of the coolant flow rate from the design nominal value is about 40 % smaller than the maximum deviation calculated with the conventional method mentioned above. The above results indicate that the hot spot temperature calculated based on the conventional method gives a considerably conservative value.

9) Based on the probabilistic distribution of fuel pin gaps under the condition of constant subassembly coolant flow rate and the probabilistic distribution of subassembly coolant flow rate under the condition of constant reactor total coolant flow rate, the probabilistic distribution of the core hot spot temperature can be evaluated. Thus obtained probabilistic distribution of the core hot spot temperature tends to shift to the higher temperature side from the normal distribution. The normal distribution of the core hot spot temperature assumed in the conventional hot spot analyses is in conflict with these tendencies. In order to optimize the reactor core performance and safety, the probabilistic distribution of the core hot spot temperature should be evaluated

based on the actual probabilistic distributions of uncertainties taking into consideration their mutual dependency through the thermomechanical correlation, the coolant flow rate correlation and the temperature dependency of material properties.

Nomenclature

location:

(x,y,z) = Cartesian coordinates illustrated in Fig. 2.1, where the vertical direction of a fuel subassembly is parallel to z direction

(x',y',z') = Cartesian coordinates illustrated in Fig. 2.14, where z' axis is oblique to z-axis by angle θ

z_0, z^+ = z coordinates of a fuel pin at the lower and the upper ends

z_0', z'^+ = z' coordinates of a fuel pin corresponding to z_0 and z^+, respectively, in the (x',y',z') coordinate system

z^* = z coordinate of the core and upper blanket interface

i = fuel pin number corresponding to the fuel pin under consideration

j = fuel pin number corresponding to any adjacent one in contact with the fuel pin i

k = number indicating the kth contact point from the lower end of the fuel pin under consideration.

$p(i,j)$ = pair number associated with fuel pins i and j

ℓ, ℓ_p = number indicating the ℓth contact point from the lower ends of the fuel pin pair $p(i,j)$

$\overset{*}{\ell}\{p(i,j),\ell|p(\xi,\eta)\}$ = number of all loads $R_{p(\xi,\eta),\zeta}$'s associated with the pair $p(\xi,\eta)$ whose points of application $z_{p(\xi,\eta),\zeta}$'s satisfy $z_{p(\xi,\eta),\zeta} \leq z_{p(i,j),\ell}$ as shown in Fig. 2.4

e = wrapper tube flat number, e = 1, 2, ·····, 6

τ = fuel subassembly number corresponding to the fuel subassembly under consideration

(μ,ν,ω) = ωth subassembly in the νth flow zone connected to the μth pressure plenum

(μ,ν) = νth flow zone connected to the μth pressure plenum

μ = pressure plenum number corresponding to the pressure plenum under consideration (in sample calculations, μ = 1, 2, 3 and 4 correspond to the high pressure plenum, the low pressure plenum, the storage rack plenum and the side wall bulk plenum, respectively)

uncertainties:

F = uncertainty of a core design parameter

F_λ = λth uncertainty

$\{F_\lambda\}$ = set of all uncertainties related to the fuel pin gap

$F^{\ell}(i,h;\lambda_\ell)$ = normalized local uncertainty of the λ_ℓth kind which belongs to the axial coordinate z_h of fuel pin i

$F^{f}(i;\lambda_f)$ = normalized fuel pin uncertainty of the λ_fth kind which belongs to fuel pin i

$F^{s}(\lambda_s)$ = normalized subassembly uncertainty of λ_sth kind (includes F^z, F^p and F^c as parameters in chapter 3)

$F^{s}(\mu,\nu,\omega;\lambda_s)$ = normalized subassembly uncertainty of the λ_sth kind which belongs to the ωth subassembly in the νth flow zone connected to the μth pressure plenum

$F^{z}(\mu,\nu;\lambda_z)$ = normalized flow zone uncertainty of the λ_zth kind which belongs to the νth flow zone connected to the μth pressure plenum

$F^{p}(\mu;\lambda_p)$ = normalized plenum uncertainty of the λ_pth kind which belongs to the μth pressure plenum

$F^c(\lambda_c)$ = normalized core uncertainty of λ_cth kind

F^{ℓ} = all uncertainties represented by $F^{\ell}(i,h;\lambda_{\ell})$ with possible combinations of i, h and λ_{ℓ}

F^f = all uncertainties represented by $F^f(i;\lambda_f)$ with possible combinations of i and λ_f

F^s = all uncertainties represented by $F^s(\lambda_s)$ or $F^s(\mu,\nu,\omega;\lambda_s)$ with possible combinations of μ, ν, ω and λ_s

F^z = all uncertainties represented by $F^z(\mu,\nu;\lambda_z)$ with possible combinations of μ, ν and λ_z

F^p = all uncertainties represented by $F^p(\mu;\lambda_p)$ with possible combinations of μ and λ_p

F^c = all uncertainties represented by $F^c(\lambda_c)$

probability:

$P(i,h;\lambda_{\ell})$ = probabilistic density function of $F^{\ell}(i,h;\lambda_{\ell})$

$P^f(i;\lambda_f)$ = probabilistic density function of $F^f(i;\lambda_f)$

$P^s(\lambda_s)$ = probabilistic density function of $F^s(\lambda_s)$

$P^s(\mu,\nu,\omega;\lambda_s)$ = probabilistic density function of $F^s(\mu,\nu,\omega;\lambda_s)$

$P^z(\mu,\nu;\lambda_z)$ = probabilistic density function of $F^z(\mu,\nu;\lambda_z)$

$P^p(\mu;\lambda_p)$ = probabilistic density function of $F^p(\mu;\lambda_p)$

$P^c(\lambda_c)$ = probabilistic density function of $F^c(\lambda_c)$

$P(\xi|\alpha,\beta,\gamma,\cdots)$ = conditional probabilistic density function that ξ is included in the interval $(\xi,\xi+d\xi)$ under the fixed parameters of α, β, γ, $\cdots$

$\overline{P}$ = probability defined by expression (4-9)

Λ = confidence level defined by eq. (1-3)

thermohydraulics:

T = core temperature distribution function (corresponds to cladding temperature in chapter 2)

T_τ = core temperature within the τth fuel subassembly

$T_\tau^{H.S.}(\Lambda)$ = calculated core hot spot temperature with confidence level Λ within the τth fuel subassembly defined by eq. (1-3)

T_τ^N = core nominal temperature at the specified point corresponding to $T_\tau^{H.S.}(\Lambda)$

T_{in} = reactor inlet coolant temperature

w = coolant flow rate

$\bar{w}$ = averaged coolant flow rate per fuel pin in a fuel subassembly

$\bar{w}_{in}$ = averaged coolant flow rate per fuel pin belonging to interior subchannels of a fuel subassembly

w_τ = coolant flow rate of the τth fuel subassembly

w^T = reactor total coolant flow rate

V = coolant flow velocity

Re = Reynolds number

$g_m(z, \{F_\lambda\})$ = mth fuel pin gap at z with respect to $\{F_\lambda\}$

$\tilde{g}_m(z)$ = nominal value of the mth fuel pin gap at z in an equilibrium pin bundle configuration calculated with nominal values of all core design parameters, i.e. $g_m(z, \{\tilde{F}_\lambda\})$

g_m^N = design nominal value of the mth fuel pin gap under non-deflected pin bundle configuration

p = static pressure

Δp = pressure drop between the inlet and the outlet plenums

Δp_1, Δp_2 = pressure drop across a core fuel subassembly and a blanket fuel subassembly, respectively

fuel pin deflection and forces:

$u(z)$, $v(z)$ = x and y coordinates of the central axis of a fuel pin at z

$x(z)$, $y(z)$ = x and y directional displacements of the central axis of a fuel pin at z from $u(z_0)$ and $v(z_0)$

ε = longitudinal strain

R = load due to fuel pin contact

$W(z)$ = normal component of the hydrodynamical force acting on a unit length of a fuel pin at z

G_b, G_g = buoyancy and gravity acting on a unit length of a fuel pin

σ = bending stress

$M(z)$ = bending moment at z

dimensions and geometries:

$r(z)$ = radius of a fuel pin at z

d = diameter of a fuel pin

r_w = radius of a spacer wire

h_p = axial length of a fuel pin

h_s = axial length of a fuel subassembly

$q(z_{i,j,\ell})$ = center to center distance of fuel pins i and j at $z_{i,j,\ell}$

$\beta_i(z)$ = directional angle of the center of fuel pin i with respect to the center of intervening wire spacer at z

$\lambda_i(z)$ = directional angle of the center of fuel pin in contact with the fuel pin i at z

θ = oblique angle of a fuel pin with respect to the flow direction

φ = directional angle of W(z) with respect to the normal to the fuel pin at z lying on the plane normal to y-axis

$\gamma(z)$ = directional cosine of load R with respect to x-axis defined by (2-8a) or (2-8a') at z

$\delta(z)$ = directional cosine of load R with respect to y-axis defined by (2-8b) or (2-8b') at z

material properties:

ρ = density of coolant

c_p = specific heat of coolant

ν_V = kinematic viscosity of coolant

ε_H = turbulent diffusivity of heat

$\alpha(T)$ = linear thermal expansion coefficient of a fuel pin under T

$E(T)$ = modulus of elasticity of a fuel pin under T

I = moment of inertia of a fuel pin cross section

$\alpha^{FB}(\mu, \nu, \omega)$ = hydraulic resistance coefficient, defined as $\alpha^{FB} \equiv \Delta p^{FB}/w^x$, associated with the fuel bundle section of the ωth subassembly in the νth flow zone connected to the μth pressure plenum

α^{OR}, α^{NS}, α^{Pl} = defined similar to α^{FB}

C_d = drag coefficient for a fuel pin

f_w = coefficient of edge-flow effect within a fuel subassembly

f^S = strain due to swelling

f^C = strain due to thermal and irradiation creep

miscellaneous:

t = time

ϕ = neutron flux

N_x, N_y = normals to fuel pin i at z lying on a plane normal to y-axis and on a plane normal to x-axis, respectively

$M_{m,n}$ = element of flexibility matrix

D_m = element of column vector

g = gravitational constant

N_z = number of subassemblies which belong to the flow zone under consideration

M_z = number of flow zones

M_p = number of pressure plenums

superscripts:

ℓ = local

f = fuel pin

s = subassembly (includes flow zone, pressure plenum and core in chapter 3)

z = flow zone

p = pressure plenum

c = core

T = due to temperature distribution (total for w^T)

R = due to loads at fuel pin contact points

H = due to hydrodynamical force

S = due to swelling

C = due to creep

M = due to bending moment

I = due to the initial bowing

OR = orifice section of a subassembly

NS = neutron shield section of a subassembly

FB = fuel pin bundle section of a subassembly

Pl = high pressure plenum section

$\overline{A}$ = mean value of A

$\widetilde{A}$ = nominal value of A

$\hat{A}$ = reference value of A at which a function of A is expanded into Taylor's series

Acknowledgement

The author would like to express his greatest appreciation to Dr. H. Hishida of Mitsubishi Atomic Power Ind., Inc. who has guided the author throughout the present study with deeply helpful discussion.

The author would also like to express his particular appreciation to Professors Dr. T. Sekiya, Dr. S. Omi and Dr. M. Hamada of Osaka University who have been giving most valuable suggestions, criticisms and encouragement.

He is also greatful to Mr. Y. Okubo for his assistance in performing this study.

Author's Personal Record

A] List of papers previously published:

(1) K. Sakai and H. Hishida, Probabilistic Evaluation of Core-Internal Coolant Flow Distribution, Trans. of A.N.S., 24 (1976) 337.

(2) K. Sakai, Y. Okubo and H. Hishida, Deflection of Wire-Spaced Fuel Pin Bundles, Trans. of A.N.S., 26 (1977) 460.

(3) K. Sakai and H. Hishida, Probabilistic Evaluation of Core-Internal Coolant Flow Distribution with Correlation Among Fuel Subassemblies, Nucl. Eng. Design, 44 (1977) 235.

(4) K. Sakai, Y. Okubo and H. Hishida, Three-Dimensional Deflection Analyses of Wire-Spaced Fuel Pin Bundles under Temperature and Hydrodynamical Force Fields with Irradiation Effects, Nucl. Eng. Design, 48 (1978) 595.

(5) K. Sakai, H. Hishida, Y. Nakai and S. Saito, Probabilistic Distributions of Pin Gaps within a Wire-Spaced Fuel Subassembly and Sensitivities of the Related Uncertainties to Pin Gaps, Nucl. Eng. Design, 48 (1978) 505.

B] List of PNC technical reports to which the author previously contributed:

(1) K. Sakai, et al., Modification of a Thermal-Hydraulic Computer Code "COBRA" for the Versatile Applications, J206 71-04, Apr. (1971).

(2) K. Sakai, H. Hishida, et al., Development of a Computer Programme for Core-Internal Flow Distribution Analyses and Evaluation of Probabilistic Flow Distribution, SJ206 75-08, May (1975).

(3) K. Sakai, H. Hishida, et al., Development of a Method of Fuel Pin Gap Assurance for "MONJU" Fuel Assemblies, SJ206 76-01, Feb. (1976).

(4) K. Sakai, H. Hishida, et al., Development of a Computer Programme for ATR Fuel Assembly Analyses III, ZJ306 76-01, Apr. (1976).

(5) K. Sakai, H. Hishida, et al., Improvement of Computer Programme ORIFS-P.F.D. for Core-Internal Flow Distribution Analyses and Evaluation of Probabilistic Flow Distributions, SJ206 76-10, Apr. (1976).

(6) Y. Yamashita, K. Sakai, H. Hishida, et al., Development of a Computer Programme for Thermal Shock Analysis of Reactor Vessel Outlet Nozzle, SJ206 76-16, July (1976).

(7) K. Sakai, Y. Okubo and H. Hishida, Development of a Computer Programme for Deflection Analysis of Wire-Wrapped Fuel Pin Bundle, PNC Report SJ206 76-17, July (1976).

(8) K. Sakai, Y. Okubo, H. Hishida, et al., Development of a Computer Programme for ATR Fuel Subassembly Analyses (IV), ZJ306 77-01, Mar. (1977).

(9) K. Sakai, H. Hishida, et al., Statistical Deformation Analysis of ATR Fuel Pin Subassemblies (I), ZJ306 77-02, Mar. (1977).

(10) K. Sakai, H. Tezuka, et al., Development of a Computer Programme for Steady State and Transient Core Thermal-Hydraulic Analyses, SJ206 77-05, June (1977).

(11) K. Sakai, Y. Okubo, H. Tezuka and H. Hishida, Development of a Computer Programme for Deflection Analyses of Wire-Wrapped Fuel Pin Bundle (II), SJ206 77-09, Mar. (1977).

(12) Y. Okubo and K. Sakai, Development of a Computer Programme for Deflection Analyses of Wire-Wrapped Fuel Pin Bundle (III), SJ206 77-34, Jan. (1978).

(13) K. Sakai, K. Ueno, et al., Development of a Computer Programme for Steady State and Transient Core Thermal-Hydraulic Analyses (II), SJ206 78-08, Mar. (1978).

C] List of oral representation:

(1) K. Sakai and H. Hishida, Probabilistic Evaluation of Core-Internal Coolant Flow Distribution, Winter Meeting of A.N.S., Washington D.C., Nov. (1976).

(2) K. Sakai, Y. Okubo and H. Hishida, Deflection of Wire-Spaced Fuel Pin Bundles, Annual Meeting of A.N.S., New York, N.Y., June (1977).

(3) K. Sakai, H. Hishida, et al., Circumferential Temperature Distribution on Fuel Cladding with Local Heat Transfer Depression, Sectional Meeting of At. Energy Soc. Japan, Oct. (1974) E21.

(4) K. Sakai, T. Koga and H. Hishida, Evaluation of Hot Spot Temperature by Monte Carlo Method, Sectional Meeting of At. Energy Soc. Japan, Oct. (1974) E22.

(5) K. Ito, K. Sakai and H. Hishida, Studies on turbulent diffusivity of coolant within a fuel pin bundle by a Mode Expansion Method, Sectional Meeting of At. Energy Soc. Japan, Oct. (1974) E24.

(6) K. Sakai, H. Hishida, et al., Evaluation of Core-Internal Coolant Flow Distribution with Correlation Among Fuel Subassemblies, Sectional Meeting of At. Energy Soc. Japan, Nov. (1975) E6.

(7) K. Sakai, H. Hishida, et al., Evaluation of Core-Internal Coolant Flow Deviation Due to Statistical Variation in Core Design Parameters with Correlation Among Fuel Subassemblies (I), Sectional Meeting of At. Energy Soc. Japan, Nov. (1975) E7.

(8) H. Kinjo, K. Sakai and H. Hishida, Three-Dimensional Core Deformation Analysis, Sectional Meeting of At. Energy Soc. Japan, Nov. (1975) E10.

(9) K. Sakai, Y. Okubo and H. Hishida, Development of an Analytical Method for Evaluating Wire-Spaced Fuel Pin Bundle Deflection,

Sectional Meeting of At. Energy Soc. Japan, Nov. (1975) E11.

(10) K. Sakai, Y. Okubo and H. Hishida, Development of an Analytical Method for Evaluating Wire-Spaced Fuel Pin Bundle Deflection (II), Annual Meeting of At. Energy Soc. Japan, Mar. (1976) A32.

(11) K. Sakai, H. Hishida, et al., Evaluation of Core-Internal Coolant Flow Deviation Due to Statistical Variation in Core Design Parameters with Correlation Among Fuel Subassemblies (II), Sectional Meeting of At. Energy Soc. Japan, Oct. (1976) B43.

(12) Y. Yamashita, K. Sakai, H. Hishida, et al., Development of a Computer Programme for Thermal Shock Analyses of Reactor Vessel Outlet Nozzle, Sectional Meeting of At. Energy Soc. Japan, Oct. (1976) B44.

(13) K. Sakai, Y. Okubo, et al., Development of an Analytical Method for Evaluating Wire-Spaced Fuel Pin Bundle Deflection (III), Sectional Meeting of At. Energy Soc. Japan, Oct. (1976) B46.

(14) K. Sakai, Y. Okubo, H. Hishida, et al., Development of a Statistically Evaluating Method for Fuel Pin Gaps within a FUGEN Fuel Subassembly, Sectional Meeting of At. Energy Soc. Japan, Oct. (1976) B47.

(15) H. Kinjo, K. Sakai and H. Hishida, Three-Dimensional Core Deformation Analyses (II), Sectional Meeting of At. Energy Soc. Japan, Oct. (1976) B48.

(16) Y. Okubo, K. Sakai and H. Hishida, Development of a Statistically Evaluating Method for Fuel Pin Gaps within a Fuel Subassembly, Annual Meeting of At. Energy Soc. Japan, Apr. (1977) C44.

(17) K. Sakai, Y. Okubo, H. Hishida, et al., Development of an Analytical Method for Evaluating Wire-Spaced Fuel Pin Bundle Deflection (IV), Annual Meeting of At. Energy Soc. Japan, Apr. (1977) C45.

(18) H. Kinjo, K. Sakai, H. Hishida, et al., Three-Dimensional Fuel Pin Deflection Analysis under Axial Load, Annual Meeting of At. Energy Soc. Japan, Apr. (1977) C46.

(19) H. Kinjo, K. Sakai and H. Hishida, Three-Dimensional Core Deformation Analysis (III), Annual Meeting of At. Energy Soc. Japan, Apr. (1977) C47.

(20) K. Ito, K. Sakai, H. Hishida, et al., Edge Flow Effect of a FBR Fuel Subassembly, Annual Meeting of At. Energy Soc. Japan, Apr. (1977) F29.

(21) K. Sakai, H. Tezuka and Y. Okubo, Development of a Computer Programme for Transient Core Thermal-Hydraulic Analyses (I), Sectional Meeting of At. Energy Soc. Japan, Oct. (1977) C52.

(22) K. Sakai, Y. Okubo and H. Hishida, Probabilistic Distribution of Fuel Pin Gaps within a Wire-Spaced Fuel Subassembly, Sectional Meeting of At. Energy Soc. Japan, Oct. (1977) C53.

(23) H. Kinjo, K. Sakai and Y. Yamashita, Development of an Evaluating Method for Turbulent Diffusivity ε_M and ε_H within a Reactor Vessel Plenum, Sectional Meeting of At. Energy Soc. Japan, Oct. (1977) C54.

(24) K. Sakai, K. Ito, H. Hishida, et al., Evaluation of the Effect of Hydrodynamical Force on Fuel Pin Deflection, Sectional Meeting of At. Energy Soc. Japan, Oct. (1977) F58.

(25) K. Sakai and H. Hishida, Development of a FBR Core Thermal and Hydraulic Design System (I) - Core Permissible Operation Temperature Bounds, Sectional Meeting of At. Energy Soc. Japan, Oct. (1978) C20.

(26) Y. Yamashita, K. Sakai and H. Hishida, Velocity Distribution of a Fluid Flow around a Wire-Wrapped Fuel Pin, to be represented at Sectional Meeting of At. Energy Soc. Japan, Mar. (1979).